JAERI-Review
94-011

Annual Report of NAKA Fusion Research Establishment for the Period from April 1, 1993 to March 31, 1994

January 1995

Naka Fusion Research Establishment

日本原子力研究所
Japan Atomic Energy Research Institute

本レポートは，日本原子力研究所が不定期に公刊している研究報告書です。

入手の問合わせは，日本原子力研究所技術情報部情報資料課（〒319-11 茨城県那珂郡東海村）あて，お申しこみください。なお，このほかに財団法人原子力弘済会資料センター（〒319-11 茨城県那珂郡東海村日本原子力研究所内）で複写による実費領布をおこなっております。

This reports are issued irregularly.

Inquiries about availability of the reports should be addressed to Information Division Department of Technical Information, Japan Atomic Energy Research Institute, Tokaimura, Naka-gun, Ibaraki-ken 319-11, Japan.

編集兼発行　日本原子力研究所

印　　刷　ニッセイエブロ株式会社

JAERI-Review 94-011

Annual Report of Naka Fusion Research Establishment for the Period from April 1, 1993 to March 31, 1994

Naka Fusion Research Establishment

Japan Atomic Energy Research Institute
Naka-machi, Naka-gun, Ibaraki-ken

(Received December 6, 1994)

Research and development activities at Naka Fusion Research Establishment, JAERI, are reported for the period from April 1, 1993 to March 31, 1994.

The main objectives of JT-60U experiments in FY1993 were to achieve and sustain high confinement regime with current drive. High-βp H-mode performance was especially highlighted among these experiments. In the mode, the highest fusion-triple-product of $1.1\times10^{21}m^{-3}\cdot s\cdot keV$, the highest stored energy of 8.8MJ, the highest neutron yield of $5.6\times10^{16}sec^{-1}$ and the highest H-factor of 3.6 were achieved. The JFT-2M experiments progressed in the systematic study of the plasma responses by applying an external helical field and also in the study of the boundary plasma with electric field or current in the scrape off layer (SOL) introduced by the divertor bias system. The study in Plasma Theory and Computation focused on the ion temperature gradient instability, the linear toroidal particle simulation, the MHD stability and the analyses of burning plasma. The progresses on DIII-D experiments were obtained in the studies of divertor radiation, cryopumping and VH-mode plasma.

As for the fusion engineering research, further developments of a ceramic vacuum pump and a high-resolution quadrupole mass spectrometer (QMS) were made in the vacuum technology area. Major evolutions of the superconducting magnet development are as follows : (1) Advanced Nb_3Sn strands were developed. (2) It was decided in the ITER Program that the US and Japan fabricate the inner and outer module of the Central Solenoid (CS) Model Coil,

Editors : Matoba T.(in chief), Nakamura Y., Matsuzaki Y., Araki M., Yamane Y.

respectively. (3) Eleven contracts were established between JAERI and Japanese industries.A high energy H^- beam of 400keV and 0.18A was produced with a current density of 13mA/cm^2 for 1s. Many efforts were made in developing the long pulse gyrotron with an output power of 410kW at 110GHz for 1.2sec and the high efficency collector potential depression (CPD) gyrotron with an efficiency of about 30% at 750kW for 1ms in the radio-frequency (RF) technology area. The main progress in the Tritium Systems Test Assembly (under US/Japan collaboration) was to demonstrate the plasma exhaust stream under non-steady tokamak operation. Heating experiments of the development 1m long divertor module for ITER were performed at a heat flux of 15MW/m^2 for 30sec. The R&D efforts of the reactor structure development were focused on the development of major components such as non-circular bellows, fail-safe first wall, etc.. The R&D efforts of the blanket technology were focused on the development of box structure for ITER shielding blanket and the out-of-reactor testing of ITER breeding blanket.

The outline design report of the ITER Engineering Design Activities (EDA) was accepted in the ITER Council Meeting on January 1994. Protocol 2 of the ITER EDA Agreement was signed in Vienna on 21 March 1994, and covers the detailed technical work up to the end of the Agreement. The DREAM tokamak reactor concept was improved regarding utilization of low activation materials and improvement of thermal efficiency.

Keywords : Fusion Research, JAERI, JT-60U, JFT-2M, DIII-D, Plasma Physics, Fusion Engineering, Fusion Technology, ITER, Fusion Reactor Design, Annual Report

那珂研究所年報（平成５年度）

日本原子力研究所
那珂研究所

（1994年12月６日受理）

原研・那珂研究所における平成５年度（1993年４月～1994年３月）の研究開発活動について報告する。

1993年度のJT-60Uの主な実験目的は、電流駆動時に高性能閉込め状態を達成し維持することであった。特に、高βpHモードが一連の実験のハイライトであった。そのモードでは、核融合積が最高値$1.1\times10^{21}m^{-3}\cdot s\cdot keV$、蓄積エネルギーが最高値8.8MJ、中性子発生率が最高値$5.6\times10^{16}s^{-1}$、及びHファクターが最高値3.6を達成した。JFT-２M実験の進展は、外部ヘリカル磁場印加時のプラズマ応答を組織的に調べたこととダイバータバイアス装置によるスクレープオフ層への電場や電流の導入による境界プラズマの研究であった。プラズマ理論・数値解析では、イオン温度勾配不安定性、線形トロイダル粒子シミュレーション、MHD安定性及び核燃焼プラズマの解析の研究が中心であった。DⅢ-D実験の進展は、ダイバータ放射、クライオポンプ及びVHモードプラズマの研究であった。

核融合工学については、真空技術では、セラミック真空ポンプ、高分解能四重極質量分析器（QMS）などの開発をさらに進めた。超電導磁石開発の主な進展は以下のとおりである。(1)先進的なNb_3Sn素線が開発された。(2)米国と日本がそれぞれCSモデルコイルの内側と外側のモジュールを製作することがITERプログラムで決定された。(3)原研と日本の企業間で11の連繋がなされた。高エネルギー負イオンビームの開発では、400keVで0.18Aの負水素イオンビームが１秒間$13mA/cm^2$の電流密度で達成された。高周波技術では、110GHzの長パルスジャイロトロンで410kWを1.2秒間発振することに成功し、また高効率CPDジャイロトロンで750kWを１ms間30％の効率で発振することに成功した。トリチウムシステム試験施設（日米協力）では、非定常トカマク運転でのプラズマ排気流の実証が主な進展項目であった。ITER用として開発した１mのダイバータモジュールの加熱実験で$15MW/m^2$の熱流束で30秒間の運転を達成した。炉構造開発としては、非円形ベローズ、フェイルセーフ第一壁等の主要コンポーネントの開発が行われた。ブランケット工学の開発では、ITER遮蔽ブランケットとして箱型構造が、及び

那珂研究所：〒311-01 茨城県那珂郡那珂町大字向山801-1
編集者：的場　徹、中村　幸治、松崎　誼、荒木　政則、山根　芳文

ＩＴＥＲ増殖ブランケットの炉外試験が主として実施された。

ＩＴＥＲ工学設計活動（ＥＤＡ）の概要設計が1994年1月のＩＴＥＲ理事会で受理された。ＩＴＥＲ・ＥＤＡ協定の議定書2が1994年3月21日にウイーンで署名された。これは、以後の協定の全期間における詳細な技術的作業内容を規定する。ＤＲＥＡＭトカマク炉の概念検討として、低放射化材料の採用と熱効率向上について進展した。

Foreword

The fusion research and development at the Naka Fusion Research Establishment, JAERI has been conducted in accordance with the Third Phase Basic Program of Fusion Research and Development laid down by the Atomic Energy Commission of Japan in June 1992. The main objectives of the Program are to realize the self-ignition condition and a long burn operation in a tokamak fusion experimental reactor, and to build up reactor technologies required for the further development of a prototype fusion reactor.

To achieve these objectives in the Third Phase activities, our emphasis should to the utmost be on a well-balanced integrated implementation of R & D's of fusion plasmas and fusion reactor technologies. At present fulfillment of the international project of the ITER Engineering Design Activities is a major and an important approach to the tokamak experimental reactor.

Extensive studies of confinement improvement and steady-state tokamak operation/ divertor physics have been continued on JT-60 Upgrade to explore an advanced tokamak concept. A quasi steady-state operation of plasmas having a good confinement property was experimentally demonstrated. A highest plasma current of up to 3.6 MA was fully driven non-inductively by lower hybrid waves in a series of experiments on non-inductive current drive. Steady progress was also made in the studies of disruption control, helium-ash exhaust and other subjects related to the ITER physics R & D.

In the reactor technology areas, the ITER engineering R & D's shared on the basis of the international task agreements got into their stride; among them the preparation for the development of ITER central solenoid coils and a remote handling system for divertor maintenance marked a significant progress. The development of a negative ion source for the future high energy neutral beam heating system and a 100 GHz range gyrotron also progressed remarkably. A Japan-US collaboration of tritium technology started a new program that emphasized safety handling aspects of tritium technology.

The ITER Engineering Design Activities entered upon their second phase activities based on the Protcol 2 in March 1994. The engineering R & D activities as described above and the design activities that contributed to the ITER outline design by the Joint Central Team were performed. We have also made efforts to support the JCT at the Naka Joint Work Site of the ITER EDA.

Sanae Tamura
Director General
Naka Fusion Research
Establishment
JAERI

Contents

目　　次

I. JT-60 PROGRAM

1. Overview

Upgrated JT-60(JT-60U) is capable of producing single-null divertor discharges with plasma current of 6 MA, with high power heating and current drive: neutral beam heating power of up to 40 MW, lower hybrid current drive (LHCD) power of up to 10 MW, and ion cyclotron resonance heating (ICRF) power of up to 5MW. Features of JT-60U are a high aspect ratio (4.0), a high toroidal magnetic field (4 T) and open divertor. From the view point of divertor heat load, 40 MW of heating power in JT-60U corresponds to alpha heating power in ITER. The main objectives of JT-60U experiments are: (1) confinement improvement, (2) impurity control and divertor studies, (3) steady-state studies, and (4) energetic particle physics. Through the pursuit of these subjects, we aim to contribute to the ITER Physics R&D, and provide data essential for the concept development of fusion power reactors like SSTR.

JT-60U experiment was commenced in March 1991. Well-controlled equilibrium in the diverted configuration was successfully achieved for Ip ≤ 5 MA with digital feedback control system. The NB power was increased up to 36 MW with perpendicular and tangential injectors. The maximum coupled LHRF power was also increased up to 7MW. The power of ICRF with a frequency range of 110-130 MHz were also increased up to 5 MW with two antennas.

The boronization using decaborane ($B_{10}H_{14}$) vapor at 100 °C was very effective for the wall conditioning. Part of the divertor tiles were replaced to the B_4C coated CFC tiles to reduce sputtering and to getter the oxygen more effectively.

The main objectives of JT-60U experiments during April 1993 to March 1994 were to achieve and sustain high confinement regime with current drive. High-βp H-mode perfermance was especially highlighted among these experiments. The fusion-triple-product $1.1\times10^{21}m^{-3}$skeV was achieved in the high-βp H-mode in which the confinement was improved in the edge region as well as the core region by the combination of the high-βp mode and H-mode. The highly improved confinement in the high-βp H-mode with both the centrally peaked profile and the edge pedestal in the pressure led to the significant H-factor up to 3.6. In the mode, the highest stored energy of 8.8 MJ and the highest neutron yield of $5.6\times10^{16}sec^{-1}$ were also achieved. This high-βp H-mode regime can be operated in quasi steady state with ELM. Plasma stored energy of 7MJ has been sustained for 1 second.

High normalized beta value $\beta_N=\langle\beta_t\rangle/(I_p/aB_t)=4.2$ was also achieved in lower field regime (B_t=1T). Disruption and MHD studies were extended addressing disruption softening and physics understanding. Progresses were made in understanding of confinement physics such as thermal confinement scaling, H-mode physics, internal transport barriers at q=3 surface etc. In the area of divertor research, particle confinement time in the main plasma was evaluated and the particle recycling characteristics showed favourable q dependence. Current drive with LHRF were

extended to drive plasma current up to 3.6MA. And the physics understanding such as "spectrum gap" were progressed. A toroidal Alfven eigen mode (TAE mode) was observed during the high power ICRF heating. The observed TAE frequency was found to be consistent with the simple theory.

These research will be a baseline for the integrated demonstration of the long pulse full current drive experiments using N-NBI and advanced closed divertor in 1997.

2. Operation of JT-60 Upgrade

2.1 Tokamak

2.1.1 Operation and maintenance for the JT-60U machine

The operation and maintenance of the JT-60 Upgrade machine have been carried out almost on schedule. Water leakage of all the toroidal field coils has been always monitored after the installation of water leak detectors. Fortunately all the coils have been operated without any trouble. The pellet injection system was improved to change the speed of the pellet from 0.9 to 1.7 km/s for deuterium. The heaters were mounted around the neutral beam injector ports to bake out the port wall efficiently. In situ boronization was carried out on two occasions, in June and February, after the improvement of the system. In August, some first wall tiles were found to be broken or detached by the inspection through the in-vessel inspection device. These tiles were replaced with new ones immediately. In February one of the plasma diagnostic devices fell down on parts of the cooling systems for the toroidal field coils and of the gas baking system for the vacuum vessel. These damaged parts were also repaired urgently.

2.1.2 Operation results of plasma facing components

Three carbon fiber composite (CFC) wall tiles were broken mechanically. This damage was probably caused by the electromagnetic force due to halo current during disruptions. The broken tile was rotated poloidally around the plasma with a speed of about 10 m/s during the following discharge. A possible driving force of this rotation might be the electromagnetic force due to the scrape-off layer (SOL) current. These results indicate that electromagnetic interaction between SOL plasma and the plasma facing components is an important issue. The in-vessel inspection also showed that one CFC divertor tile was detached and about 80 units of divertor tiles were loosened by the imperfect spot-welding of the bolt. Seven tiles were eroded by 3-4 mm in depth due to protrusion during discharges. These damaged tiles were replaced with new ones after improvement of the structure.

The B_4C-converted CFC divertor tiles which have been used since January 1993 exhibited good material behavior in the NB-heated divertor operation and the B_4C-converted surface was effective in reducing carbon impurity, but slight erosions were observed on almost all tile edges as

shown in Fig. I.2.1-1. The additional B_4C-converted tiles were installed on the divertor plate in December 1993. The oxygen impurity was reduced by strong evaporation of the B_4C-converted layer due to oxygen gettering by the deposited boron for a long period of the high power operation.

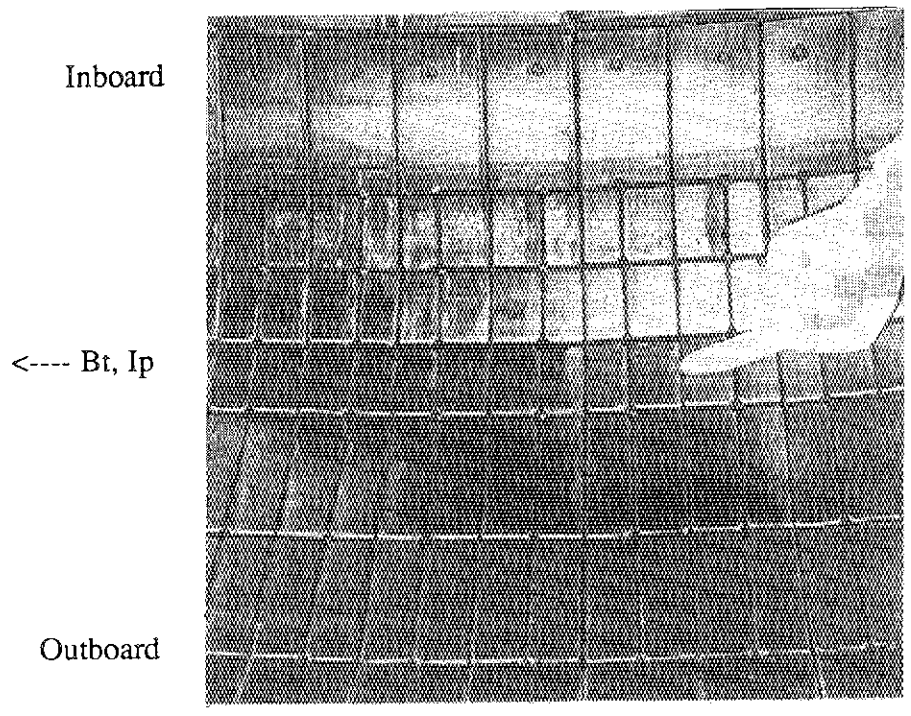

Fig. I.2.1-1 Typical view of the divertor tiles after operation until October 1993, showing no significant damage except for slight erosions at tile edges

2.2 Control system

The control system was fully used in the JT-60U experiments in this fiscal year. Improvements were made on some functions in the central control system corresponding to the experiments. New control algorithms were installed in the plasma position and current control system [2.2.1] for the studies on plasma initiation by low loop voltage and slow build-up of plasma current. A new system with workstations (SPARC Station 2) was installed in the central control room for a session leader easily announcing the JT-60U operation status, which is displayed on the TV screens in the control room and offices.

For the maintenance of the control system, annual inspections were made of the computer system, control boards, the signal processing system for plasma control and the hard X-ray monitors in the shut-down period of November and December. In conjunction with the maintenance of the central control computer system, five consoles of the minicomputers (HIDIC-80Es, Hitachi Ltd.) were superseded by a UNIX workstation (SPARC Station IPX), where a newly-developed emulator of the consoles were installed. The workstation is connected to the minicomputers via RS-232C interfaces. (Fig.I.2.2-1) Furthermore, an annual inspection of the

interlock functions on neutron production and the doors of controlled area was made in accordance with the inner rules for the prevention of radiation hazards at Naka Fusion Research Establishment before the re-start of the operation in January.

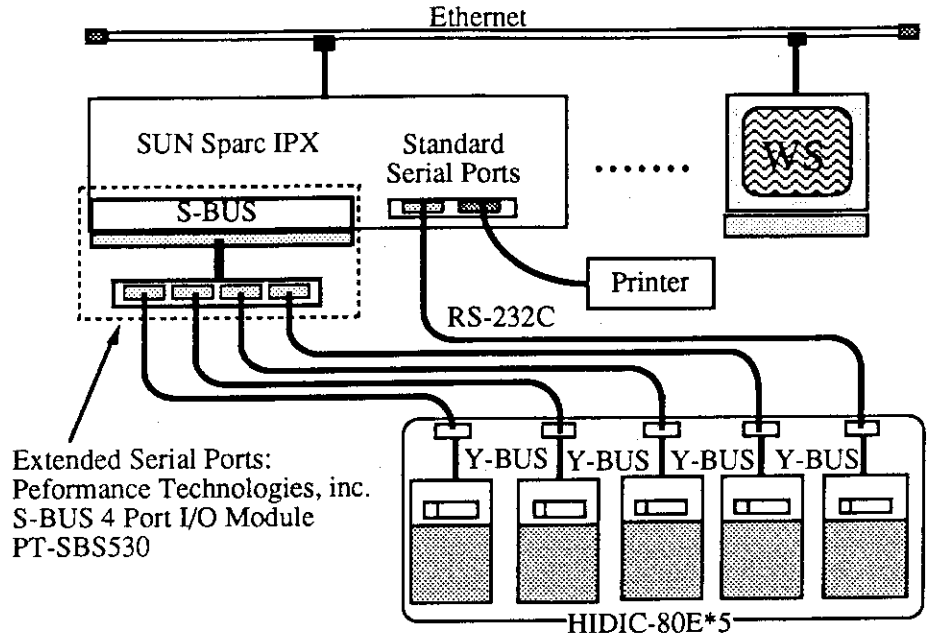

Fig.I.2.2-1 A minicomputer (HIDIC-80E) console emulator with an engineering workstation.

Reference

[2.2-1] T. Kimura, et al., IEEE Trans. on Nuclear Science 35 (1989) 1554.

2.3 Power supply

The JT-60 toroidal field power supply (TFPS), the poloidal field power supply (PFPS), and the motor-generator for the heating system (H-MG) have been operated smoothly and functioned very well in 9 operation-cycle and so on in the fiscal year . The operating hours and the number of sequence-stops of operation of TFPS, PFPS and H-MG were 1,230, 1,369 and 1,273 hours and 13, 95 and 1 times, respectively. Almost all the stops have arisen from the CAMAC control system and by plasma disruptions, and they scarcely stopped the JT-60U machine. Some faults, however, stopped the JT-60U machine, which were vacuum circuit breakers (VCB) of the TFPS and power supplies of the controllers of the PFPS.

The utility power distribution facility and the second cooling facility have also been operated smoothly. These facilities have been operated over ten years from their operation start, so not a few parts of the equipment have been growing worse and some parts have to be exchanged. In this fiscal year, rubber expansion joints used in second the cooling facility as shown in Fig.I.2.3-1 were replaced with new ones. These rubber joints were checked by eye-check, hardness, distortion and so on. As the results, cracks and distortion had been observed on a half of the rubber joints, and Shore hardness HS of the rubber turned into worse about HS=77-79, whose

limit is HS=80, of all rubber joints. From the checks eighty of one hundred joints have been exchanged. In the utility power distribution facility almost all the electrolytic capacitors of the smoothing circuits in uninterruptible CVCF AC power supply were exchanged.

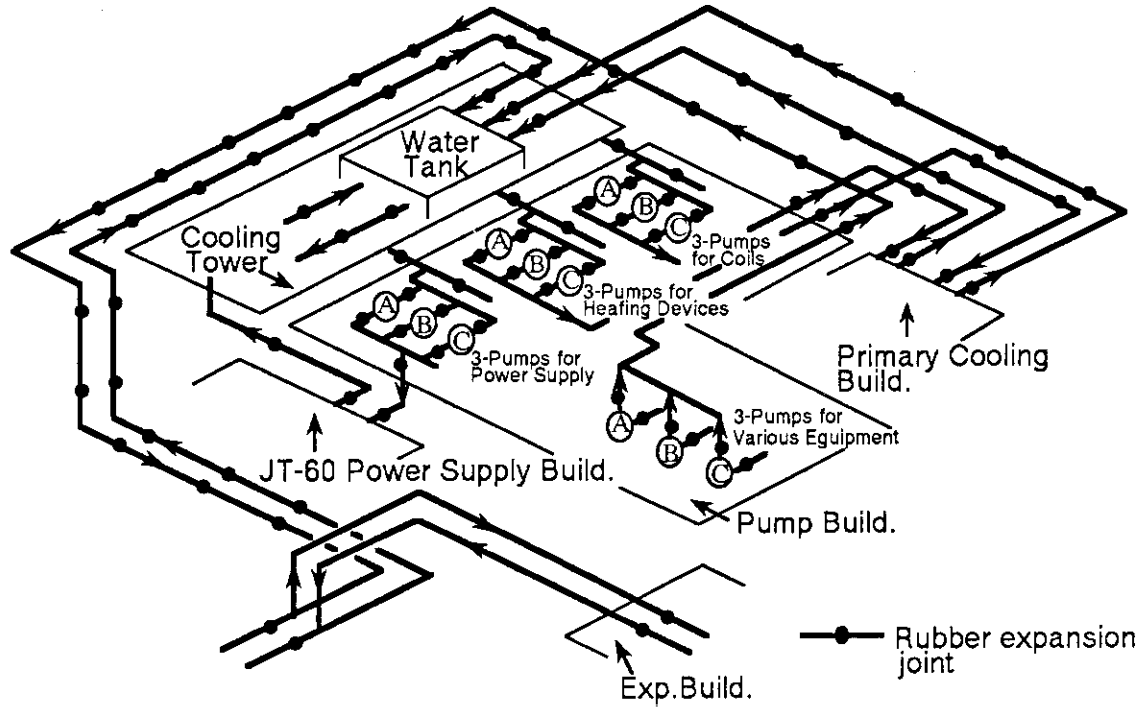

Fig.I.2.3-1 Pumps, pipes and rubber expansion joints of JT-60 second cooling facility

2.4 Neutral beam injection system

The operation of the JT-60 neutral beam injection system (JT-60 NBI) ,which is composed of four tangential and ten quasi-perpendicular beamline units, was carried out almost on schedule under the JT-60 experiment plan in this fiscal year.

A high power deuterium beam injection was required to get a high performance plasma. We have tried to increase beam injection power with a beam energy of more than 90 keV. The JT-60 NBI was designed to inject hydrogen beams with 75 keV of beam energy in the standard-rated operation. Since the ion source was also designed to operate this voltage region, we observed frequent flashovers on the outer-surface of the short ceramic insulators succeeding to the inner electrode breakdowns in the second-stage acceleration grids in the extraction of deuterium beam above 90 keV. Such a surface-flashover gradually contaminated the ceramic surface and hence deteriorated the voltage holding characteristics. We decided to add a set of sphere gap for bypassing the surge currents at the accelerator. After having adjust the sphere gap to be an optimization length of 22 mm, we extracted stably deuterium beam at an energy of 95 keV.

We have tried to increase extraction beam currents further from the ion source. A new operation field had to be examined to extract more than the rated beam current, where a heat load of electrodes increased because of increasing beam divergence angle. To reduce the beam

divergence angle with a large current beam acceleration at a given beam energy, the second accelerative voltage ratio of two stage accelerator was stepped down from 0.8 to 0.7. The beam current have increased by about 40 % under the allowed heat load of electrodes. We, so far, achieved up to an injection power of 36 MW at a beam energy of 95 keV .

^{3}He beams were injected into the JT-60 plasma with four quasi-perpendicular beamline units for D-^{3}He fusion experiment. The injection power with ^{3}He reached 5 MW per four beamline units at a beam energy of 78 keV. ^{3}He gas was pumped out using a cryo-sorption with an argon-condensed layer. The sorption pumping speed for ^{3}He gas is 550 m^3/s per one beamline unit.

2.5 Radio-frequency system

2.5.1 LHCD system

The LH system for JT-60U has three sub-systems to inject ~10MW at the frequency of 1.74 to 2.23GHz. Each sub-system has eight klystrons and can control the frequency, the power and the phase between adjacent klystrons during RF pulses. One of the sub-system has been operated at the power level of 2-3 MW by using the 24x4 multijunction launcher (CD-1'). Two of the sub-systems have been arranged to drive the simple launcher (CD-2) where operation started in 1993. The CD-2 launcher consists of 4 (toroidal) x 4 (poloidal) multijunction modules [2.5-1]. RF power in the module has been divided toroidally into 12 sub-waveguides at a junction point through an oversized waveguide. In this system, the output power of the klystron is directly feeded to the multijunction module as shown in Fig.I.2.5-1.

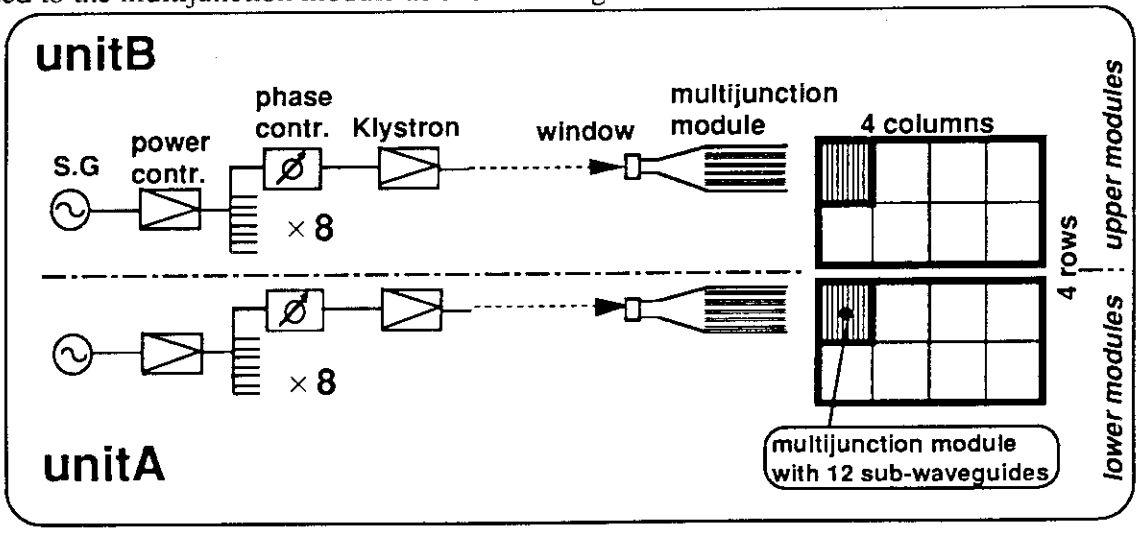

Fig. I.2.5-1 Block diagram of CD-2 Launcher

This method simplifies the LH system of the multijunction launcher with a large number of sub-waveguides. On the CD-2 launcher, the maximum power density up to 25MW/m^2 was achieved with a low reflection coefficient less than 2%. The coupling and current drive efficiency were well explained by the designed wave spectra without taking account of higher modes in the oversized waveguides. Thus, the simple multijunction launcher has been demonstrated to excite

expected wave spectra with high power handling capability. Up to now, the total injection power has been achieved up to ~7MW using the CD-1' and CD-2 launchers, and high current drive up to 3.6MA has succeeded.

2.5.2 ICRF heating system

The ion cyclotron range of frequencies (ICRF) heating system for JT-60U has been operated very well in this fiscal year 1993. The antennas showed very good coupling to the plasma, that is, the antenna loading resistance was more than 4 W at the gap of 0.13 m between the antenna and the plasma [2.5-2]. ICRF power of 5 MW was coupled in the first ICRF experimental campaign in April. From the experimental requirement, the output power of the amplifiers has been increased to 8 MW from 6 MW for 3 sec by upgrading final stage amplifier or replacing with a new tube since last fiscal year, as described in detailed in the following subsection. Then, the maximum coupled power of 6.4 MW was achieved in the last experimental campaign in October, which contributed the study of TAE mode induced by high power ICRF heating.

The increase of the output power of the final stage amplifier is not easy because the maximum plate voltage E_p is limited at 18 kV. Figure I.2.5-2 shows a schematic circuit of the final stage amplifier. Consequently in order to increase the output, we have increased the voltage of the control and screen grids (E_{g1}, E_{g2}) and performed tuning of the output cavity, that is, of its inductance and capacitance carefully. These works were much difficult for the tetrode Eimac 8973 because the power level was marginal beyond its maximum rating, but easier for a new tube 4CM2500KG which was developed as a replaced tetrode with the tetrode 8973 according to Japan-US fusion technology collaboration [2.5-3]. Adjustment of the neutralization circuit was not needed for a frequency range of 108-132 MHz at higher power because the neutralization was quite sufficient at an original power level. Major parameters of the final stage tetrodes are listed in Table I.2.5-1. It was shown that the efficiency increased as well as the output power through this improvement. Therefore, it was possible to increase total output to more than 10 MW by replacing the tetrodes with 4CM2500KG ones without the upgrade of the high voltage power supply.

References

[2.5-1] Seki M., et al., Proc. 10th Topical Conf. on Radio Freq. Power in Plasmas, Boston (1993).
[2.5-2] Saigusa M., Moriyama S., Fujii T., et al., "High coupling performance of JT-60U ICRF antennas", Nucl. Fusion **34** (1994) 276.
[2.5-3] Moriyama S., Ogawa Y., Fujii T., et al., "Test results of X2242 and X2274 high power tetrodes with the JT-60 ICRF amplifier in a frequency range of 110-130 MHz", Fusion Engn. and Design **19** (1992) 41.

Table I.2.5 - 1 Major parameters of final stage tetrodes

	8973 (Original)	8973 (Upgraded)	4CM2500KG (New tube)
E_p	18 kV	18 KV	18 kV
E_{g1}	250 V	490 V	490 V
E_{g2}	800 V	1200 V	1400 V
Efficiency	55 %	65 %	71 %
Output	0.75 MW	1.1 MW	1.4 MW

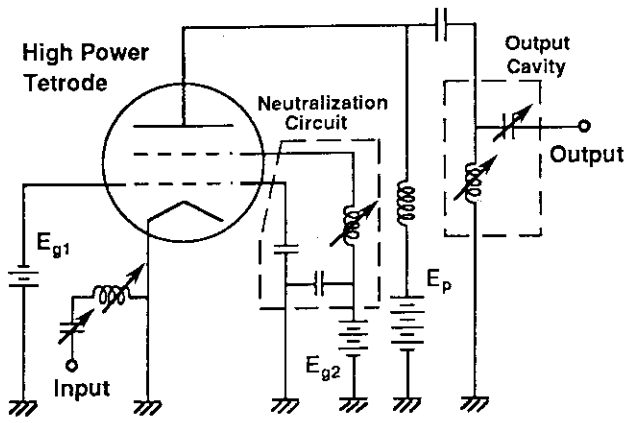

Fig. I.2.5-2 Schematic circuit of the final stage amplifier

2.6 Diagnostic system

During the period from April 1993 to March 1994, a YAG Thomson scattering subsystem, a laser blow off subsystem, a fast $H\alpha/D\alpha$ sampling array, a bolometer array for divertor, a scintillating fiber neutron detector, a reciprocation probe, triple probes for divertor, saddle loops for locked mode detection, a quadrupole mass analyzer subsystem for the divertor region, and Penning gauges were newly installed. Significant progress was also made in the diagnostic subsystems such as a Thomson scattering subsystem, a charge exchange recombination spectroscopy, an alpha particle charge exchange analyzer, a γ-ray PHA and a motional Stark polarimeter and so on. The JT-60U diagnostic subsystems and their status at the end of March 1994 are summarized in Table I.2.6-1. Here, the alpha particle charge exchange analyzer, the saddle loops , the Thomson scattering subsystem and the quadrupole mass analyzer subsystem are described in the following sections.

Table I.2.6-1 Present status of JT-60U diagnostic system

Diagnostic System	Subsystem	Specification	Status Mar.1994
Electron Density	FIR Interferometer	CO2 Pumped CH3OH Laser Vertical 2 chords	Operational
	CO2 Laser Interferometer	Tangential 1 chord	Operational
	Millimeter Wave Reflectometer	2 density points fluctuation	Operational
	Electromagnetic Wave Scattering	2 points, $0.5< k\theta\rho_i <4.5$, Δf~5MHz	Under construction
Electron Temperature	Thomson Scattering	60 points Δz=8~22mm, 2 Ruby Lasers, 2ms at burst mode YAG Laser 2J/10pps vertical	Operational Under construction
	ECE Michelson Interferometer	512 points,Δt~20ms,Δf~3.7GHz	Operational
	ECE Grating Polychromator	20 points,Δt~20μs,Δf~2GHz	Operational
	ECE Heterodyne Radiometer	12 points,Δt~20μs,Δf~0.5GHz	Operational

Ion Temperature	Charge Exchange Recombination Spectroscopy	20 points (tangential) 28 points (perpendicular)	Operational
	Fast Charge Exchange Recombination Spectroscopy	6 x 2 Points,Δt~1ms	Operational
	Active Beam Scattering	He Beam 200keV, 3.5A 1 point (center)	Out of Operation
	Charge Exchange Neutral Particle Energy Analyzer Arrays	2 chords (tangential) 1 chord (perpendicular) 1 chord (tangential)	Operational Under construction
Impurity	X-ray Crystal Spectrometer (Doppler &Wide Wavelength Range)	1 chord (vertical) Ti,Ni,Kr-Kα Rotating Crystal, 0.1~0.8 nm	Operational
	VUV Spectrometer	1 chord, 0.5~130 nm (Main) 1 chord, 30~156 nm (Div.)	Operational
	Light Impurity Spectrometer (Doppler)	1 chord, 100-200 nm (Div.)	Operational
	Grazing Incidence Monochromator	1 chord, 10-130 nm Absolutely Calibrated	Operational
	Visible Monochromator	1 chord, 200-700 nm Absolutely Calibrated	Operational
	Visible Spectrometer (Periphery)	Mirror Scan, 200-700 nm	Operational
	Visible Spectrometer (Divertor)	Spectrometer (2 chords) Fiber Optics & Filters (38 chords) Spectrometer (Doppler;10 chords)	Operational Under construction
	Visible Bremsstrahlung (Zeff)	10 chords, 523.2 nm Fiber Optics & Filters	Operational
	Laser Blow-off Impurity Monitor	YAG laser 70J, 10ms (Main,Div.) Selectable target Al,Ni,Fe,Ti,W,Mo,SUS	Under construction
Current Profile	Motional Stark Polarimeter	5 point tangential view	Operational
Radiation Flux	Hα / Dα Arrays	Poloidal 15(30) chords Toroidal 3(6) chords, Δt~1ms	Operational
	Hα / Dα Array (Fast Sampling)	Poloidal 8(16) chords (10~500 kHz)	Operational
	Pellet Ablation Monitor	Poloidal 8 chords Midplane 1 chord	Operational
	Soft X-ray Array	Poloidal 64 chords	Operational
	Bolometer Arrays	Poloidal 32 chords Divertor 14 chords Toroidal 2 chords	Operational
	Hard X-ray PHA	Poloidal 7 chords Co 1 chord, (Counter 1 chord)	Operational (plan)
	γ - ray PHA	1 chord (vertical)	Operational
	X-ray Image TV	Tangential 1 chord (5-500keV)	Operational
Neutron	Fission Chamber	3 points, Δt~10ms	Operational
	Neutron Spectrometer(NE213)	1 chord, ΔE~10%	Operational
	Neutron Spectrometer (^{3}He Ionization Chamber)	1 chord, ΔE~ 2%	Operational
	Neutron Activation	1 point	Operational

Neutron (continued)	14MeV Neutron Detector (SBD)	1 point	Operational
	Scintillating Fiber Detector	2 points	Operational
α particle	Neutral Particle Analyzer	1 chord(perpendicular), 0.5~4MeV, ΔE~10%	Operational
Peripheral Plasma & Wall Surface	Infrared TV	Divertor 1 camera,100-1200°C	Operational
	Visible TV	Tangential 4 chords	Operational
	High Speed TV	Tangential 1 chord, 1 frame/ms	Operational
	Electromagnetic Probes (Mirnov Coils)	40 points (Poloidal & Toroidal arrays)	Operational
	Electromagnetic Probes (Rogowski for Halo Current)	4 points	Operational
	Electromagnetic Probes (Saddle loops)	8 loops (Toroidal arry)	Operational
	Electro Static Probes	Divertor 2 x 16 probes	Operational
	Reciprocation Probe	Triple probe array (SOL)	Under construction
	Triple Probe	2 points (Divertor)	Under construction
	Quadrupole Mass Analyzer	3 ports (Inner/Outer divertor ports)	Operational
	Penning Gauge	3 ports (Horizontal ports)	Operational

2.6.1 Alpha particle charge exchange analyzer

The alpha particle charge exchange analyzer introduced from the A.F.Ioffe Physical-Technical Institute (Russian Federation) was installed, under the collaboration between the Ioffe Institute and JAERI, in JT-60U. In order to increase the charge-exchange flux and to obtain spatially resolved energy distribution of ions, the analyzer was installed in the line-of-sight of two heating-beam injection zones. The line-of-sight of the analyzer on JT-60U is shown in Fig. I.2.6-1. The major radius of the line-of-sight is 3.56 m and the angles between the line-of-sight and beam line are 55° and 125°. About 10% of the beam (1.4 A for $^3He^0$ beam of 80 keV and 2 A for D^0 beam of 90 keV) passes the observation field in the absence of the plasma. The analyzer makes a special feature of the data processing system. A 16-channel pulse height analysis (PHA) system has been adopted in this analyzer to distinguish pulses from energetic ions from noise arising from

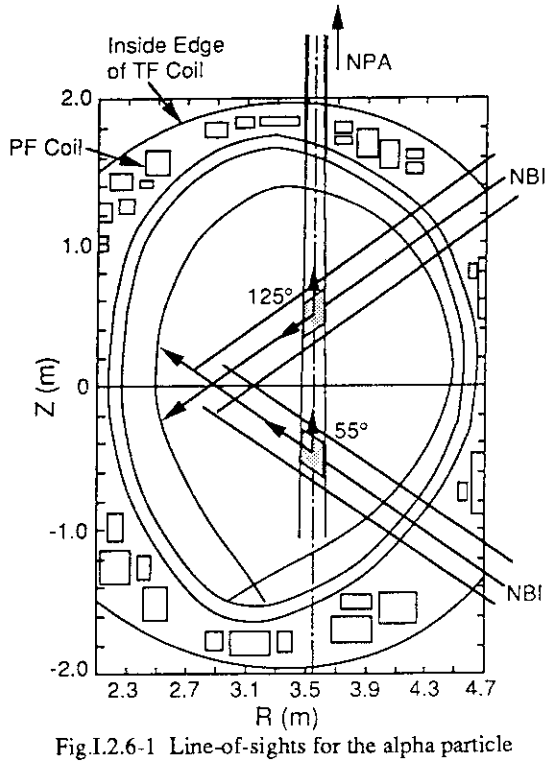

Fig.I.2.6-1 Line-of-sights for the alpha particle charge exchange analyzer on JT-60U

neutrons, γ-rays and optical lights. The validity of the PHA system were confirmed in the radiation environment of deuterium-beam-heated plasmas of JT-60U [2.6-1].

2.6.2 Saddle loops for locked mode detection

The objectives of saddle loops are to obtain absolute amplitude (B_R component) of locked modes and low frequency modes in which always observed befor disruptions. Eight saddle loops were installed inside the vacuum vessel at every 45° separated toroidal angle (Fig.I.2.6-2). The poloidal location is at the outside midplane enclosing the horizontal ports. A pair of saddle loops consists of two 180° toroidally separated loops. Using the four sets of the pairs, Fourier component of four toroidal mode number of n=0,1,2,3 are easily separated by adding and subtracting the B_R signals. The typical integrated signal amplitude is 10^{-2} ~ 10^{-3} Volt•second. The signal to noise ratio of the fluctuation of B_R ~ 1 gauss is expected to be over 3.

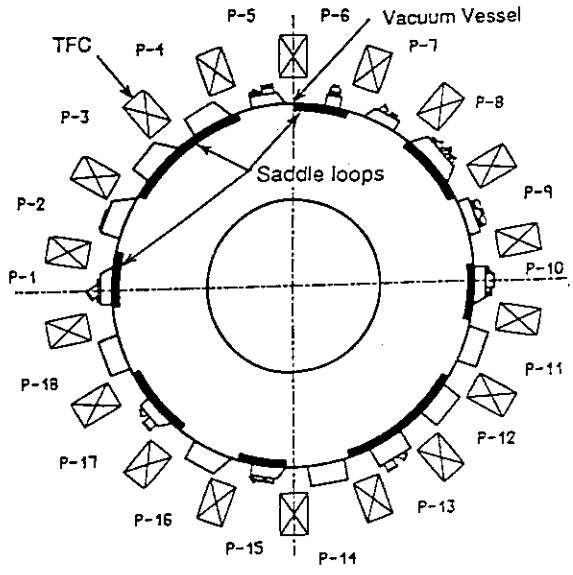

Fig.I.2.6-2 Top view of toroidal arrangement of saddle loops.

2.6.3 Thomson scattering subsystem

The third Littrow type spectrometer (f=275 mm, F/2.9) was introduced in the ruby Thomson scattering to measure low n_e (higher than 0.5×10^{18} m^{-3}) and high T_e (less than 20 keV) precisely in the core plasma region. The output image of this spectrometer was connected to a glass fiber bundle, which was divided into 10 spatial ch and 6 by spectral ch (420~680 nm). As a result, the spatially measurable points in ruby Thomson scattering subsystem added up to 60: 40 points through photomultiplier tubes and 20 points through a photodiode array. The arrangement of YAG Thomson scattering was initiated from 1993. The improved YAG laser has capability of 2 J output energy with repetition frequency of 10 Hz. The input optics and the collection optics were shared among the ruby lasers and the YAG laser. The beam line of YAG laser was identical with that of ruby lasers. The 20 spatial points has been planned to be measured. The production of corresponding 20 polychromator and 120 avalanche photodiodes (APD) is almost completed. The adjustment of data processing system is also finished. Each polychromator has 6 interference filters and lens system. The silicon APD had quantum efficiency of 30 % and internal gain of 100, and was controlled by a RISC I/O processor.

2.6.4 Quadrupole mass analyzer subsystem

A measurement subsystem for partial pressure of gaseous impurities and deuterium gas was installed to JT-60U during the shut down period from November to December in 1993. Figure I.2.6-3 shows a diagram of this subsystem. The subsystem is composed of three quadrupole mass analyzers (QMA (BALZERS QMA125, ULVAC QMS400)), three optical Penning gauges (OPeG) and four ionization gauges (IG). The OPeG, which is the same type as the Penning gauge developed in TEXTOR [2.6-2], is used for measuring the pressure of deuterium and helium gases. The maximum measurable partial pressure of the QMA is 3×10^{-3} Pa for CO gas. The design value of the maximum measurable partial pressure of the OPeG is 4×10^{-1} Pa. With a combination of QMA's and OPeG's, it is possible to measure a wide range of partial pressures, from 0.1 Pa of deuterium gas to 10^{-5} Pa of impurity gases, at the same time. These detectors are connected to the vertical diagnostic ports (P9U1, P9U2, P4U2, ϕ0.138 m, L=3.7 m) at the inner and outer divertor regions, and to the horizontal diagnostic port (P5, ϕ0.1 m, L=3.5 m) at the mid-plane. The distances between the separatrix strike zones and the vertical diagnostic ports are about 0.3 m for the inner side and about 0.4 m for the outer side. The delay time of the measurement system for the deuterium gas is about 0.2 s for the vertical diagnostic ports and 0.3 s for the horizontal port.

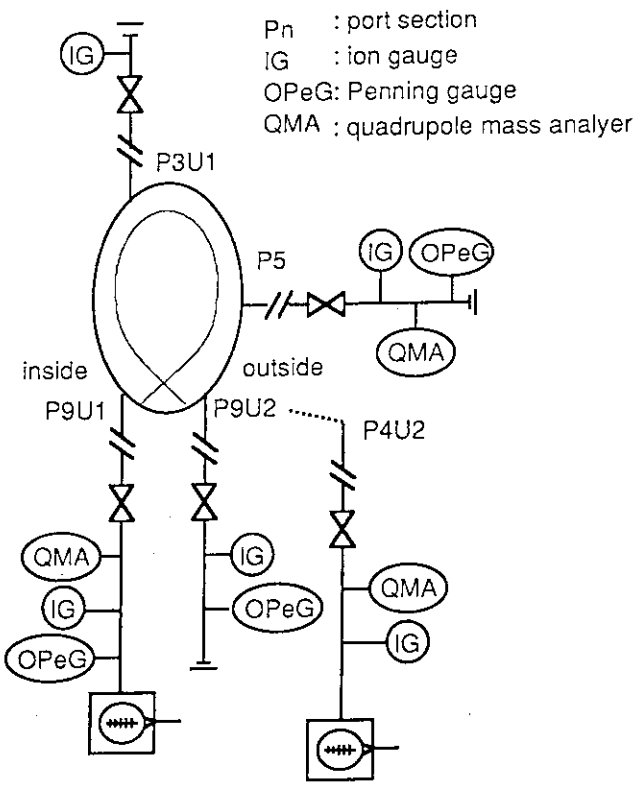

Fig.I.2.6-3 Diagram of quadrupole mass analyzer subsystem.

References

[2.6-1] Y. Kusama, et al., 'Charge-Exchange Neutral Particle Measurement in MeV Energy Range on JT-60U' (presented at the 10th Topical Conference on High-Temperature Plasma Diagnostics, Rochester, NY, USA, May 8-12,1994).

[2.6-2] K. H. Finken et al., Rev. Sci. Instrum. **63** (1992) 1.

3. Experimental Results and Analysis

3.1 Disruption and plasma control

Six types of the disruptive termination have been observed in JT-60U, which are caused by the density limit, the error field, the β_p-collapse, the high l_i during the plasma current ramp-down with low density, the low l_i during the plasma current ramp-up, and the vertical positional instability (Vertical Displacement Event, VDE). All of these disruptions have been investigated

thoroughly, and operational scenarios to avoid them have been developed successfully[3.1-1]. These developed scenarios are general, and can be applied to tokamak fusion reactors like ITER.

3.1.1 Density limit disruption

MARFE and the radiative contraction are good precursors for the density limit disruption[3.1-1]. At the subsequent phase of precursor MHD instabilities, heat pulses on to the divertor plate are observed. Then the energy quench occurs with an asymmetric erosion of the soft X-ray emission profile in JT-60U[3.1-2]. At the end of the energy quench, spikes are observed in all channels of soft X-ray emission and ECE, and then the current quench starts[3.1-1,2,3].

The fast time evolution of the heat power on to the divertor plate, the carbon impurity emission (C III) in the main plasma, and the central electron temperature has been measured in JT-60U at energy quench[3.1-1]. The heat flux on to the divertor plate has been observed after the start of the asymmetric erosion of the electron temperature profile. Then the carbon-emission jumps up with the simultaneous spikes in all channels of the ECE and soft X-ray emission.

3.1.2 Methods to avoid or soften the current quench

The rate of the plasma current quench increases with the rise in the radiation loss at the energy quench for the density-limit disruption of OH divertor plasmas in JT-60U[3.1-2]. The direct measurement of the electron temperature in the central region just after the energy quench by ECE heterodyne, shows that the current quench does not occur for higher electron temperature of $> \sim 200$ eV[3.1-3]. Thus the following three methods have been proposed for avoiding or softening the current quench, and have been demonstrated in JT-60U[3.1-2].

1) Minimization of the impurity generation at the energy quench.
2) Minimization of impurity influxes to the main plasma just after the energy quench.
3) Minimization of the electron temperature drop just after the energy quench.

3.1.3 Scaling of the plasma stored energy for avoiding the current quench

According to 3.1.2, reduction of the plasma-surface interaction at the energy quench is essential to realize the concept of the disruption-free tokamak. A scaling of the stored energy for getting the non-disruptive termination has been proposed[3.1-3] as,

$$W_{store} < \alpha \cdot C^{-1} \Delta T_{crit} t^{0.5} \cdot n_e^{0.45} q_{eff}^{0.67} R^{2.65} \qquad [3.1\text{-}1]$$

Here C is a constant, dependent on the material, t is the time duration of the energy quench, ΔT_{crit} is the necessary increase in the tile temperature to generate the required carbon impurities by sublimation and/or evaporation, R is the location of the separatrix line on the divertor plate, and α is the constant. This equation suggests that higher plasma density and higher q_{eff} are better to reduce the generation of the impurity, and that the dependence on R is very high. The stored energies of non-disruptive discharges in JFT-2M (R ~1 m) and JT-60U (R ~3 m) with carbon tiles

and t=~1 ms are compared using eq.[3.1-1] as shown in Fig.I.3.1-1, and the obtained threshold stored energy has been scaled as,

$$W_{store}\,[J] < 3 \times 10^{3} \cdot (n_e\,[\times 10^{19} m^{-3}])^{0.45}\, q_{eff}^{0.67} (R[m])^{2.65} \qquad [3.1\text{-}2]$$

That for ITER (R ~ 7.75 m) with the same carbon tiles and t=~1 ms can be predicted as ~5 MJ (Fig.I.3.1-1), which is only about ~1% of a stored energy. Thus, in order to get the non-disruptive condition for ITER, the threshold stored energy should be raised much largely, or the plasma stored energy should be reduced to be low enough just before the energy quench within a short time. According to eq.[3.1-1], W_{store} increases with $t^{0.5}$. In JT-60U, energy of 5~6MJ has been released for t=20~30 ms without causing the subsequent current quench. Thus the long time-duration of the energy quench is one method to avoid the current quench.

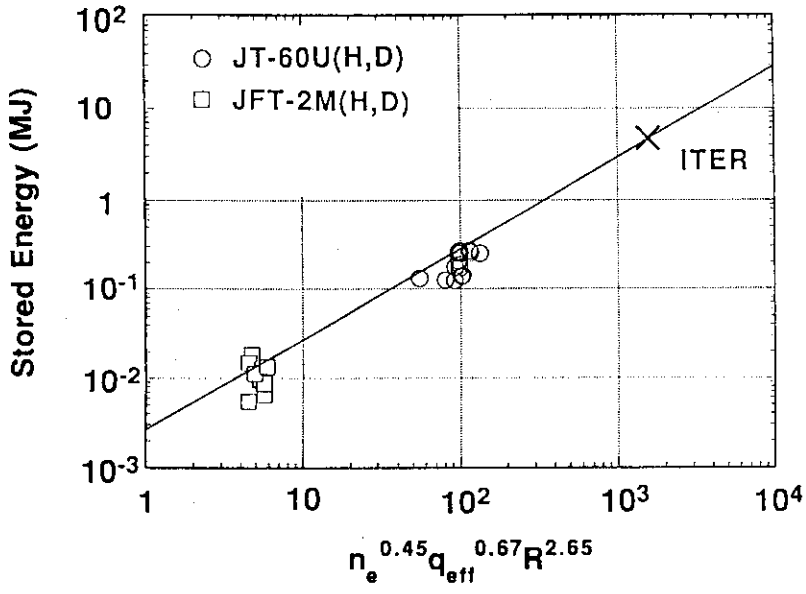

Fig.I.3.1-1 The plasma stored energy just before the energy quench versus $n_e^{0.45}\, q_{eff}^{0.67} R^{2.65}$ for non-disruptive discharges in JT-60U and JFT-2M [3.1-3]. Units of parameters are n_e[10^{19} m^{-3}] and R [m].

3.1.4 Error field instability

Low Density Lock Mode (LDLM) for OH plasmas is one of the error field instability, which has been observed in DIII-D, COMPASS, and JET, has appeared in JT-60U at the plasma current flattop for $q_{eff} \leq 3.7$, $n_e \leq 0.9 \times 10^{19}$ m^{-3}, and the plasma elongation κ of >1.48 with higher excitation of the divertor coil[3.1-1].

The error field instability has been also observed in Neutral Beam (NB) heated plasmas for the same κ and the same excitation rate of the divertor coil current as in OH plasmas. However the occurance region of q_{eff} is much larger of 3~6 for NB heated plasmas, which suggests the destabilizing effect of NB. The internal inductance of the target plasma, the power and the composition of NB heating, the plasma density during NB heating decide the stability of the plasma[3.1-1].

3.1.5 Vertical positional instability

Vertical Displacement Event (VDE) occurs for elongated plasmas. In JT-60U, VDE is very few in the normal operation, because its growth rate is as small as ~50 s^{-1} owing to relatively low

plasma elongation of 1.3~1.75 (defined at the outermost flux surface), high stabilizing force of vacuum vessel, and long resistive current penetration time of 8 ms in the vacuum vessel for a dipole magnetic field. Thus VDE is observed only in plasmas with high l_i or high n_{index}, because the destabilizing force increases with l_i and n_{index} as,

$$\Delta F_Z = -\mu_0 \Lambda \; n_{index} I_p^2 \Delta Z / (2R_J) \qquad [3.1\text{-}3]$$

Here Λ is $\beta_p + l_i/2$. Thus VDEs has been observed in the plasma initiation with the first wall of high retention of hydrogenic gas, in the plasma current ramp-down with the low plasma density, and during the plasma current quench[3.1-1]. The reduction of the shrinkage of the plasma current channel (or the increase in l_i) is essential to avoid VDE. Especially the slowing down of the current quench obtained by methods 1)~3) in 3.1.2 is powerful to avoid VDE during the current quench. Halo current observed during the plasma current quench with high toroidal asymmetry of 2.5 [3.1-4] can be reduced largely at the same time.

3.1.6 Plasma-current quench after the β_p-collapse

The β_p-collapse caused by some ideal MHD modes owing to high pressure gradient[3.1-5] terminates a discharge, only when a plasma touches the inboard first wall with high plasma stored energy of >3 MJ. This plasma current quench caused by the βp-collapse (up to the drop of 5 MJ within 20 ms) has been be avoided by mitigating the plasma surface interaction with keeping the divertor plasma configuration during the β_p-collapse[3.1-1]. Thus a larger clearance between the inboard first wall and the outermost flux surface is necessary to avoid the disruptive termination.

References

[3.1-1] R.Yoshino, et al., "Operational Scenarios to Avoid Disruptions in JT-60U", J. of Plasma and Fusion Research, in press (in English) (1994).
[3.1-2] R.Yoshino, et al., Nuclear Fusion 33 (1993) 1599.
[3.1-3] R.Yoshino, "Avoidance and Softening of Disruptions by Control of Plasma Surface Interaction" , Proc. of 11th PSI Conf., Mito (1994) 25, J. of Nucl. Materials, in press (1994).
[3.1-4] Y.Neyatani, et al., submitted to Fusion Technology.
[3.1-5] Y.Neyatani, et al., Proc. 20th European Conf. on Cont. Fusion and Plasma Physics, Lisboa, I (1993) 215.

3.2 High-β_p mode and High-β_p H-mode study

In March 1993, high-β_p mode with a superposition of the H-mode, namely high-β_p H-mode, has been achieved in JT-60U, and as a result, the record fusion triple product of $n_D(0)T_i(0)\tau_E = 1.1\times10^{21}$ m^{-3}keVs, has been achieved[3.2-1]. The high-β_p mode and the high-β_p H-mode have been investigated intensively in FY 1993 to understand the way for further improvement and to make optimized scenario in future experimental campaign with 500 keV neutral beam injection.

3.2.1 Dependence of plasma performance on plasma current

It has been found that the high-β_p H-mode with high plasma current (I_p > 2 MA) is necessary to achieve further increase in the plasma performance, as shown in Fig.I.3.2-1, where the plasma performance is represented by product of volume averaged pressure (<P>) and tE instead of the fusion triple product: the product of the central pressure and τ_E. The highest performance was achieved in the High-β_p mode at I_p < 2 MA (q_{eff} > 5), and was limited by the β_p-collapse occurring in the plasma core. Since the achievable value of β_p limited by the β_p-collapse increases with the value of I_p, the performance is improved with Ip. At a plasma current of about 2 MA (q_{eff} ~ 5), the plasma performance was improved significantly with the high-β_p H-mode. Since the β_p-collapse has to be avoided with higher plasma current even in the high-β_p H-mode, the discharge at the plasma current of I_p>2MA has to be optimized to achieve higher performance.

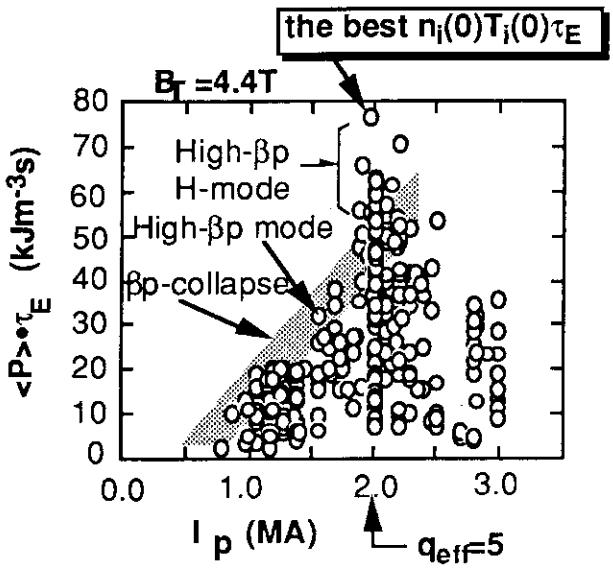

Fig.I.3.2-1. Plasma performance in the High-β_p mode and High-β_p H-mode experiments

3.2.2 Internal transport barrier in the high-β_p mode

It was found from the measurement of charge exchange recombination spectrum that the High-β_p mode is characterized by formation of internal transport barrier[3.2-2], inside which the gradient of the ion temperature profile and the gradient of the toroidal rotation velocity profile are significantly high compared with those in the L-mode phase; the energy confinement and the momentum confinement are improved in the core region. The position of the transport barrier depends on the value of q_{eff}, as shown in Fig.I.3.2-2, where possible regions of rational q surfaces evaluated by the equilibrium calculation is represented by shaded regions. From this figure, the transport barrier in the High-β_p mode seems to appear at the q=3 surface[3.2-2]. Further investigation is needed

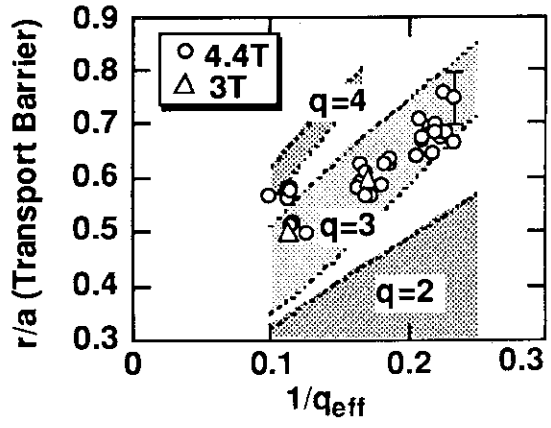

Fig.I.3.2-2 Position of internal transport barrier in High-β_p mode
Open circles correspond to the high-β_p mode in the filed of 4.4 T, and open triangles corresponds to B_T = 3T discharges.

to understand why the internal transport barrier appears at the q=3 surface.

3.2.3 Ion thermal diffusivity and electron thermal diffusivity

To estimate the plasma performance in the reactor correctly, it is necessary to discuss the ion transport and the electron transport distinctively in the improved confinement mode. For this purpose, the ion thermal diffusivity (χ_i) and the electron thermal diffusivity (χ_e) have been evaluated in the High-β_p mode and the High-β_p H-mode using profile data[3.2-3], as shown in Fig.I.3.2-3. The value of χ_i is significantly reduced in the core region ($r/a < 0.7 \sim 0.8$) of the High-β_p mode and the High-β_p H-mode. However, reduction of χ_e is not evident. Therefore, the improvement in the High-β_p mode is brought about chiefly by the reduction of the bulk ion thermal transport.

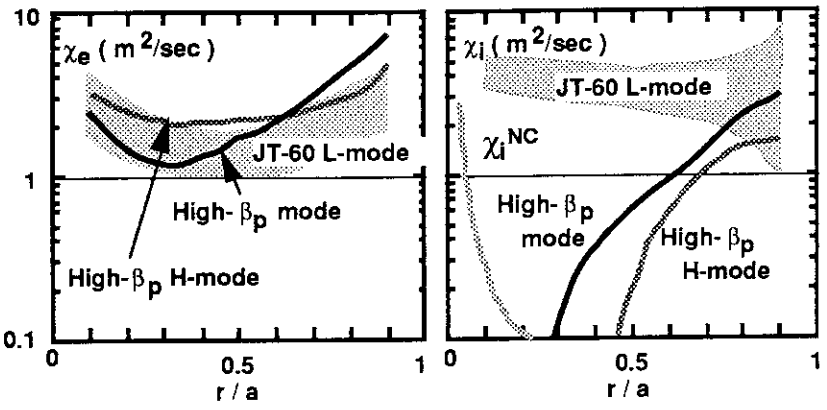

Fig.I.3.2-3 Transport analysis in High-β_p mode and High-β_p H-mode. The shaded region corresponds to many L-mode data with different configurations in JT-60 and JT-60U, and gives us a rough expectation of the diffusivities in the JT-60U L-mode. χ_i^{NC} represents neo-classical ion thermal diffusivity.

References

[3.2-1] Mori M., Ishida S., et al., 1993 *'Achievement of High Fusion Triple Product in JT-60U High-β_p H-Mode', to be published* in *Nucl. Fusion*

[3.2-2] Koide Y., Ishida S., et al., Phys. Rev. Lett. 72 (1994) 3662.

[3.2-3] Shirai H., Takizuka T., and Azumi M., in Proc. of ISPP-14 <<PIERO CALDIROLA>> Local Transport Studies in Fusion Plasmas, Varenna, 1993, p.33

3.3 H-mode study

To understand H-mode physics, we have investigated intensively edge localized modes (ELMs) and particle confinement property in the H-mode. Furthermore, a new approach to evaluate local diffusivity has been developed, and preliminary results show good correlation between the evaluated diffusivity and the confinement mode.

3.3.1 Edge localized mode

Improvement in confinement is limited by the appearance of ELMs in the JT-60U H-mode. Strong correlation between the estimated pressure gradient just before the ELMs and the ballooning parameter, $B_t^2/(Rq_{eff}^2)xl_i$, seems to indicate that ELM activity is caused by the ballooning mode[3.3-1], where B_t is toroidal field, R major radius, q_{eff} the effective safety factor, and l_i the internal inductance, respectively. This idea has been confirmed by stability analysis of the ballooning mode including the estimation of the plasma current profile evolution by using a

time-dependent 1.5 D-transport code; the result indicates that the ballooning mode is possibly unstable at the edge[3.3-2].

3.3.2 Evaluation of local diffusivity by density fluctuation analysis

To understand structure of transport phenomena in the H-mode, local diffusivity has to be evaluated quantitatively. We are trying a new approach to evaluate local diffusivity in a peripheral region by analyzing density fluctuations propagating in the radial direction. For the density fluctuation measurements at two different positions, phase-resolved reflectometers with two different frequencies were used. The reduction of the density fluctuations at positions of r/a = 0.97 and r/a=0.84 in the frequency range of 50 kHz - 100 kHz was clearly observed across the conventional H-transition, as shown in Fig.I.3.3-1(b). The time behavior of the evaluated local diffusivity, $D_{fluct.}=\lambda_c^2/\tau_c$, had a good correlation with the confinement modes qualitatively; the value of $D_{fluct.}$ in the H-mode was quite low compared with that in the L-mode (see Fig.I.3.3-1), where τ_c is the correlation time, and λ_c is the correlation length of the fluctuations. Since the density fluctuation measurements were possible at only two positions, we made a very rough estimation of λ_c using a cross correlation of the fluctuations at these two positions. More accurate estimation of λ_c with increased radial observation points will be available in the near future.

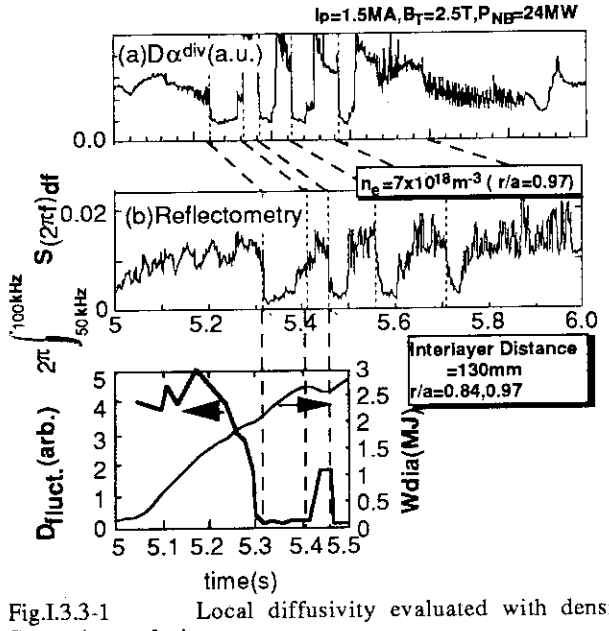

Fig.I.3.3-1 Local diffusivity evaluated with density fluctuation analysis

3.3.3 Particle confinement in H-mode

The particle confinement has also been studied intensively in the H-mode plasma and has been compared with that of the L-mode plasma. To evaluate a value of the particle confinement time (τ_p) in the main plasma, the charged particle source due to the ionization of deuterium atoms penetrating into the main plasma has been estimated based on the measured D_α emission intensity combined with a simulation using a Monte-Carlo neutral particle transport code (DEGAS). The electron density, the electron temperature and the ion temperature in the divertor plasma and the scrape-off-layer (SOL) were calculated using an interpretative simple divertor code[3.3-3], which solves 1-D fluid equations along a magnetic filed, where n_e-profile and T_e-profile at the divertor plate were obtained using 15 sets of Langmuir probes.

In Fig.I.3.3-2(a), the particle confinement time is plotted as a function of the line averaged electron density in H-mode plasmas (open symbols) with high power NB heating (P_{NB} > 10 MW). The value of τ_p increases with the density in the H-mode. The value of τ_p in the L-mode (closed triangle) also increases with $\bar{n}_e$. It should be noted that the values of τ_p in the H-mode are not so different from that in the L-mode.

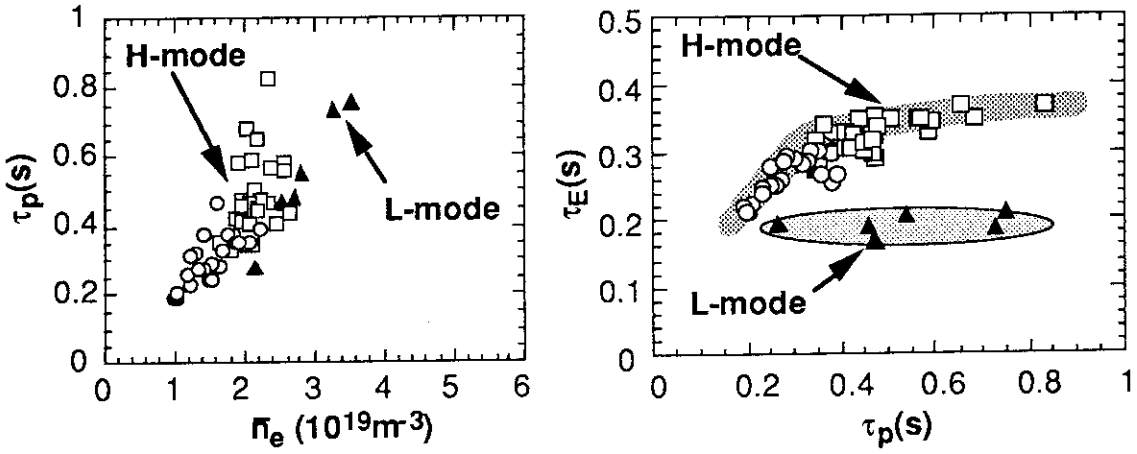

Fig.I.3.3-2 (a) τ_p as a function of $\bar{n}_e$ (b) τ_E vs. τ_p in H-mode and L-mode
Open circles correspond to the H-mode with plasma current of 2 MA, and open squares to the H-mode with current of 3 MA. The toroidal field was fixed at 4 T. Closed triangles correspond to the L-mode data in discharges of (I_p = 2 MA, B_T = 4 T), (I_p = 2 MA, B_T = 3 T), and (I_p = 3 MA, B_T = 4 T). In spite of high heating power (P_{NB} > 15 MW), the plasma was in the L-mode due to its high recycling operation.

The value of τ_E does not change with τ_p in the L-mode (see Fig.I.3.3-2(b)). In the H-mode, the value of τ_E is proportional to τ_p until a certain value of τ_p, and is saturated above this value. From a viewpoint of the density control in a fusion reactor, the value of τ_p^*/τ_E should be lower than 15, where τ_p^* is effective particle confinement time including particle recycling rate (R): $\tau_p^*=\tau_p/(1-R)$. To satisfy this condition, the ratio of τ_p/τ_E has to be low enough. The value of τ_p/τ_E in the H-mode is about 1-2, and would be in acceptable range for a reactor design.

References

[3.3-1] Kamada Y., et al., Plasma Phys. Control. Fusion **36**(1994) A123-A128.
[3.3-2] Mori M., the JT-60 Team, and the JFT-2M Team, Plasma Phys. Control. Fusion **36**(1994) A39-A49.
[3.3-3] Shimizu K., et al., J. Nucl. Mater. 196 & 198 (1992) 476.

3.4 Steady state high performance

It is necessary to achieve the following conditions simultaneously: i) high confinement improvement (high H-factor= $\tau_E^{EXP}/\tau_E^{ITER89P}$), ii) high power density (high normalized β: β_N), iii) high bootstrap fraction (high β_p) and iv) high efficiency of heat & particle exhaust. To achieve the condition iv), we adopted the ELMy H-mode as an operation mode in the steady state. For achievement of this highly-integrated performance in steady state, the optimization of current and pressure profiles to control ELMs and the low (m,n) pressure driven instability, and selection of safety factor, q_{eff}, have been clarified as the key issues in JT-60U.

3.4.1 ELM control

Since the H-factor for ELMy H-mode increases with decreasing ELM frequency f_{ELM} and asymptotically reaches the level of ELM free H-mode, control of f_{ELM} is necessary to sustain high confinement. We found that value of f_{ELM} is proportional to the heating power divided by the ballooning parameter, $B_t^2/(Rq_{eff}^2)xl_i$. Based on these results, the high H-factor at high β_p in the ELMy H-mode was achieved by controlling edge magnetic shear and heating power.

3.4.2 Suppression of low (m,n) pressure driven instability

The value of β_p in JT-60U was limited by the low (m,n) pressure driven mode located in the central region (β_p-collapse: ● in Fig.I.3.4-1). Recently, it has been demonstrated that the β_p-limit can be improved by 60% (Fig.I.3.4-1) by combination of a peaked current profile and a broad pressure profile, and as a result the values of β_N of 4 and $\varepsilon\beta_p$ of 1.1 have been obtained. The MHD mode observed at the β_p-limit has pressure driven type structure with n=1-2 and m=2-5. These results agree with the β-limit estimated by stability analysis of kink-ballooning mode with ERATO code(Fig.I.3.4-1 solid lines).

3.4.3 Effects of safety factor

We found that the β_p-limit increases with q_{eff}. Therefore, to achieve high bootstrap fraction, high q operation is essential (e.g. for β_p>2.5, q_{eff}>6-7). The H-factor also increases with q_{eff}, and to obtain H-factor of 2 in ELMy H-mode, q_{eff}>6-7 is required. This H-factor dependence on q_{eff}>6-7 is mainly caused by the facts that l_i decreases with decreasing q_{eff} and that the degradation by sawtooth activity becomes stronger with decreasing q_{eff} [3.4-1]. In addition, the profile of heat flux on to divertor plates becomes broader with increasing q_{eff} [3.4-2]. By summarizing these effects, high-q operation (q_{eff}>6-7) is essential for the steady state highly-integrated performance based on the JT-60U results.

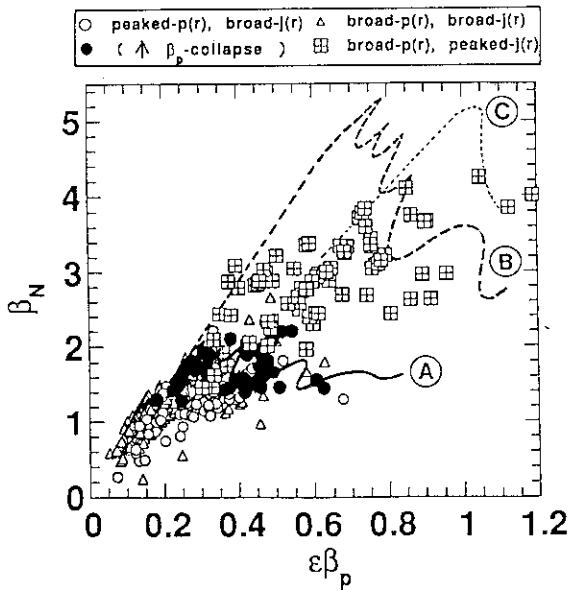

Fig. I.3.4-1 Operating region of JT-60U on the β_N-$\varepsilon\beta_p$ plane.
By the modification of current and pressure profiles, β-limit was improved. Solid lines describe the stability boundary of the ideal kink-ballooning mode calculated with ERATO code, where A: a peaked pressure profile ($dp/d\Psi \sim (1-\Psi)^2$) with $q_{surface}/q(0)=4$, B: a broad pressure profile ($dp/d\Psi \sim (1-\Psi)^{0.5}+0.7$) with $q_{surface}/q(0)=4$, and C: the broad pressure profile with $q_{surface}/q(0)=6$.

3.4.4 Progress of plasma performance in steady state

We carried out the experiments aiming at the steady highly-integrated performance with optimization of current profile, pressure profile, and the value of qeff in the two operational regions: low field (1.5T) operation for high β_N and high field (4.4T) operation for high fusion product.

(1) Fully current driven High β_N ELMy H-mode at low field

Highly-integrated performance with β_N~3, β_p~3 and H-factor~2 was sustained quasi-steadily (>>τ_E) under the full current drive condition (bootstrap current 60% and NB driven current 40%) at B_t=1.5T, I_p= 0.5MA, qeff = 8.5, $T_i(0)$ = 8 keV, $<T_e>$ = 1 keV (Fig.I.3.4-2). Co-tangential off-axis NB (4MW) was injected for current drive. The values and profiles of driven current were calculated with the ACCOME code, and it is found that this discharge has negative magnetic shear in the central region. When the counter-tangential NB was injected into the identical target plasma, the beam driven current compensated the bootstrap current and a monotonic q(r) profile was produced. In this case, the energy confinement time, τ_E, was 80% of that in Fig.I.3.4-2. This result suggests that the negative magnetic shear possibly improves energy confinement if the stability condition is satisfied.

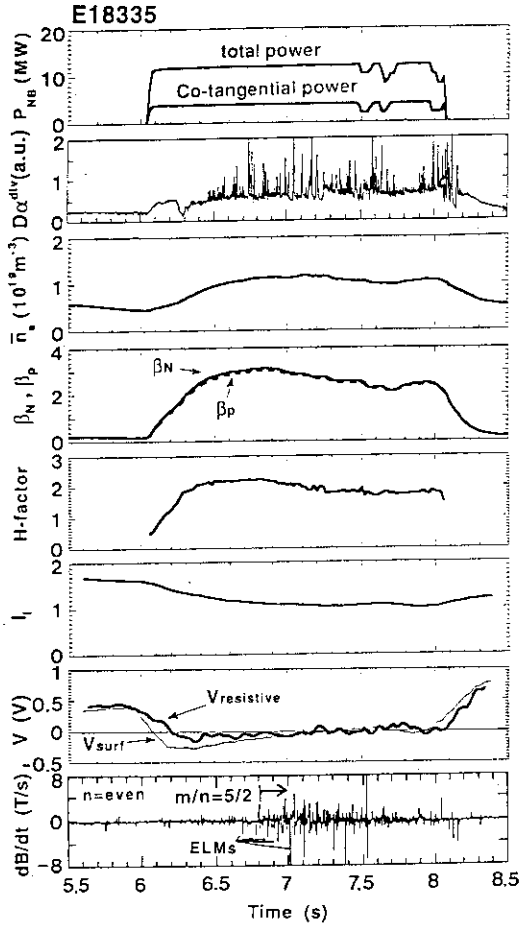

Fig. I.3.4-2 Highly integrated performance (β_N~3, β_p~3, and H-factor~2) was sustained in quasi-stationary under the full current drive condition at B_T=1.5 T and I_p=0.5 MA.

(2) Sustainment of high temperature ELMy H-mode at high field

High value of the fusion product, $n_i(0)\tau_E$ $T_i(0)$=5x$10^{20}m^{-3}$skeV, was sustained in the ELMy H-mode plasma for 0.7s with B_t=4.4T, I_p=2.2MA, qeff =4.2, P_{NB}=28MW, $T_i(0)$=39keV, H-factor=2.2, τ_E =0.3s, β_p=1.4 and bootstrap fraction of 45%. Since the threshold heating power for the L-H transition increases with B_t (>20MW at 4.4T), the enhanced plasma wall interaction tends to prevent the steadiness. Therefore ELM control at the high field was the critical factor to diffuse the heat flux onto the divertor plates.

References
[3.4-1] Kamada Y., et al., in Plasma Physics and Controlled Nuclear Fusion Research. Proc.14th Int. Conf., Wurzburg, 1992, (IAEA, Vienna, 1993), Vol.I., p.219
[3.4-2] Itami K., et al., J Nucl. Materials **196-198** (1992) 755

3.5 Impurity and divertor characteristics

Quantitative studies of radiative divertor, particle recycling, helium, impurity and heat transport have been performed on JT-60U divertor plasmas to explore the steady-state operation of tokamaks and to contribute to the ITER physics R&D.

3.5.1 Divertor radiation

The divertor radiation in the L mode was investigated with spatially resolved bolometer arrays [3.5-1]. The divertor radiation loss fraction increased with the electron density in the main plasma as shown in Fig. I.3.5-1. Its dependence on the safety factor was roughly proportional to $q_{eff}^{0.5}$ similarly to the divertor particle flux [3.5-2]. When the ion grad-B drift was towards the divertor, a radiative region developed between the strike points and the X-point accompanied by a gradual decrease in the heat flux to the target plates. A divertor radiation loss fraction up to 60% of the input power lasted for a few seconds without particle detachment from the divertor. This radiative state finally triggered a MARFE near the X-point (closed symbols). In contrast, the MARFE was never formed at the X-point when the ion grad-B drift was away from the divertor. Nonetheless there was no significant difference in the maximum radiation power level.

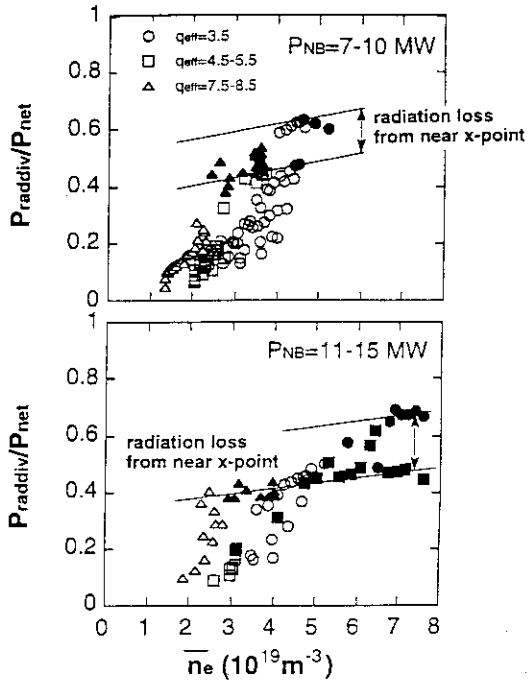

Fig. I.3.5-1 The divertor radiation power fraction as a function of the main electron density with the ion grad-B drift towards the X-point. Open and closed symbols stand for before and after the occurrence of the MARFE.

3.5.2 Particle and heat transports

A two-dimensional impurity code based on Monte Carlo techniques (IMPMC) was developed to study impurity transport in divertor/SOL plasmas [3.5-3]. The model includes 1) impurity generation at the target plates, 2) ionization of sputtered neutrals, 3) parallel motion of impurity ions along the field lines, 4) Coulomb scattering, 5) cross-field diffusion and 6) atomic processes. Fig. I.3.5-2(a) shows that the measured spatial profile of the C IV line at the divertor in a beam heated L-mode plasma agrees well with the calculated one with a cross-field diffusion

coefficient of around 1 m^2/s. The contribution of charge exchange recombination to the C^{3+} ion density was clarified as displayed in Fig. I.3.5-2(b).

The helium ion transport was investigated with He beam injection as known central fuelling [3.5-4]. Transport analysis reveals that the measured He^{2+} ion profile in ELMy H mode plasmas with an H-factor of 1.5 can be explained with D = 1~2 m^2/s and the inward pinch parameter C_V = 1~1.5 [3.5-5], which values are similar to the transport coefficients of the bulk ions, deuterons. No central accumulation of He ions was observed in the ELMy H mode. The helium ion density in the core plasma was reduced by the ELM activity with higher frequency.

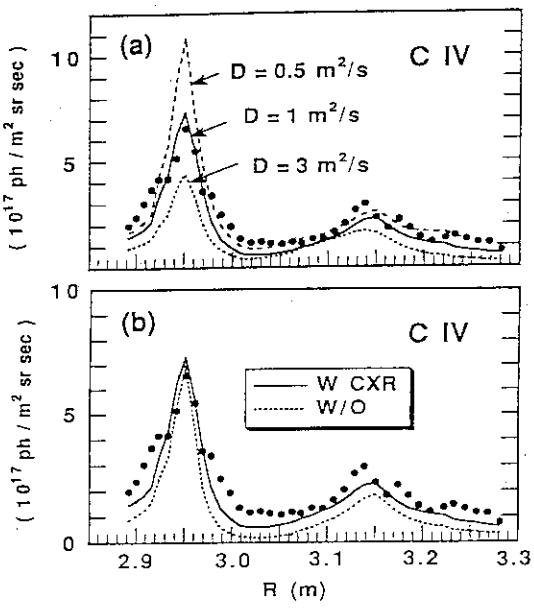

Fig. I.3.5-2 C IV line intensity profiles calculated with different diffusivities (a) and with and without charge exchange recombination (b). Experimental data are indicated by closed circles.

B_T reversal experiments were carried out to study the asymmetries of particle and heat profiles on the target plates [3.5-6]. The total particle influx in the L mode increased with the main density and the safety factor not depending on the B_T direction. However the in-out asymmetry of the particle recycling reversed with the B_T reversal; the enhanced recycling in the inboard side with the ion grad-B drift towards the X-point swapped to the outboard side. A measure of the asymmetry increased with $\overline{n_e} \times q_{eff}^{0.5}$ similarly to the total particle flux. The relatively symmetric heat load profile changed to outboard-dominated one with increasing $\overline{n_e}$ and q_{eff} when the ion grad-B drift was towards the X-point, while the inboard-dominated heat load changed to be symmetric with the B_T reversal.

Transient heat and particle fluxes in the ELMy H mode were studied by fast sampling of divertor diagnostics [3.5-7,8]. The heat flux density reached several hundreds MW/m^2 in 250 μs and decayed within one ms in ELMy phases under P_{NB} ~ 10 MW. However a multi-peak structure of the heat flux due to the ELM activity was confirmed to reduce the time-averaged peak heat load at the target plates. The pulsed heat and particle fluxes due to ELMs behaved differently. About 80% of the pulsed heat flux was deposited to the inboard side, while about 40% was deposited during ELM-free phases. The in-out asymmetry was little affected by the ion grad-B drift direction. In contrast, the ELM and ELM-free particle fluxes were similarly asymmetric. The in-out asymmetry in the ELM particle flux was exchanged with the B_T reversal.

3.5.3 Divertor modification

Divertor modification to a closed configuration was analyzed with the UEDA code [3.5-9]. Although baffle plates can reduce the neutral density around the main plasma, the particle recycling and heat load on the baffle plates can not be neglected. In JT-60U, the aperture between the inner and outer baffle plates was calculated to be optimum around 50 cm in the case of $D_\perp = \chi_\perp = 1$ m^2/s. Closing the private region is effective to reduce the return of neutral particles to the X-point. Cold divertor plasma with particle fluxes at an H-mode level was found to be possible only in a slot-like divertor shape with divertor gas puffing.

References

[3.5-1] Hosogane N. et al., 11th PSI conf. (1994), to be published in J. Nucl. Mater.
[3.5-2] Asakura N. et al., submitted to Nucl. Fusion.
[3.5-3] Shimizu K. et al., 11th PSI conf. (1994), to be published in J. Nucl. Mater.
[3.5-4] Sakasai A. et al., 20th EPS Conf. on Control. Fusion and Plasma Phys. Vol. 17C (1993) Part I. 67.
[3.5-5] Sakasai A. et al., 11th PSI conf. (1994), to be published in J. Nucl. Mater.
[3.5-6] Asakura N. et al., 11th PSI conf. (1994), to be published in J. Nucl. Mater.
[3.5-7] Itami K., Asakura N., Tsuji S., Shimada M., Plasma Phys. Control. Fusion. **36** (1994) A177.
[3.5-8] Itami K. et al., 11th PSI conf. (1994), to be published in J. Nucl. Mater.
[3.5-9] Tsuji S. et al., 11th PSI conf. (1994), to be published in J. Nucl. Mater.

3.6 Fast ion studies

3.6.1 Ripple loss study

The loss rate of total beam ions was evaluated from the neutron decay measurement, reflecting all loss processes of beam ions, after the short-pulse beam injection. The plasma parameters were $n_e=(0.2\text{-}1.2)\times10^{19}$ m^{-3}, $T_{eo}=1.2\text{-}4.6$ keV, $Z_{eff}=2\text{-}6$, $V_p=40\text{-}80$ m^3 and $I_p=0.4\text{-}1.3$ MA. In the case of $V_p=40$ m^3(toroidal field ripple $\delta \sim 0.1$ %), the time constant of the neutron decay was almost equal to the value evaluated from a classical slowing-down time of beam ions and no significant loss of beam ions was observed. However, the significant loss was observed for larger V_p. It was also observed that neutron decay time decreased with decrease in I_p. These correlations with V_p and I_p were consistent with those of the ripple well region. The decay of the neutron emission rate was compared with the calculation using the OFMC code and the neutron decay was reconstructed fairly well by the OFMC calculation. The calculated total ripple loss fraction, which was a summation of the ripple-trapped and the banana drift loss, was compared with the experimental one. It was shown that the OFMC code could explain the experimental results within ±20 %, irrespective of the evaluated fraction of the banana drift loss. These results demonstrated newly that the OFMC code could predict the banana drift loss in addition to the evaluation of the ripple-trapped loss [3.6-1,3.6-2].

3.6.2 TAE modes in the ICRF heating

In JT-60U, minority proton second harmonic ICRF heating is employed in He or deuterium discharges at toroidal field B_T of 3.8T on magnetic axis. Toroidicity-induced Alfvén eigenmodes

(TAE modes) [3.6-3] appeared in a number of ICRF heating shots for relatively wide range of experimental conditions: plasma current I_p=2~4MA (q_{eff}=5.1~2.8) and line-average electron density $\bar{n}_e$ =1.1~4.5×$10^{19}m^{-3}$ [3.6-4]. TAE modes were identified by checking mode frequencies measured by magnetic probes (Mirnov coils) installed inside the vacuum vessel. The measured frequencies are in the range of 200-300kHz and are well fitted by the electron density dependence of the theoretical TAE frequency. The threshold fast ion stored energy is around 0.3MJ or the threshold beta-value of tail ions, $<b_{tail}>$, is 0.05%.

One of features of TAE experiments on JT-60U is observation of dynamic plasma behaviour associated with TAE modes. Typical example is shown in Fig. I.3.6-1. Experimental conditions are following; I_p=3.5MA, q_{eff}=3.3, $\bar{n}_e$=2.2×$10^{19}m^{-3}$, He+H mixture plasma and ICRF power of 5.3MW. Temporal evolution of the diamagnetic stored energy and the central electron temperature is well correlated with Mirnov coil signals indicating TAE modes. Neutron yield and γ-ray counts which reflect MeV-range protons also show the decrease and increase according to the growth and suppression of TAE modes. Here, an origin of the neutron yield is considered to be a nuclear reaction $^{11}B(p,n)^{11}C$ with threshold proton energy of about 3MeV. Those for ~2.1MeV and ~4.4MeV γ-rays are inelastic scattering of high energy proton with boron or carbon with threshold proton energy of 2.5MeV and 5MeV, respectively. Neutron and γ-ray counts decrease by 60-70% by the TAE modes, although the reduction rate of the tail stored energy ($\delta W_{tail}/W_{tail}$) is only 20%. It is thus demonstrated that TAE modes affect population of fast protons of several MeV significantly. It is also discovered that TAE modes are suppressed for a period as long as 0.6sec after giant sawtooth crash. Such a long suppression of TAE modes is not simply due to loss of energetic ions [3.6-4].

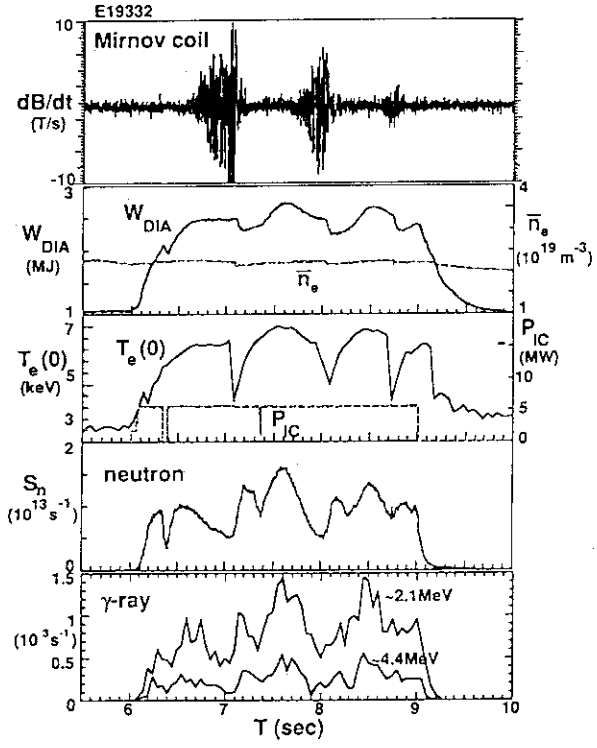

Fig. I.3.6-1 Typical time evolution of plasma parameters in ICRF heated low-q discharge where TAE modes appeared.

References

[3.6-1] K. Tobita, et al., to be published in Nuclear Fusion.
[3.6-2] K. Tani, K. Tobita, Y. Neyatani, et al., Proc. IAEA Technical Committee Meeting on Alpha Particles in Fusion Research, Trieste, 1993, IAEA, Vienna (1993) 67.
[3.6-3] C. Z. Cheng and M. S. Chance, Phys. Fluids 29, 3695 (1986).
[3.6-4] H. Kimura et al., submitted to Physical Review Letters.

3.7 LHRF experiments

A new multijunction launcher has been installed in JT-60U[3.7-1]. The newly developed multijunction launcher has a very simple structure with oversized waveguides. The launcher is fed by 16 klystrons. Each feeding waveguides from a klystron connects directly to its 12 subsidiary waveguides through an oversized taper, composing a single module. The launcher consists of 4 (toroidal) x 4 (poloidal) modules. A typical half width of the $N_{||}$ spectrum is $\Delta N_{||} \sim 0.2$. Even at a plasma-launcher distance of ~ 10cm, LH can couple to the plasma with a reflection coefficient of $R_{ref} < 2\%$. The total couple power of the LH system, including that from the previous 24x4 multijunction launcher, has reached a value of 7MW.

By using the new launcher, a maximum driven current of 3.6MA has been achieved at a relatively low density ($n_e \sim 10^{19}m^{-3}$)[3.7-2]. Figure I.3-7-1 shows the current drive product $n_eR_pI_{CD}$ against the injected LH power, where the previous JT-60 results are shown as the open circle. Solid lines in Fig.I.3.7-1 corresponds to the current drive efficiency. The current drive product is enlarged up to $1.75x10^{20}m^{-2}MA$. The driven current by LH power is plotted against the current drive efficiency in Fig.I.3.7-2. The current drive efficiency tends to increase with the

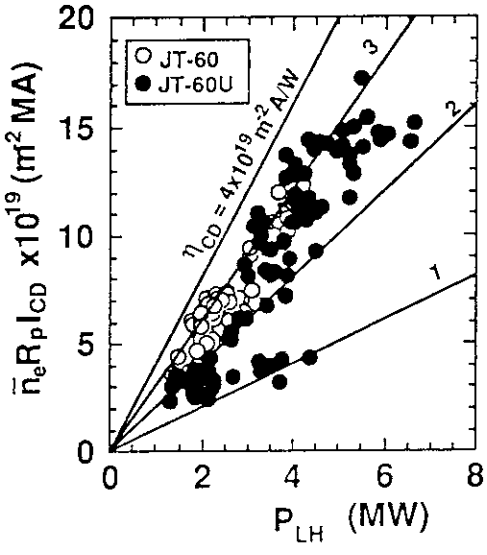

Fig. I.3.7-1 The current drive product against the injected LH power.

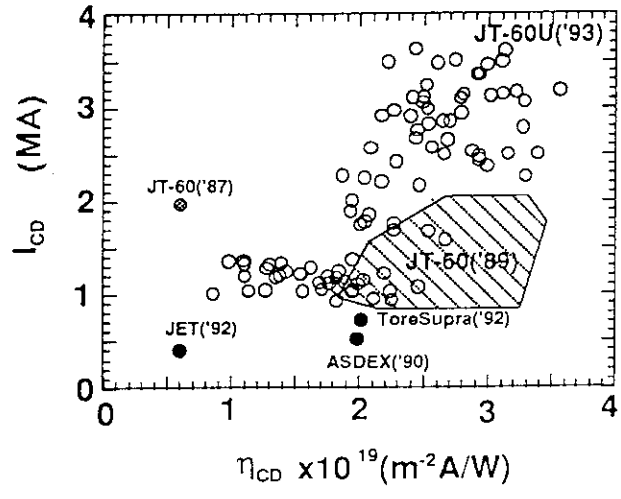

Fig. I.3.7-2 The LH driven current versus the current drive efficiency.

driven current and the current drive efficiency of $3.5x10^{19}m^{-2}A/W$ has been achieved at I_{CD}>3MA. The observed current drive efficiency was consistent with the JT-60's empirical scaling[3.7-3].

The following facts on the driven current profile were found in LHCD experiments. (1) Driven current profile tends to be broad at higher current regime with the same wave spectrum. (2) The driven current profile can be controlled by changing the launched peak $N_{||}$; the low, narrow and the pure $N_{||}$ spectrum produces the peaked current profile. (3) Higher component of $N_{||}$

spectrum and the wide spectrum enhance edge deposition of RF power, and produce a broad current profile. (4) The driven current profile depends on the poloidal launcher location consistently with the ray tracing analysis. (5) The current profile can be also controlled by current drive in the direction opposite to the original OH current. These results demonstrates the feasibility of the current profile control by LHCD.

References

[3.7-1] Y. Ikeda et al., Fusion Engineering and Design 24(1994)287.
[3.7-2] O. Naito et al., Plasma Phys. Control. Fusion 35(1993)B215.
[3.7-3] K. Ushigusa et al., Nuclear Fusion 29(1989)1052.

3.8 Development of fusion plasma analysis codes

The numerical codes required for the experimental data analysis and the theoretical prediction of plasma performance in JT-60U, JFT-2M and a tokamak reactor are systematically developed and updated. The efforts of code development and update in FY1993 have been concentrated on the more accurate evaluation and verification of the improved plasma performance, the detail analysis of physical mechanisms and the increased functions in utility softwares.

3.8.1 Experimental data time slice monitoring software : SLICE

The "SLICE" code maps various kinds of plasma experimental data such as n_e, T_e, T_i, measured at the different geometrical position of JT-60U and JFT-2M onto the equilibrium magnetic configuration calculated by the first boundary identification and MHD equilibrium calculation code FBI/SELENE. Experimental data are treated as a function of volume averaged minor radius r in SLICE. The experimental data measured as line integrated values such as interferometer data for n_e, bolometer data for radiation loss, bremsstrahlung and etc. are transformed by the Abel inversion technique. Plentiful commands of SLICE make it easy to process the mapped data and fitted data. For example, the profile of effective charge number is calculated by n_e, T_e and Abel inverted bremsstrahlung profiles in SLICE. The mapped data are fitted to a functional form and saved to the database MAPDB. SLICE can read the data from MAPDB, display them as the function of r and fit them in another functional form. SLICE also creates the run data of orbit following Monte-Carlo code OFMC and tokamak predictive and interpretation code system TOPICS, and initiates the detail analysis of experimental data.

3.8.2 Tokamak prediction and interpretation code system : TOPICS

The code system TOPICS for analyzing the tokamak plasma performance and plasma characteristics, based on the 1-1/2 transport model, has been updated according to the progress in JT-60U experiments. The major efforts were made for the improvement of interface routines with plasma profile database. By this modification, the SLICE output can be easily transferred to

TOPICS input data and it made easy the transient transport analysis of JT-60U plasma, in addition to the steady state analysis. Physics models also updated to meet the requirements for data analysis in the series of 1994 experiments on JT-60U. Several load modules are now running for both the snap-shot analysis and the time-evolutional analysis of transport properties based on experimental data and for studying the operation scenario in the self-ignition phase of the steady-state tokamak reactor.

3.8.3 Orbit-following Monte-Carlo code : OFMC

Detail comparison between the TF ripple losses of NB-injected fast ions observed by IRTV camera and the numerical calculation by using the OFMC code shows that the electric field plays very important roles in the heat load deposition profile on the first wall; that is, the location of heat deposition on the first wall is sensitive to the electric field. In order to analyze the loss process of ripple trapped particles, the electric field between the plasma surface and the first wall is included in the system code of OFMC. As the same time, the modification of OFMC code into the high level computer with parallel processors, which is scheduled to be introduced in the FY 1994, is also going on.

3.8.4 Divertor simulation code : SOLDOR

In order to simulate the SOL and divertor plasmas in a tokamak, a divertor simulation code with fluid model, SOLDOR, is under development. Fluid equations for two-dimensional SOL and divertor plasmas are discretized in space by using the finite volume method with the total variation diminishing scheme in convective terms. The equations are solved time-dependently by using a implicit scheme with the Newton-Raphson method. The numerical scheme was successfully tested in the slab geometry and the code is now under modification to the toroidal geometry.

3.8.5 Impurity transport Monte Carlo code : IMPMC

A two-dimensional impurity code based on Monte Carlo techniques (IMPMC) has been developed, in order to study the impurity behavior in the divertor and SOL plasmas of JT-60U. The code follows impurity ions in the toroidal geometry and includes the various physics processes, such as (1) impurity generation at the divertor plate, (2) ionization of sputtered neutrals, (3) parallel motion of impurity ions along field lines, (4) Coulomb scattering, (5) cross-field diffusion, and (6) atomic processes[3.8-1].

3.8.6 Fast analyzer for MHD equilibrium : FAME

FAME is the system that solves the time sequence of MHD equilibria by using the parallel processing technique on the small scale parallel computer with 20 processor elements of 250 MFLOPS and 64 MB. The Multi Instruction Stream and Multi Data Stream is employed as the

architecture type of parallel processing. After the first release of the system, the data flow has been modified from the original one such that both FBI and SELENE codes run in series on the parallel processor. By this modification, the calculation of 103 time-slices of MHD equilibria is completed within 9 minutes after the JT-60U database access. As the result, the time sequence of MHD equilibria can be refereed for the data analysis within 22 minutes after the each discharge.

3.8.7 Database retrieval system : DARTS

Database Retrieval System (DARTS) has been developed to support users of experimental database of JT-60U and JT-60U. In this fiscal year, in order to improve a handling of the database, followings are updated. DARTS database is automatically prepared from ZENKEI system, diagnostic system and FBI system in each interval of plasma discharge. An information of the research theme is added to the index database. The interface between SAS-system and DARTS are newly developed. DARTS can support the database, which are created by SAS, with help of the interface.

3.8.8 Data instruction system : DAISY

DAISY is the software program to monitor the experimental data on graphic terminals and the first version was released in 1989. The code has been successively updated to increase its functions to meet requirements from the JT-60U experimental data analysis. The main efforts in 1993 has been devoted to improve the manual commands. For example, the DEFINE command was improved to increase the number of user definitions for evaluating the correlation function. DAISY, which was originally developed on the large scale computer, was transplanted to the SUN workstation in order to enhance the efficiency of data analysis. By this transplantation, experimental data can be monitored not only on the graphic terminal but also on the workstation through the computer network.

Reference

[3.8-1] K.Shimizu, et. al., "Impurity Transport Modeling and Simulation Analysis of Impurity Behavior in JT-60U", to be published in J.Nucl.Mater.

4. Related Developments and Maintenance

4.1 Research on hydrogen content and hydrogen isotope exchange in decaborane-based boronization

In JT-60U a mixed gas of decaborane ($B_{10}H_{14}$) and helium has been used as a substance for boronization so that the deposited boron film contains hydrogen of about 10 atomic % in H/B ratio, which requires a few ten tokamak discharges to reduce hydrogen contents in the boron films after the boronization. This is disadvantage to perform a D-D discharge just after the boronization

because of the dilution of the deuterium plasma. In order to reduce the hydrogen content in the boron film or deuterate it, there are two ways. The first is to use deuterated decaborane and the second is to deuterate the boron film during boronization using the deuterium glow discharge. The latter will be applicable to JT-60U at the present but the former is not, since it is not possible to get the deuterated decaborane. In this fiscal year the laboratory experiments of decaborane-based boronization have, therefore, been performed to clarify the details of the hydrogen contents in the boron film such as the hydrogen contents as a function of wall temperatures[4.1-1] as well as the efficiency of deuterium to hydrogen isotope exchange using deuterium/helium-decaborane gas mixture[4.1-2]. The results are as follows: (1) the hydrogen content decreases with increasing wall temperature. (2) the deuteration ratio D/(D+H) achieves 80-95% when deuterium-decaborane gas mixture is used as a feeding gas for boronization. (3) the total concentration (D+H) for deuterium-decaborane mixture is at most 50% lager than that for helium-decaborane mixture. From these results the next boronization session in JT-60U is planned to use a mixed gas of deuterium and decaborane for boronization.

References

[4.1-1] M. Yamage et al., Jpn. J. Appl. Phys. 32 (1993) 3968
[4.1-2] M. Yamage et al., to be published in J. Nucl. Mater.

4.2 Development of a handler for a VME bus-based CAMAC driver related to rejuvenation of the control system

Since the JT-60 control system has been in operation for some ten years, troubles of the hardware have been gradually increased due to the worse of the CAMAC crates and modules, signal conditioners, etc. It has become difficult to supply repairing parts such as old-type ROM chips with small capacity housed in the CAMAC module. Then, the cost for the maintenance has increased consequently.

Since the first plasma of JT-60 in 1985, the control system has been extended to cope with the changing requirements of the tokamak. At present the upgrade of the control system is required corresponding to the development of a new plasma heating device of negative ion source based neutral beam injection (N-NBI) system and a long pulse operation of the poloidal field coil power supply (PFPS) for tests of super conducting magnets. However, no more room to install new programs for the above developments is left in the original computer system because of a smaller size of their memories than that of modern computers. Moreover, the software development in the computer system is not so efficient as that in modern computers.

In order to cope with the developments of the control systems for the PFPS and the N-NBI heating system, the following countermeasures will be taken in the central control layer ZENKEI. We will change only the communication routes between ZENKEI and the subsystem controllers, because a lot of application software exists in the original minicomputer system. Besides the LAN

for the presentation layer, another LAN of Ethernet connected to the discharge data file server will be provided for the data communication as shown by the dashed line in Fig.I.4.2-1 [4.2-1].

On the other hand, in the subsystem controller for the PFPS, obsolete 16-bit microcomputers of Intel-8086 distributed in about twenty CAMAC crates will be superseded by 32-bit microcomputers of MVME147 (Motorola Inc., USA) embedded in two VMEbus crates, where the CAMAC serial highway driver module SD-2140-Z1A (we shall call it VSD, Kinetic Systems Inc., USA) will be installed to form two loops of the subsystem highways. Hence, the I/O modules housed in the original CAMAC crates can be entirely used in the new system. The VMEbus-based front end computers will be also connected to an Ethernet LAN at the subsystem level with the modern workstations, which in turn will be bridged to the central control Ethernet LAN.

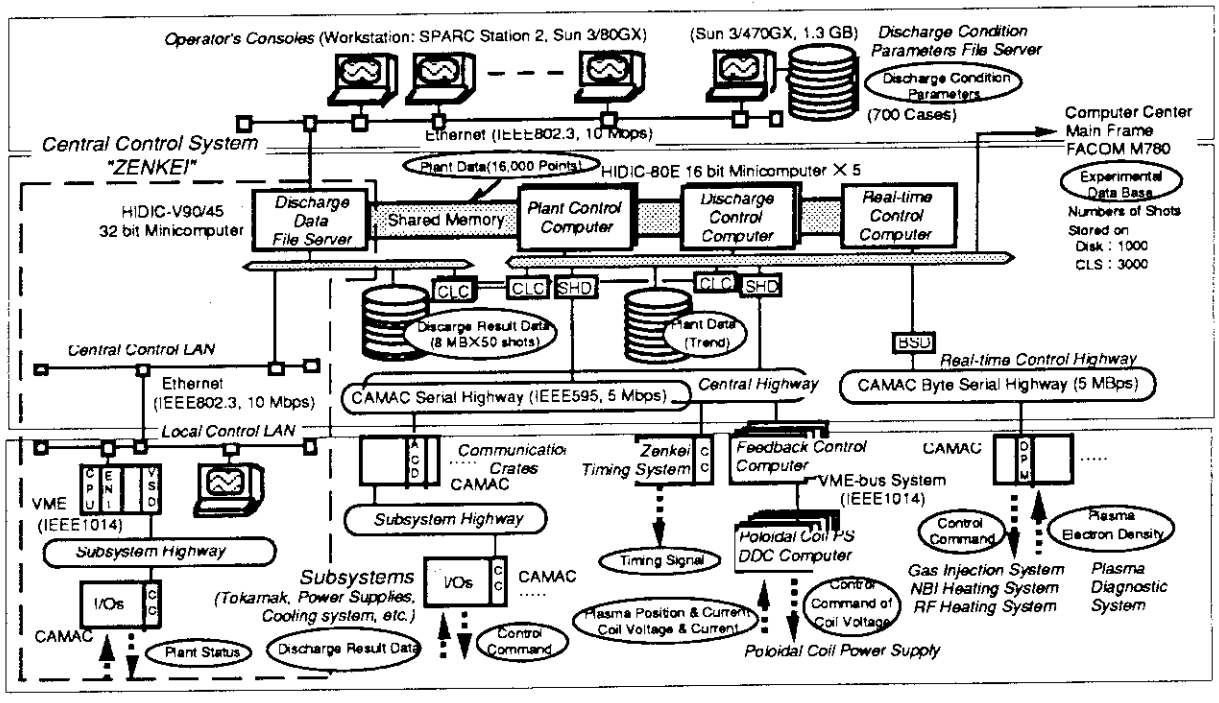

Fig.I.4.2-1 Computer configuration of the JT-60U control system.

For the migration to the new configuration, throughput of the data transfer in the new system has to be examined beforehand. For the data transfer in the local control system, a CAMAC handler has newly developed for the VSD [4.2-2]. This handler, which is a series of subroutine programs written in C language, runs on the MVME147 microcomputer under the real-time OS of Vx-Works. The capability of executing single command and block transfer and of handling of LAM demand has been measured with a test system. The measured values of the execution are shown in Table I.4.2-1. In addition to the above validation of the local communication, data throughput of the second LAN for the communication between the central control computer and the local control system and the CPU load of the SVP computer have been also tested under the

real operation of the JT-60U tokamak. These test results proved the communication systems to have sufficient data throughput and time response for extending the VME and network applications to the local control layer.

Table I.4.2-1. Test results of data transfer rate from CAMAC I/Os to a workstation via CAMAC highway.

Transfer Mode	Bit serial (5 MHz)
Single Command	250 μs/word + 20 μs
Block Transfer	46 μs/word
LAM demand	350 μs

References
[4.2-1] T. Kimura, , in Proceedings of International Conf. on Accelerators and Large Experimental Physics Control Systems, Berlin, 1993, to be published in NIM.
[4.2-2] T. Totsuka, JAERI-M 93-158 (1993) (in Japanese).

4.3 Rejuvenation of the CAMAC system in the PFPS

The control system of the poloidal field power supplies (PFPS) mainly consists of three CAMAC systems, that is the plant support CAMAC system which controls and monitors PFPS machines, the discharge control CAMAC system which performs pre-conditioning such as setting the MG and the timing system and making the circuits by changing circuit breakers and line switches for requirements of the discharge modes and the DDC CAMAC system which is engaged in real-time control of plasma. The DDC system has already been modified largely to a new system, where engineering-workstations and VMEbus based 32-bit microcomputers were adopted and the programs were written by C language [4.3-1].

As ten years has passed since the start of JT-60 operation, troubles of CAMAC crates and modules have been increased and it has become more difficult to get repairing parts such as old-type ROM chips and so on, so we need rejuvenation of the CAMAC control system. Taking the opportunity of modifying the control systems for delivering the power of PFPS to ITER CS superconducting coils, the modification of the other two CAMAC have started from this fiscal year. The system 16-bit microcomputer modules are replaced VMEbus based 32-bits micro-computers and workstations and the programs were written by C language. In this fiscal year, we have designed the basic

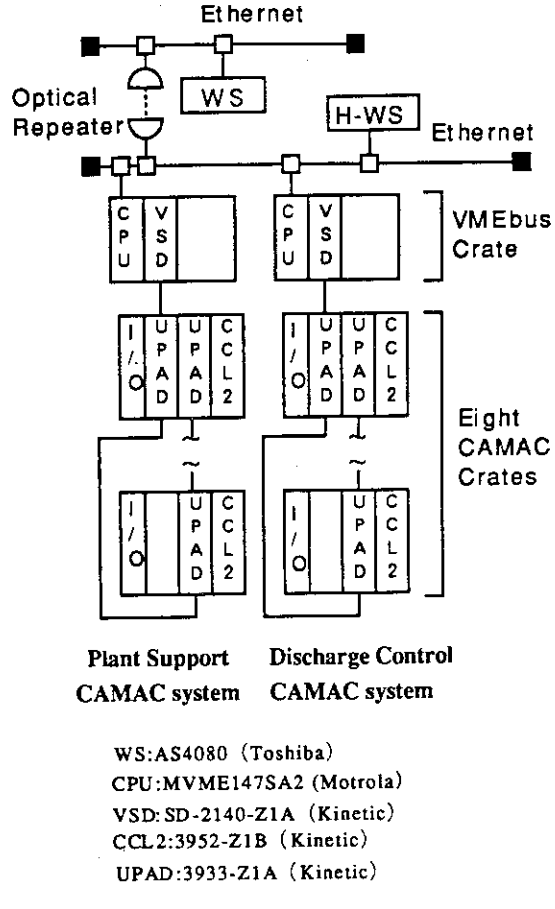

Fig. I. 4.3-1 New plant support and discharge control system of PFPS

specifications of the whole system, its hardware, its software, communication format between workstations, microcomputers and CAMAC. We also made software design of discharge sequence control of the PFPS. The new system is shown in Fig. I.4.3-1. Two workstations will be located in the central and local control room, respectively. The workstation are connected to two VMEbus crates via Ethernet LAN. A 32-bit microcomputer MVME147SA2 (Motorola) and a CAMAC serial driver SD-2140-Z1A (Kinetic) are installed on each VMEbus crate. The original CAMAC crates with I/O modules are used in the new system. Their programs are written by C language and run under a real-time OS VX-works.

Reference

[4.3-1] Y. Matsuzaki et al., Proc. 16th Symp. on Fusion Technology, (1990)1482.

4.4 Negative-ion-based neutral beam injection system

The JT-60 negative-ion-based neutral beam injection system (JT-60 N-NBI) has been building to be completed in spring 1996 for plasma heating and current drive experiment[4.4-1]. The JT-60 N-NBI is composed of two ion sources, one beamline, a dc 500 kV power supply system, a control system and an auxiliary system. The specification of the JT-60 N-NBI is shown in Table I.4.4-1. Since the JT-60 N-NBI is used aiming at the studies of the current drive and plasma core heating of high density plasma, the beamline is installed in the JT-60U as shown in Fig I.4.4-1 so that the beams are injected tangentially. The beamline consists of an ion source tank, a neutralizer tank , an ion dump tank and a NBI port.

Table I.4.4-1 Specifications of the JT-60 N-NBI

Beam Energy	500 keV
Injection Power	10 MW
Beam Pulse	10 s
Beam Species	D^0/H^0
Injection Angle	tangential/co-injection
Number of Beamline	1
Gas Influx to the JT-60U	less than 0.1 Pa·m^3/s

In the design of JT-60 N-NBI, there were many technical difficulties such as extraction of high negative ion current and handling of high voltage ,etc.[4.4-2]. It was necessary to confirm the performance of the ion source and the power supply system until the completion of the whole JT-60 N-NBI. A part of components; one ion source and the power supply system, is under manufacturing, so that these performance tests will be able to start in spring 1995.

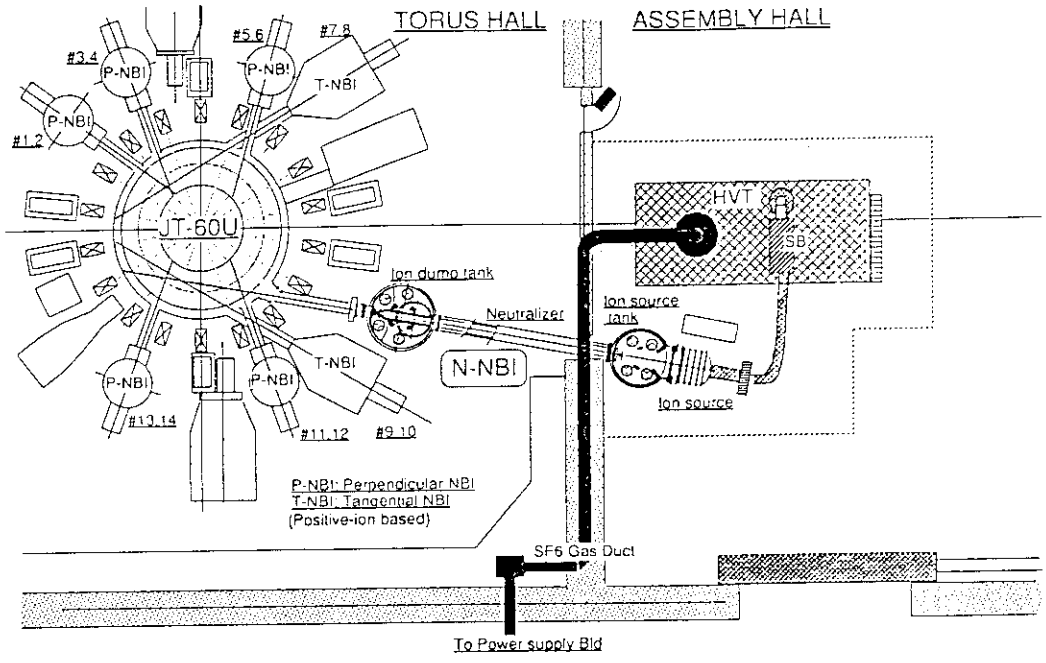

Fig I.4.4-1 JT-60U Negative-ion based NBI System

References

[4.4-1] M.Mizuno et al, Plasma Devices and Operations, 1994,Vol.3,pp.199-210
[4.4-2] T.Inoue et al, Plasma Devices and Operations, 1994,Vol.3,pp.211-222

II. JFT-2M PROGRAM

1. Toroidal Confinement Experiments

1.1 Overview

The progresses on JFT-2M experiments in FY 1993 are summarized. There are two main efforts, one is the systematic study of the plasma response by applying an external helical field, and the other is the study of the boundary plasma with introducing electric field or current in the scrape off layer (SOL) by the divertor bias system. In the rotating m=2/n=1 external helical field experiment, the possibility to control the rotation of m=2/n=1 island is demonstrated, and the frequency response of the m=2/n=1 island is systematically studied. In the static high-m/high-n external helical field experiment, the understanding of the control of an edge localized mode (ELM) is extended by the study of the different ELM behavior with changing safety factor. In the boundary plasma modification experiment, the particle and heat transport in the SOL and divertor region are summarized in the cases of Ohmic heating, L-mode and H-mode.

1.2 Experimental results

1.2.1 Rotating m=2/n=1 external helical field experiment

The plasma response of the rotating external helical field is studied with a circular plasma configuration which has a large saturated stable m=2/n=1 magnetic island. The typical plasma parameters are $q\sim3$, $\bar{n}_e \sim 1\times10^{19}m^{-3}$, $B_T\sim1.2T$, $I_P\sim240kA$. The natural frequency of the m=2/n=1 island is about 3kHz and the width of the island is measured to be about 5cm. A set of eight saddle coils installed inside the vacuum vessel are driven by two independent power supplies to generate an external rotating magnetic field with m=2/n=1 as a major helical component. The direction of the rotation , frequency (<5kHz) and amplitude (<5G) of the magnetic field perturbations are controllable. The

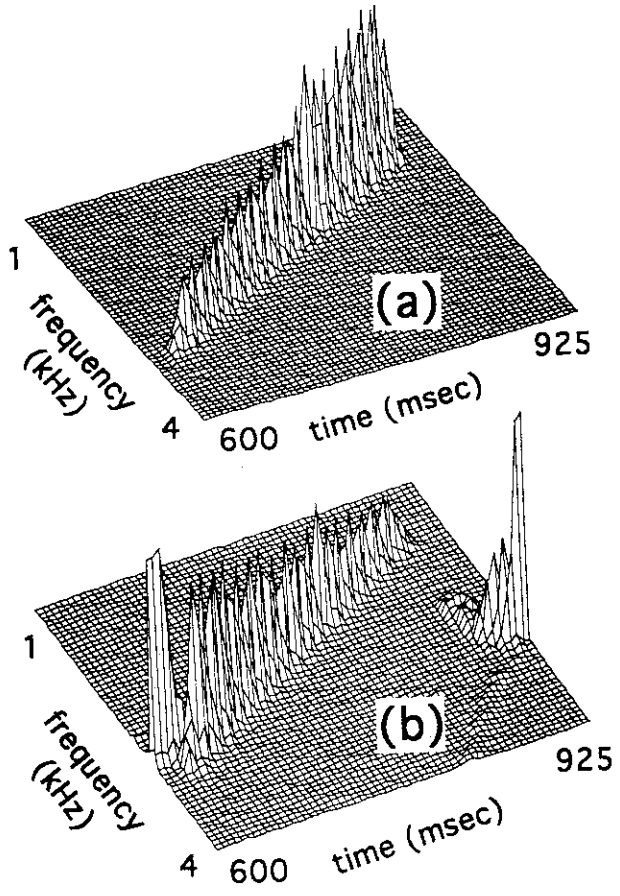

Fig.II.1.2-1 (a)Fourier spectrum of the external coil current. (b)Fourier spectrum of the magnetic probe data.

Fourier spectrum of the external coil current and that of the magnetic probe data are shown in Fig.II.1.2-1 (a) and (b), respectively. In this case, the rotating field is applied from 620 msec to 870msec with changing its frequency from 3kHz to 1.6 kHz continuously. The m=2/n=1 island is synchronized with the applied rotating field and its frequency resumes the natural frequency of 3kHz after switching off the external field. Such a synchronization[1.2-2] is not observed if the direction of the rotation of the external field is reversed, and if the initial frequency gap between the applied field and the natural m=2/n=1 oscillation exceeds about 0.3kHz. There are several conditions to synchronize the island rotation with external rotating field, however, the result clearly demonstrates the controllability of the island rotation.

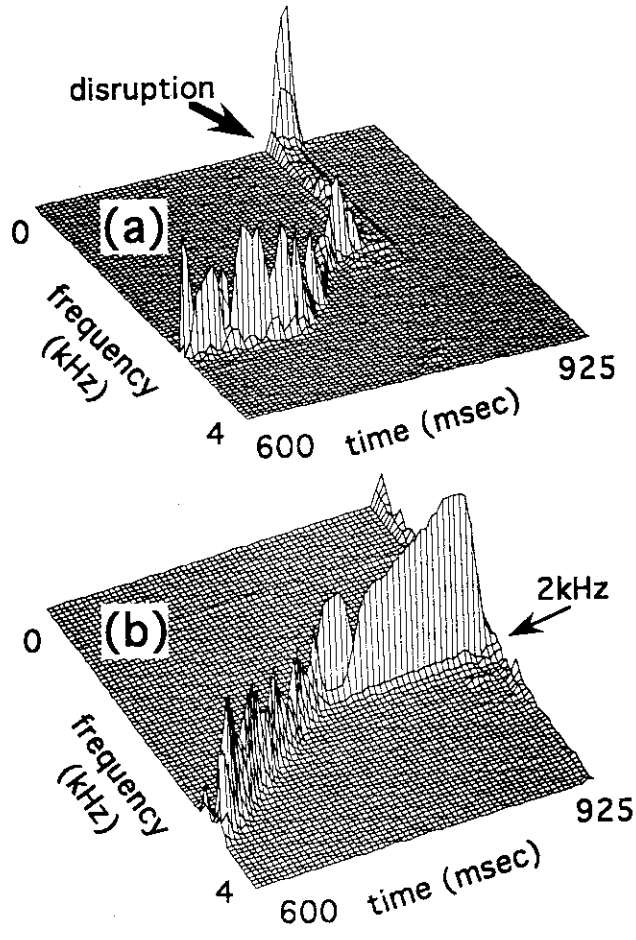

Fig.II.1.2-2 (a)Fourier spectrum of a magnetic probe data at the density limit disruption, (b)Fourier spectrum of a magnetic probe data when rotating external field is applied.

It is known that the density limit disruption occurs as the frequency of the m=2/n=1 mode decreases and goes to zero with increasing density. We tried to keep the m=2/n=1 rotation speed constant at the density limit disruption by the external rotating field. The Fourier spectrum of a magnetic probe data at the density limit disruption is shown in Fig.II.1.2-2 (a). The density is increased from 700msec and the disruption occurred at 825 msec. In Fig.II.1.2-2 (b), the rotating external field is applied with its frequency of 2kHz from 725msec to 900msec. In this case, m=2/n=1 island keeps rotating at 2kHz, resulting in the avoidance of disruption during the application of external helical field, and the disruption occurs just after switching off the external field. It shows that if the density were decreased during the application of the rotating helical field, it is possible to avoid density limit disruption.

1.2.2 ELM control by the static high-m/even-n external helical field

At present, only H-mode which has an edge localized mode (ELM) shows stationary state with improved confinement in JFT-2M. The ELM is actively controlled by the external helical

field. We have found that the effective helical field component to produce ELMs is high-m (≥12) and high-n (≥4) at fixed safety factor about q~3.5[1.2-1]. In FY 1993, the different ELM behavior with changing the safety factor is studied. The change of ELM behavior with fixed external helical field of high-m/even-n and ladder (M=10/N=2) is shown in Fig.II.1.2-3. The ELMs disappears with increasing q, or its amplitude is increasing with decreasing q. In the calculation of external helical field component in this case, the poloidal component of m=8 has the peak value at n=4. It suggests that the m=8 or 10 with n=4 might also have an effect to produce ELMs at low q of 2.5. This means that the toroidal helical component of n≥4 may be more important to produce ELMs than the poloidal one. The poloidal components only determines the resonance position around the pedestal (about 2cm from the separatrix). No ELMs in the case of large q is understood as follows. There is no large helical component with n≥4 which has the resonance condition around the pedestal region. There are m=12/n=4 which has a resonance with q=3, but the position may be further inside from the pedestal. Then it does not give effects to produce ELMs.

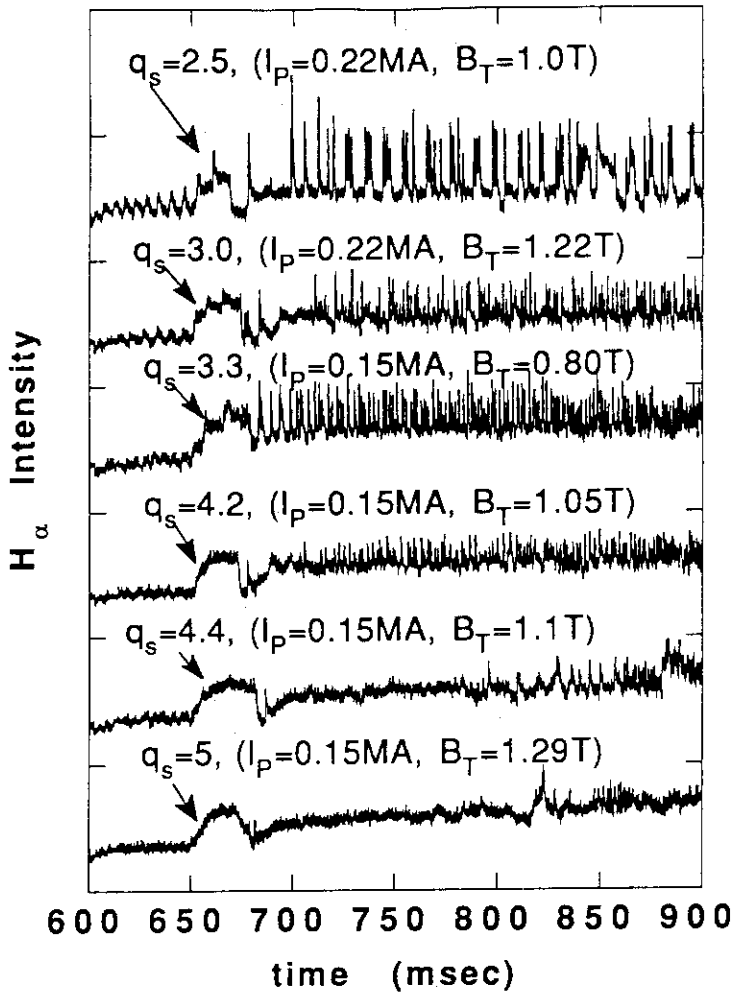

Fig.II.1.2-3 The change of ELM behavior at different q from 2.5 to 5 with fixed external helical field of high-m/even-n and ladder (M=10/N=2).

1.2.3 Particle and heat balance in the scrape-off layer and the divertor region

The transport mechanisms in the scrape-off layer and the divertor region have been extensively studied over the past few years. Transport phenomena in these regions have been treated using quite complicated models, and various atomic processes. Numerical simulation is usually adopted in this area. In the simulations, some important physical quantities are dominated by radial transport processes, which are recognized as anomalous, the same as those in main

plasma. Hence, experimental investigation of the radial transport is an important task, in addition to the detailed numerical simulations.

Particle and heat balance are studied in the scrape-off layer and the divertor region, in order to investigate the radial transport and determine the perpendicular diffusivity in JFT-2M. Particle flux parallel to the magnetic field at the divertor plates was estimated from ion saturation current of the divertor probes. From this measurement, profiles of electron density n_e, electron temperature T_e and floating potential ϕ_f were also obtained. Radial electric field was evaluated as $E_x=-\partial\phi_f/\partial x-3\partial T_e/\partial x$, and the poloidal particle flux Γ_y was calculated[1.2-3]. In this analysis, the density gradient and the particle diffusivity $D_\perp$ were assumed to be constant in the poloidal direction. Figure II.1.2-4 shows the obtained diffusivity as a function of electron density in the scrape-off region. The values obtained from ohmic and L-mode plasmas have the same tendency: they decrease with increasing the electron density. The values in H-mode plasmas are smaller than those in L-mode by a factor of 2-3. The obtained diffusivity has no clear dependence on plasma current I_p (or surface safety factor q_s). The heat balance is also studied. The evaluated heat diffusivity has almost the same dependence as the particle diffusivity and the ratio of $\chi_{eff}/D_\perp$ is about 2. In the case of the formation of a low temperature (≤10eV) divertor plasma of a broad temperature profile on the divertor plate, the parallel and perpendicular transport to the magnetic field would play an important role. Then this study will be extended further. Preliminary experiments of introducing electric currents in the SOL by divertor biasing, clearly show the modification of the divertor plasma. The physics of this phenomena will also be studied further to control the divertor plasma.

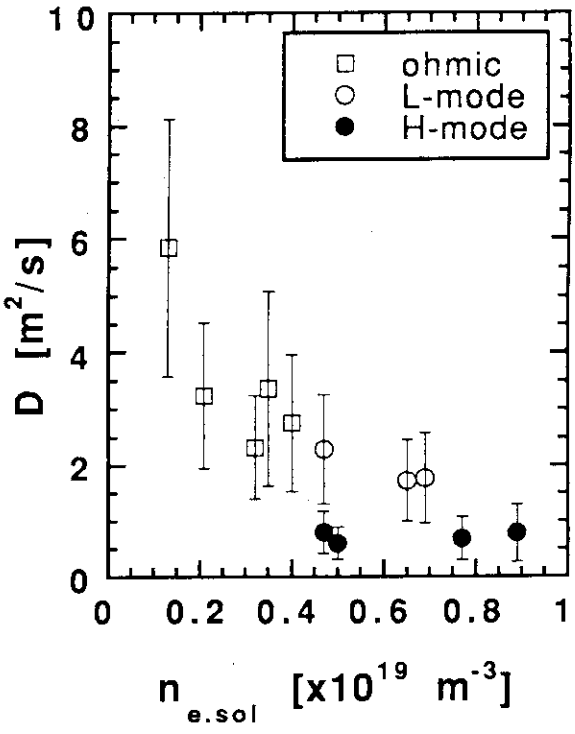

Fig.II.1.2-4 Particle diffusivity as a function of electron density in the scrape-off region.

References

[1.2-1] Mori M., et al., in Proc. 14 th International Conference on Plasma Physics and Controlled Nuclear Fusion Research, Würzburg, (1992) IAEA-CN-56/A-5-5.
[1.2-2] Oasa K., et al., to be published in Proc. 15 th International Conference on Plasma Physics and Controlled Nuclear Fusion Research, Seville (1994).
[1.2-3] Nagashima K., et al., to be published in J. Nucl. Mat.

2. Operation and Maintenance

2.1 Introduction

The JFT-2M tokamak has been operated from 1983 in cooperation with two divisions (Experimental plasma physics laboratory and JFT-2M facility division). The main duty of JFT-2M facility div. is to operate the facility smoothly and to develop new equipment necessary for new experiments. The JFT-2M experimental plan and operation schedule are arranged every week at the group leader meeting. In this fiscal year, a trouble on the toroidal field coil decreased experimental time . In other period, each apparatus was operated smoothly according to the experimental plan, and the careful examination of machine status was carried out daily and periodically. As for developing study of equipment, the divertor-biasing system and high speed helical magnetic field system were improved. Additional heating apparatus (ECH and FW) were adjusted to irradiate more RF power.

2.2 Operation and Maintenance

Summary of operation records for main apparatus is listed in Table II.2.2-1. The main apparatus such as the flywheel motor-generator(MG), the JFT-2M machine, the neutral beam injection system(NBI), the electron cyclotron heating system (ECH) and the fast wave current drive system(FW) were operated in a minimum loss time according to the experimental schedule .

Table II.2.2-1 Summary of operation records for main apparatus

		FY 1992	FY 1993				
			Apr-Jun	Jul-Sep	Oct-Dec	Jan-Mar	total
MG	#1MG (hour)	1,036	225	217	291	0	733
	#2MG (hour)	1,037	223	216	291	1	731
JFT-2M	Shot number (shot)	5,329	451	908	1,576	0	2,935
	TDC (hour)	252	20	72	59	0	151
	Baking (times)	3	0	0	0	0	0
	Pellet injection (day)	0	0	1	3	0	4
NBI	Operation (day)	70	7	15	20	0	42
	A-line Injection(times)	16,684	1,238	1,564	7,056	0	9,858
	B-line Injection(times)	22,802	1,718	1,523	7,257	0	10,498
ECH	Operation (day)	19	13	15	0	0	28
	Injection (times)	23,610	44,846	45,418	0	0	90,264
FW	Operation (day)	32	0	0	0	0	0
	Injection (hour)	256	0	0	0	0	0

A trouble on the toroidal field coil occurred. Electric insulation to the earth decreased less than the control value. Surveys on broken points of the electrical insulation indicated that a little water leak from a connection cap of the cooling water penetrated into a small gap between the insulator and coil conductors. As a result, the insulating resistance decreased less than the control value of 1 mega-ohm. Repair of the connection cap was comparatively easy. However, recovery of electric insulation required a long period of about 2 months to dry up the wet coil with a temporary thyristor power supply. From this experience, the tight covering of water pipe with epoxy resin was changed to a loose covering with rubber sheet to prevent the water penetration into the coil. Another trouble was same electric insulation problem on the old motor-generator used over 20 years. Dropping of electric insulation during the wet season and increasing distortion on the generator shaft resulted in one conclusion that the motor-generator has to be renewed. The renewal plan has started in 2 year's schedule. During the machine stop phase, repair of the divertor-bias equipment installed inside the vacuum vessel and necessary checks and regular examinations of the devices were carried out by the help of industries.

2.3 Development of equipment and apparatuses

In collaboration with the experimental plasma physics laboratory, some improvements on apparatuses have been carried out as follows. As for the divertor biasing system, fast acting fuses have been inserted in 34 feeder lines to prevent serious damage on the divertor plate by arcing, whose main cause was insulation breaking. The IGBT power supply was improved to feed high frequent current separately to the saddle coils(m/n=2/1) and excited rotating magnetic field with fixed frequency for the MHD control experiment. For the wall conditioning, the modification of the titanium RF sputtering system has been completed to work as a boron coating system. The merit of this method seems to be safe from diboran gas and to be a short operation time of about half an hour. In additional heating apparatuses, a new type of fast-wave antenna with back faraday shield was prepared to check the loading resistance. The transmission line components of 60 GHz ECH were examined carefully to reduce transmission loss and to decrease breakdown phenomena. Rearrangement of components and adjustment of wave-guide axis contribute to input more power into the plasma.

III. PLASMA THEORY AND COMPUTATION

In JFY1993, the extensive theoretical and computational works have been carried out on the topics of Analyses of Confinement and Heating Processes; MHD Equilibrium and Stability Analyses; Analyses of Burning Plasma in Tokamaks. The reports in detail are shown in each section.

1. Analyses of Confinement and Heating Processes

1.1 Critical gradient transport model for ion temperature gradient instability in toroidal plasma

It is found in toroidal particle simulations [1.1-1,1.1-2,1.1-3] that the characteristics of η_i /ITG instabilities in a toroidal system show remarkable differences compared with those in a cylindrical configuration including the development of radially extended potential structure and the radially increasing heat conductivity [1.1-1]. We found that the excited global mode and the related transport provide a strong constraint on the plasma so that the plasma profile is self-organized. This feature originates from the global nature of the mode. Here, we describe the self-organization of the plasma profile and propose a *critical gradient model* to theoretically explain the transport. The critical gradient model is described by the coupled time dependent equations for the potential energy φ^2 and the inverse scale length $\mu = 1/\varepsilon_T$:

$$d\varphi^2/dt = 2[\ \gamma_0\ (\mu-\mu_c) - \gamma_N\ \varphi^2\ ]\ \varphi^2\ ,$$

$$(3/2)d\mu/dt = -\ g\ \varphi^2\ \mu + P_h\ ,$$

where $\gamma_0 \sim \omega_d$, $\gamma_N = \gamma_{NL}/\varphi^2 \equiv (k_\theta \rho_i) k_r^2 R v_i$, $\mu_c = R/L_{TC}$ (L_{TC} : the critical gradient), $g = \chi_h/a^2$ and $\chi_h = (\rho_i v_i) k_\theta R$, $P_h = (R/a) P_{in}/T_i n_i$: the normalized input power. Note here that the former equation is identical to Landau equation and the latter is derived from the energy equation by assuming that L_T is spatially independent. We solve the those equations in the steady state and the heat conductivity scaling $\chi_i \equiv (\rho_i v_i)^{1/2}\ a\ P_{in}^{1/2}\ (T_i n_i)^{-1/2}$ and the energy confinement scaling $\tau_E \equiv B^{1/2}\ a n_i^{1/2} P_{in}^{-1/2}$, which reproduce the confinement degradation proportional to $P_{in}^{-1/2}$.

References

[1.1-1] M.J. LeBrun, T. Tajima, M.G. Gray et. al. Phys. Fluids **B5** (1993) 752.
[1.1-2] Y. Kishimoto, T. Tajima, M.J. LeBrun, J-Y. Kim, W. Horton, IFSR #589.
[1.1-3] T. Tajima, Y. Kishimoto, M.J. LeBrun et. al. "Transport in the self-organized relaxed state of ion temperature gradient instability", in Ion Temperature Gradient-Driven Turbulent Transport, AIP Conference Proceedings **284** (January 1994) p.255.

1.2 Linear toroidal particle simulation in the presence of poloidal shear flow induced by the radial electric field

It has been found in the simulation by TPC (Toroidal Particle Code) [1.2-1,1.2-2] that the characteristics of η_i /ITG instabilities in a toroidal system shows remarkable features, showing the development of the mode structure which has the long correlation length in the radial direction as shown in Fig.III.1.2-1(a). These remarkable features are primary due to the toroidicity induced coupling of mode rational surfaces over radial region. We here take into account the poloidal shear flow in the simulation and investigate the influence on the global mode and the transport.

An external electric field is introduced by $E_r(r) = \alpha r$, where $|\alpha|$ is chosen so that the potential difference between r=0 and r=a becomes $\Delta\phi = 0.1 - 0.2\ T_e/e$. Figure III.1.2-1(b) shows the potential structure in the case that the direction of the flow is same ($\alpha>0$) as the one of the mode rotation. It is found that the mode is localized in the radial direction and the saturation level and the related transport become lower. On the other hand, Fig.III.1.2-1(c) shows the result when the flow direction is opposite ($\alpha<0$) from the one of the mode rotation. The mode excitation is hardly excited compared with the $\alpha>0$ case. Thus, we found that the turbulence and the transport characterized by the toroidal coupling has the strong correlation with the direction of the flow. This is a direct result of the global extent of the mode.

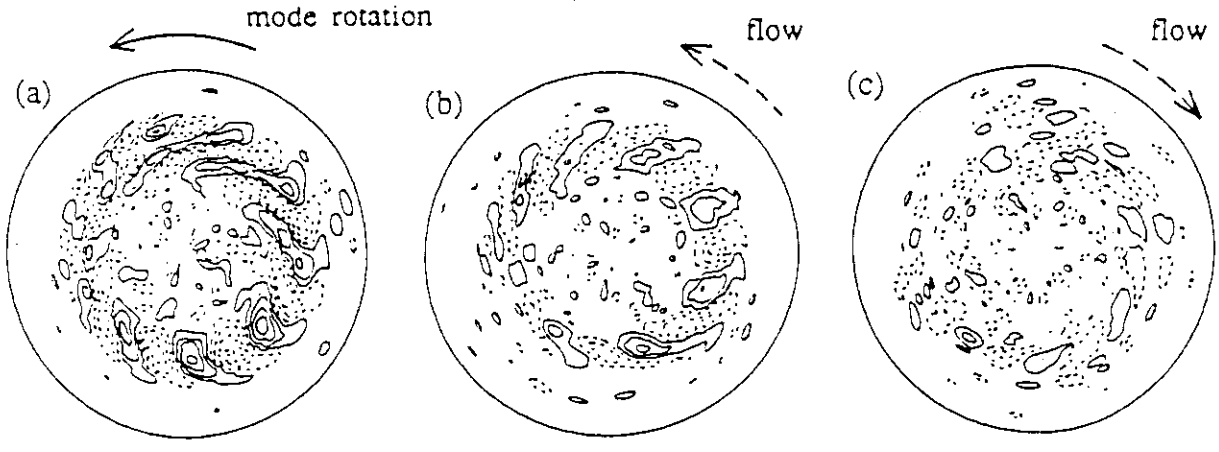

Fig.III.1.2-1 Potential contour plots around the saturation for the aspect ratio A=4 and the normalized Larmor radius $<\rho_i/a>\approx 0.02$ (a) without the radial electric field and shear flow, (b) with the shear flow directed to the mode rotation ($\alpha>0$), and (c) with the oppositly directed shear flow ($\alpha<0$).

References

[1.2-1] Y. Kishimoto, T. Tajima, M.J. LeBrun, J-Y. Kim, W. Horton, IFSR #589.

[1.2-2] T. Tajima, Y. Kishimoto, M.J. LeBrun et. al. "Transport in the self-organized relaxed state of ion temperature gradient instability", in Ion Temperature Gradient-Driven Turbulent Transport, AIP Conference Proceedings **284** (January 1994) p.255.

1.3 Interpretation of L-mode physics based on current diffusive ballooning mode [1.3-1,1.3-2,1.3-3,1.3-4]

The physics of the tokamak L-mode is studied based on the current-diffusive ballooning mode. Various phenomena which were observed in tokamak L-mode plasmas are predicted based on this instability. This instability shows β dependence is important factor on confinement time. Therefore from dimensionally similar experiments in which β is held fixed, we can deduce nothing about the confinement time from considering this β dependence. Also the Bohm versus gyro-Bohm argument is meaningless for MHD modes such as a current diffusive ballooning mode and is valid only for drift waves. This is because if β is held fixed in this model, it gives rise to Bohm scaling but this mode is the short-wavelength mode not the long-wavelength mode.

References

[1.3-1] Yagi M., Itoh K., Itoh S.-I., et al., "Analysis of the Current-Diffusive Ballooning Mode", Phys. Fluids **B5** (1993) 3702.
[1.3-2] Itoh K., Yagi M.., Azumi M.., et al., "L-mode confinement model based on transport-MHD theory in tokamaks", Plasma Phys. Controlled Fusion **35** (1993) 543.
[1.3-3] Yagi M., Itoh K., Itoh S.-I., et al., "Analysis of Current Diffusive Ballooning Mode", American Physical Society Meeting, Nov. 2, 1993, St. Louis, MO.
[1.3-4] Yagi M., Itoh K., Itoh S.-I., et al., "Interpretation of L-Mode Physics Based on Current Diffusive Ballooning Mode Instability", Transport Task Force Meeting, March 10, 1994, Dallas, TX.

1.4 Nonlinear simulation of the current diffusive interchange mode [1.4-1]

We have done the numerical simulation based on the three-field equations to investigate the nonlinear process driven by the electron convective term. Although the ballooning effect plays an important role in a tokamak, we concentrate on convective nonlinearity and take the electrostatic interchange as the target mode. In these simulations, we have observed the transition between linear and nonlinear instability. Comparing the analytic growth rate of the electrostatic interchange mode and the spontaneous growth rate of the simulations, we confirmed the nonlinear instability driven by electron convection. We have also observed self-organization of dipole vortex in the pressure field by the convection of the electron parallel current.

Reference

[1.4-1] Yagi M., Itoh K., Itoh S.-I., et al., "Nonlinear Simulation of the Current Diffusive Interchange Mode", Invited Talk, Sherwood Fusion Theory Conference, March 16, 1994, Dallas, TX.

1.5 Kinetic MHD model for analyses of plasma turbulence

Three kinds of models for analyses of the plasma turbulence have been developed.

The first one is a set of "reduced Braginskii equations" [1.5-1], which is derived without assuming flute ordering and the Boussinesq approximation. This model conserves the direct physical energy integral but does not contain the compressional Alfven time scale although the conventional reduced MHD model does not conserve the physical energy. It is a natural extension of the model derived by Drake et al.[1.5-2].

The second is a set of "hybrid model equations" in toroidal (or more general) geometry for magnetically confined plasmas [1.5-3]. This is suitable for low frequency toroidal modes for example, for trapped electron and current diffusive ballooning instability. This model consists of fluid ions and drift kinetic electrons. The numerical algorithm of this model equations is discussed. Also we have shown that this model in fact reproduces two limits of fluid and kinetic electron dynamics correctly.

The last one is a set of fluids moment equations with kinetic effects [1.5-4], which is a class of exact closures based on the Chapman-Enskog approach and formulated a new approach for the closures which allow to recover the exact kinetic results from the standard fluid equations at least in the linear limit. We have found that there exists the more direct way to derive the Chapman-Enskog closure relations, which provides the more compact form of closures and shown the closure relations in ref.[1.5-5] can be identically transformed to our form.

References

[1.5-1] Yagi M., and Horton W., "Reduced Braginskii Equations", IFSR #632.
[1.5-2] Drake J. F., and Antonsen T. F. "Nonlinear Reduced Fluid Equations for Toroidal Plasmas", Phys. Fluids. **27** (1984) 898.
[1.5-3] Yagi M., Tajima T., and Lebrun M. J., "Hybrid Toroidal Simulation", Numerical Tokamak Project Meeting, March 16, 1994, Dallas, TX.
[1.5-4] Private Communication with Smolyakov A. I. and Callen J. D.
[1.5-5] Chang Z., and Callen J. D., "Unified Fluid/Kinetic Description of Plasma Microinstabilities. Part I: Basic Equations in a Sheared Slab Geometry", Phys. Fluids **B4** (1992) 1167.

1.6 Numerical analyses of electron cyclotron resonance heating

To analyze the efficiency of electron cyclotron heating (ECH) in tokamak plasmas, the propagation and absorption of electron cyclotron waves were numerically analyzed by using the ray tracing method. Firstly, the extraordinary wave heating was studied in the frequency range of second harmonic resonance. The dependence of the power absorption rate on plasma parameters, i.e., electron density and temperature, was obtained. Secondly, both the ordinary and extraordinary waves were also analyzed in the fundamental resonance frequency range. The position of power deposition can be scanned along a major radius by controlling the injection angle of electron cyclotron wave. As for the extraordinary wave heating, the down shift of effective cyclotron resonance frequency due the relativistic effect is investigated. In the case of that the electron temperature exceeds about 10keV, the wave frequency can be sifted down to about 65% of the cyclotron resonance frequency at the plasma center and the heating of central region is possible [1.6-1]. This shows that the toroidal magnetic field can be increased by about 35% without the change of wave frequency.

Reference

[1.6-1] K. Hamamatsu, M. Azumi, JAERI-M 94-062 (1994).

1.7 Linear beam orbit analysis in a wiggler by using a non-canonical perturbation method

A high power free electron laser (FEL) in a millimeter wavelength has been applied for heating and the current-drive of a tokamak plasma. In a FEL with a long wiggler, an additional focusing field is required to keep beam particles from diverging. An additional long scale transverse motion induced by the focusing field modulates the longitudinal motion and sometimes destroys the axial phase relation between the beam particles and radiation field even if the beam is successfully transmitted. In order to investigate such a delicate phase relation under a complex wiggler configuration, a systematic perturbation method which employs non-canonical variables and Lie transformation developed by Cary and Litrtlejohn [1.7-1] is presented. This method is applied to a focusing wiggler which has a parabolically curved pole face [1.7-2,1.7-3]. Radial space charge force is taken into account in the analysis and the maximum current which can propagate that wiggler is estimated as a function of the transverse emittance for an electron beam which energy is around 1MeV. The effect of the beam current on the axial phase relation is investigated and found to be small. The present non-canonical approach is found to be transparent and comprehensive for this kind of problem and applicable to arbitrary complex wiggler recently developed.

References

[1.7-1] J.R. Cary, R.G. Littlejohn, Annals of physics **151** (1983) 1.
[1.7-2] E.T. Scharlemann, J. Appl. Phys. **58** (1985) 2154.
[1.7-3] K. Sakamoto, T. Kobayashi, S. Kawasaki, Y. Kishimoto et. al., J. Appl. Phys. **75** (1994) 36.

2. MHD Equilibrium and Stability Analyses

2.1 Up-down asymmetric version of the JAERI ERATO code

The JAERI ERATO code, an ideal MHD spectral code in a toroidal configuration, has been adapted to up-down asymmetric equilibria. This asymmetric version of the JAERI ERATO code incorporates two newly developed modules: one is a solver of the eigenvalue problem for a Hermitian matrix and the other is a module to compute the energy of the perturbed magnetic field in the vacuum [2.1-1]. The code was applied to symmetric equilibria given analytically and the eigenvalues (growth rates) obtained are good agreement with those obtained from the symmetric version of the JAERI ERATO code (ERATOJ).

Reference

[2.1-1] S. Tokuda, "Analysis of unstable modes in tokamak", Simulation **12** (1983) 89 (in Japanese).

2.2 Calculation of a 'big solution' in a tokamak plasma [2.2-1]

A code has been developed to calculate a 'big solution' of the two dimensional linearized ideal MHD equation for a marginally stable tokamak plasma (Newcomb equation). The big solution is necessary to obtain the outer region solution in non-ideal MHD stability analysis by the

asymptotic method. The big solution is expressed in the Frobenius series around a rational surface and the coefficients of the Frobenius series are numerically computed for a MHD equilibria of a tokamak plasma. The equilibria is obtained by an inverse equilibrium solver (INVEQ) which gives the solution of the Grad-Shafranov equation ($R(\psi, \theta)$,$Z(\psi, \theta)$) and their derivatives with respect to ψ with high accuracy.

Reference

[2.2-1] S. Tokuda, "Resistive MHD stability analysis by asymptotic matching method", in Proceeding of "1993-Workshop on MHD Computation", The Institute of Statistical Mathematics Cooperative Research Report 55, pp85-96 (1994).

2.3 Eigenvalue method for a 'small solution' in a tokamak plasma

The usual asymptotic matching method (Δ' method) for non ideal MHD stability analysis in a tokamak plasma expresses the outer region solution of the Newcomb equation $L\xi(r) = 0$ as a form of the response of the 'small solution' to the big solution: $\xi_L(r) = \xi_L^{(b)}(r) + \Delta'_L \xi_L^{(s)}(r)$, where the 'left' solution in the one dimensional problem is considered for simplicity (the differential operator L has the regular singular point $r = r_s$). This form breaks down when the plasma is marginally stable against the mode considered (for example, m = 1 mode) because $|\Delta'_L| = \infty$ for this case. We have extended the matching method to the marginally stable case by expressing the outer region solution as $\xi_L(r) = \xi_{L0}^{(s)}(r) + \xi_L^{(s)}(r) + \delta_L H(r) \xi_L^{(b)}(r)$ where $H(r)$ is a support function and $\xi_{L0}^{(s)}(r)$ the eigen-function of the equation $L\xi(r) = \lambda \rho(r) \xi(r)$ with eigenvalue λ_0 the absolute value of which is minimum among the eigenvalues ($\rho(r) > 0$ and $\rho(r = r_s) = 0$). The equation for $\xi_L^{(s)}(r)$ is $L\xi_L^{(s)}(r) = - \lambda_0 \rho(r) \xi_{L0}(r) - \delta_L (LH(r) \xi_L^{(b)}(r))$. From the solvability condition $(\xi_{L0}, \rho\xi_L^{(s)}) = 0$ the factor δ_L is given by $\delta_L = - \lambda_0 / (\xi_{L0}, \rho H(r) \xi_L^{(b)})$ ((f,g) denotes the inner product between f and g). In this formulation the eigen-function $\xi_{L0}(r)$ must be obtained and can be numerically computed by the finite element method using a singular element. A code based on this formulation is under developing.

2.4 Effect of local heating on m=2 tearing mode in a tokamak [2.4-1]

Effect of electron temperature perturbation induced by local heating on a tearing mode activity is investigated by simulations based on the reduced set of resistive MHD equations with the transport equation of electron temperature. Effect of poloidal plasma rotation is also considered in the simulations. It is shown that the local heating can suppress m=2 tearing mode instability when O-point of the rotating magnetic island is effectively heated as shown by solid line in Fig.III.2.4-1. X-point heating affects little the width of magnetic island (dashed line). While the perpendicular thermal conduction imposes a lower limit to the degree of localization of the heating that is achievable, the ratio of parallel to perpendicular conduction is shown to determine the heating power necessary for complete stabilization of the tearing mode.

Reference
[2.4-1] G. Kurita, T. Tuda, M. Azumi, T. Takeda, JAERI-M 93-224 (1993).

2.5 Axisymmetric tokamak simulation by using the TSC code

The improved version of TSC code (Tokamak Simulation Code) was applied to the position control analyses of fusion plasmas and gave a good efficiency in the time-consuming computational practice [2.5-1]. It is proved that there can be a good solution of ITER build-up scenario satisfying the control requirements such as plasma contact with limiter and shaping of plasma cross-section within a demanded tolerance. The time-evolution of ITER positional instability due to a failure in feedback control loop was also demonstrated and the growth rate of vertical displacement partly stabilized by the passive shell structure was clarified.

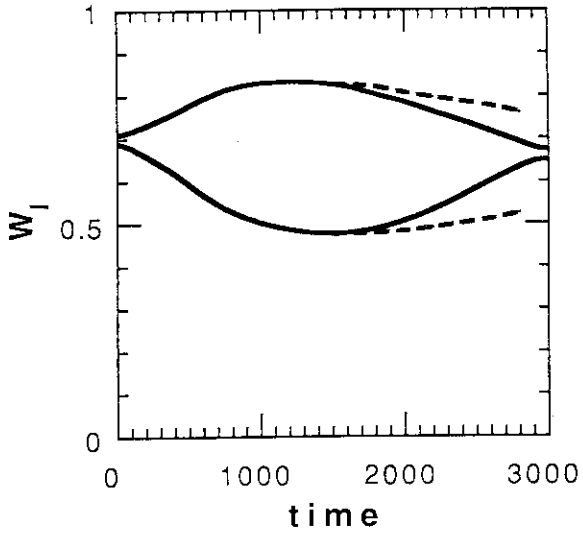

Fig.III.2.4-1 Time evolutions of the width Wi of rotating magnetic island for O-point heating (solid line) and for X-point heating (dashed line).

Reference
[2.5-1] Y. Nakamura, " Position Control Analyses of Fusion Plasmas - Axisymmetric Tokamak Simulation - ", Proc. 1993 Workshop on MHD Computations (The Institute of Statistical Mathematics, Nov. 24-26, 1993) 97 (1994).

3. Analyses of Burning Plasma in Tokamaks

3.1 Possible measurements of rf-induced radial diffusion of tritons using 14 MeV neutrons due to triton burnup

The possibility of measurements of ICRF-induced radial diffusion of tritons (T) through the detection of emission profiles of 14 MeV neutrons due to triton burnup was examined for deuterium (D) plasmas of JET with combined D^0 beam injection (to enhance the triton production rate due to D-D reactions) and triton cyclotron range of frequencies heating. The frequency range available in JET is f = 25 - 50 MHz, which corresponds to $\omega = 2\omega_{cT} - 4\omega_{cT}$ for $B_t = 2.5$ T. A simple calculation [3.1-1] shows that the neutron emission profile may possibly be flattened by rf-induced radial diffusion of fast tritons in D(^{3}He) plasmas with ICRF heating in the fundamental minority regime, where the tritons are in the second harmonic resonance. The effect of rf-induced radial diffusion on the tritons is expected to manifest in comparing the 14 MeV neutron signals with and without ICRF heating. Successful experiments could lead to simulation of profile control of fusion produced alpha particles by ICRF waves in D-T plasmas.

Reference
[3.1-1] M. Yamagiwa, Physics Plasmas **1** (1994) 205.

3.2 Ripple loss of alpha particles in a tokamak reactor with a non-circular plasma cross-section [3.2-1]

The geometric effect of a non-circular plasma cross-section on the loss of alpha particles induced by a toroidal field ripple is investigated theoretically and numerically by using a orbit following Monte Carlo code. The ripple-enhanced banana drift and the critical field ripple for ergodic orbits are very sensitive to the elongation. The effect of the triangularity on these parameters is not as important as that of the elongation. The ripple-enhanced banana drift loss shows a drastic decrease with plasma ellipticity. As the banana drift loss is reduced with ellipticity, the ripple trapping begins to dominate the total loss and shows a sharp increase with ellipticity. The resulting beneficial effect of elongation on reducing ripple-enhanced losses is weakened. Two key parameters that affect the fraction of ripple-trapped loss, the non-uniformity of the elongation and the gap between the plasma surface and the first wall, have been found. The geometrical effect is very important, not only for the basic loss mechanisms but also for the global ripple losses of alpha particles in connection with the distribution of field ripple.

Reference
[3.2-1] K. Tani, T. Takizuka, M. Azumi, Nucl. Fusion **33** (1993) 903.

3.3 OFMC plus Mapping Hybrid code for high energy ion ripple loss analysis in the up-down asymmetric configuration

New version of a Mapping code for the up-down asymmetric configuration is developed. Combination of Mapping with OFMC (Orbit-Following Monte-Carlo), Hybrid code, provides an effective tool for reliable calculations of high energy ion ripple losses in a tokamak including both total loss fraction and lost power distribution over the first wall. The code gives 10-30 times faster calculation than a pure OFMC code. Hybrid code calculations for NBI ion ripple losses in JT-60U are in good agreement with experimental and previous OFMC data.

3.4 Comparison of Monte-Carlo calculations between of "velocity scattering model" and of "spatial diffusion model" for impurity transport simulation

The impurity transport in a divertor plasma and a SOL plasma is very important problem for the remote-radiative cooling by impurities and the shielding of impurities in a reactor. In order to study the impurity transport, Monte-Carlo codes are used, in which two kinds of models for the impurity motion parallel to the magnetic field line have been adopted. One is a "velocity scattering model" [3.4-1], where Coulomb collisions scatter the velocity and result in the spatial spread, and the other is a "spatial diffusion model" [3.4-2], where the parallel motion is described directly as the diffusive one. We compare the difference between these models. The former model simulates

the physics processes, while the latter model cannot correctly simulate the parallel transport especially when the characteristic time and length of the transport become comparable to or less than collision time and mean-free path.

References

[3.4-1] K. Shimizu, H. Kubo, T. Takizuka, M. Azumi et al., "Impurity transport modelling and simulation analysis of impurity behavior in JT-60U", to be published in J. Nucl. Mater.
[3.4-2] e.g., P.C. Stangeby, J.D. Elder, J. Nucl. Mater. **196-198** (1992) 258.

IV. COOPERATIVE PROGRAM ON DIII-D (DOUBLET-III) EXPERIMENT

1. Introduction

The primary goal of the DIII-D tokamak research program is to provide data to develop a conceptual physics blueprint for a commercially attractive electrical demonstration plant (DEMO) that would open a path to fusion power commercialization. Specific DIII-D program is addressing these objectives in an integrated fashion with high beta and with good confinement. The long-range plan is organized into two major thrust; the development of an advanced divertor and the development of advanced tokamak concepts. These two thrust have a common goal: an improved DEMO reactor with lower cost and smaller size than the present DEMO which can be extrapolated from the conventional ITER operation scenario. In order to prepare for the long-range program, in FY93 the DIII-D research program concentrated on three major areas: Divertor and Boundary Physics, Advanced Tokamak Studies, and Tokamak Physics.

The major goals of the Divertor and Boundary Physics studies are the control of impieties, efficient heat removal and understanding the strong role that the edge plasma plays in the global energy confinement of the plasma. The advanced tokamak studies initiated into new techniques for improving energy confinement, controlling particle fueling and increasing plasma beta. The major goal of the Tokamak Physics Studies is the understanding of energy and particle transport in a reactor relevant plasma.

2. Highlight of FY 1993 Research Results

Success on DIII-D during fiscal year 1993 include: the installation of an all carbon wall which allowed VH-mode without boronization and a rapid recovery from vents, cryopumping of the divertor which for the first time in any tokamak made the density in H-mode controllable and allowed pumping of neutral injected helium giving promise of alpha ash control, deuterium or neon puffing at the divertor with concomitant divertor radiation greatly reducing the divertor heat flux while little affecting global confinement and in the case of the neon puffing also producing an edge region of high radiation which encircles the plasma. $n_D(0)Ti(0)\tau_E$ was more than doubled to $5x10^{20}m^{-3}keVs$, the ratio of plasma pressure to magnetic field pressure β was increased to 12.5%, a new quiescent high βp (ratio of plasma pressure to poloidal magnetic pressure) high performance regime was identified and advances were made in fast wave current drive and efficiency. In addition to controlling the plasma shape, the digital control system was successful in controlling (1) the plasma density by feedback on the cryopumping and gas fueling rate, (2) the radio frequency ion cyclotron power loading by adjusting the gap between the plasma and antennas, and (3) in maintaining constant beta (stored plasma energy) by feedback control of the neutral beam power.

Divertor radiation by D_2 or Ne injection:

Power flow from the plasma core through the scrape-off layer (SOL) and into the divertor represents a serious design challenge. A successful means of reducing the peak flux was found in FY93 by radiating the power away before it strikes the divertor plate by use of deuterium and/or neon injection with cryopumping to limit the density rise; peak heat load on the divertor plate was reduced by as a factor of five. The effect of Ne gas puffing, which has only a small effect on global confinement but a large effect on the profile of divertor heat flux as measured by an absolutely calibrated IRTV camera.

Divertor cryopumping and particle control:

For the first time in any tokamak with H-mode, density can now be controlled successfully. The advanced divertor cryopump was effectively brought into operation allowing: density control, observation of helium exhaust and a systematic measurement of the dependence of confinement on density. Plasma density control, for example, is shown in Fig. IV.2-1. Obviating the usual H-mode density rise is of major importance for successful, efficient rf current drive for a steady-state reactor with current profile control.

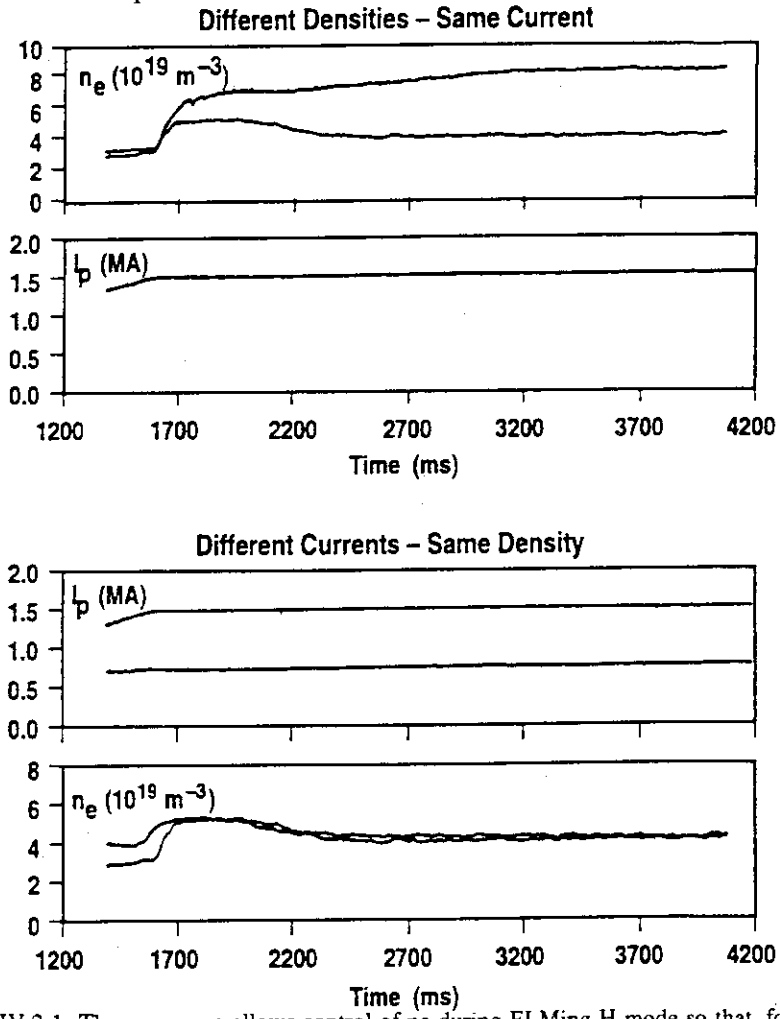

Fig. IV.2-1 The cryopump allows control of ne during ELMing H-mode so that, for example, n_e can be reduced at constant Ip and beam power or kept constant at different Ip.

Helium exhaust using the cryopump:

A major potential problem for ITER and fusion reactors in general is buildup of helium ash as a result of alpha particles produced during fusion reactions; too much dilution of the DT plasma by helium will stop the fusion power output. (The sun is now about 28% helium and will eventually become a " red giant " because of a lack of He ash removal.) The use of the new cryopump was successful in pumping away the helium density in DIII-D after a short He gas puff. See Fig. IV.2-2. The decay rate of the He density during the pumping is fast enough to be acceptable for ash control in ITER or a reactor.

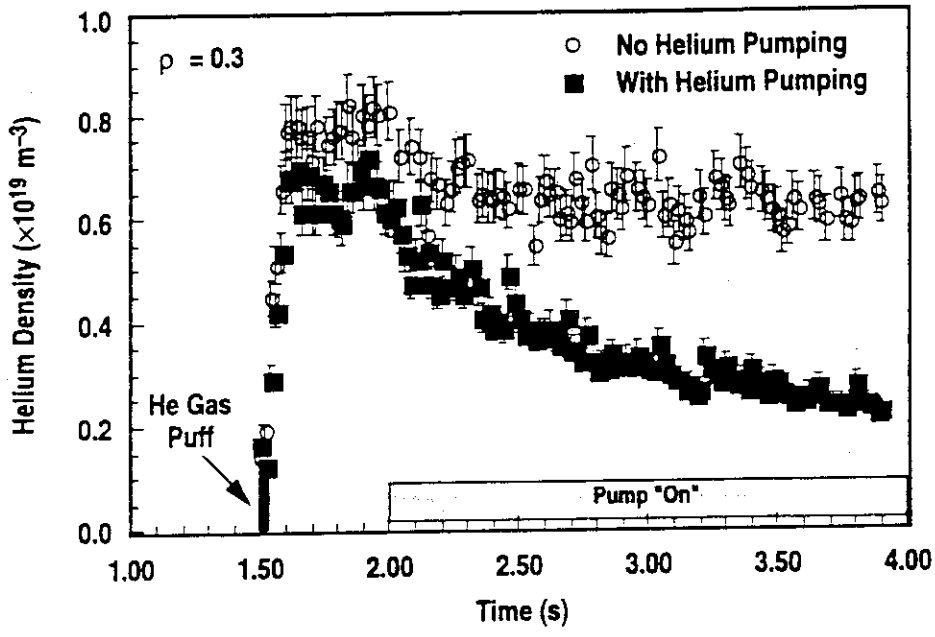

Fig.IV.2-2 First He exhaust experiment on DIII-D using Ar frosting of the ADP cryopump.

Improved understanding of VH-mode:

VH-mode plasma with confinement up to twice the usual H-mode value were successfully reproduced in an all-carbon vessel without boronization, confirming that clean wall condition is required but the means are not unique. The hypothesis that the VH-mode core confinement improvement is due to entry into a positive feedback loop in which core flow shear increases, particularly deeper inside the core, decreasing turbulence and concomitant transport, increasing flow shear, etc., was confirmed by using 'magnetic braking" of core flow as an independent control of toroidal plasma rotation. Where the VH-mode flow shear is decreased by magnetic breaking, turbulence and transport increase back to "normal" levels.

V. TECHNOLOGY DEVELOPMENT

1. Vacuum Technology and Fuel Injection

1.1 Introduction

Vacuum technology is one of the most important technology for the realization of a fusion experimental reactor like ITER. R&D's of innovative vacuum components and techniques are essential in this technology area.

For this fiscal year, the research activity of a high resolution quadrupole mass spectrometer should be noted. Development of the ceramic turbo-viscous pump, ceramic coating and joining technology, and ceramic-insulated cables was also advanced.

Efficient fueling and ash exhaust are essential to confine and control near-ignition fusion plasmas. To meet the ITER Engineering Design Activity, a new R&D program was started to establish fueling and pumping systems of tokamak fusion experimental reactors in FY1991. In this fiscal year, the pneumatic pipe-gun/railgun combined accelerator was studied to develop a fuel pellet injector with variable speed and repetitive acceleration capabilities. Two types of large rotor disks with full pump blades and upper and lower touch-down bearings for accidental heavy loads up to 1 ton were fabricated and tested for the development of a large turbomolecular pump with a pumping speed of 25 m^3/s.

1.2 Progress in ceramic vacuum pump development

The conditions needed for the torus pumping system of a nuclear fusion reactor are a large pumping speed and the robustness against radiation, tritium, and high magnetic fields. To establish such a system by using dynamic oil-free pumps, we developed two types of ceramic pumps;ceramic turbomolecular pump and ceramic turbo-viscous pump.

By the previous year, we performed the pumping speed measurements and an atmosphere air rushing tests as a performance test of the fabricated large-size turbo-viscous pump whose rotor assembly consisted of seven rotor disks 200 mm in diameter and hybrid gas bearings.

In this fiscal year, the measurements of the radial bearing acceleration changes in the start-stop cycle test for a large-size turbo-viscous pump were made under the

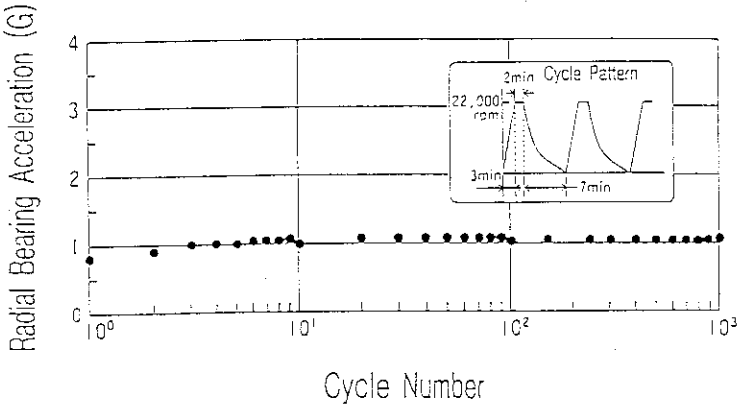

Fig.V.1.2-1 Change in the radial bearing acceleration during a 1000 start-stop cycle test.

following regular time intervals; 3 min. (start-up time) -2 min. (rotation keeping time)-7 min. (stopping time) in Fig.V.1.2-1. The experimental results revealed that the radial bearing acceleration values were approximately 1 G constant in Fig.V.1.2-1 and the operation behavior was the stable rotation during 1000 cycle tests.

1.3 Improvement of high-resolution quadrupole mass spectrometer (QMS)

In this fiscal year, the high-resolution QMS was improved to detect a 10^{-4} helium peak in a deuterium atmosphere and to expand an analyzable mass range [1.3-1], [1.3-2].

Figure V.1.3-1 shows the QMS improved, which is equipped with two resolving powers, i.e., a high resolution mode and a normal one, and voltages for realizing the two modes are supplied by a common circuit. The high resolution mode adopts a condition of the second stability zone in the Mathieu diagram and can analyze a range of 1 to 9 amu. By switching to the normal mode, we have an analyzable range of 1 to 60 amu.

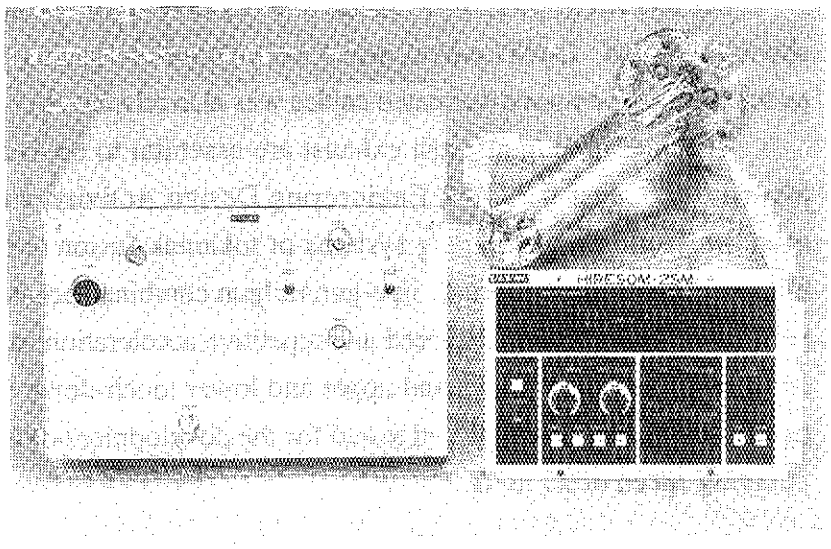

Fig. V.1.3-1 Photo of the improved QMS. A drive unit is on the left and an analyzer head without an envelope are on the right.

1.4 Progress in joining technology using ultra-fine particles

The ceramics-to-ceramics joining is a fundamental technique for the production of large-size ceramic components. In conventional ceramics bonding technique, the metals as a bonding binder the melting point of which is lower than these of the ceramics are inserted in the interface between the both ceramics parts to bond each other and to release the thermal stresses. However, the conventional technique has an inevitable problem, i.e., when those bonded ceramics components are exposed to an atmosphere of higher temperature than the binder's melting point, those components will not be able to keep the bonded shape because the bonding binder will melt down. In order to increase the thermal resistance properties of bonding binder, we proposed a new ceramics joining technique which utilizes as a bonding binder the ultra-fine particles(UFP, diameter< 50 nm) consisting of ceramic materials.

In the previous year, we fabricated the joined bodies of two Si_3N_4 bulk ceramics by using Si_3N_4 UFP as a bonding binder at 1700 °C , 10^8 Pa in N_2 atmosphere . The average bending

strength of those joined bodies ; 3 x 4 mm cross section (JIS-R1601 standard) sample showed 85 MPa .

In this fiscal year, in order to increase the bending strength the joined body of Si_3N_4 bulk ceramics was fabricated by using Al_2O_3 UFP as a bonding binder at 1700 °C , 10^8 Pa in N_2 atmosphere . The bending strength of 3 x 4 mm cross section (JIS-R1601 standard) samples in Fig.V.1.4-1 showed approximately 970 MPa up to 800 °C in contrast to 1050 MPa for bulk Si_3N_4. The bending strength for the case of Al_2O_3 UFP binder is ten or more times that of Si_3N_4 UFP binder.

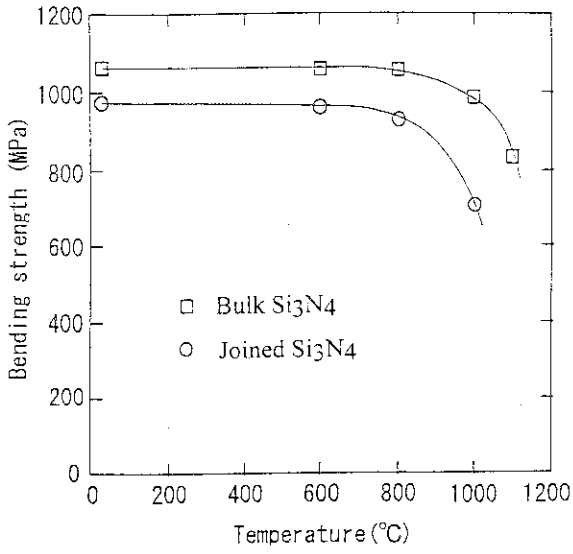

Fig.V.1.4-1 Temperature dependence of bending strength.

1.5 Study on railgun pellet injector

A two-stage type railgun injector was studied to develop a repeating-type and variable speed pellet injector for reactor-like plasmas and to improve plasma properties (confinement time, density limit etc.). A final goal of this R&D is to develop the injector with the following characteristics: 1) Pellet speeds can be variable in the range of 1-5 km/s during a repeating injection. 2) Pellets can be repeatedly ejected at 1-2 Hz. 3) A plasma armature is produced by a laser, so the supplied voltage to the rails is reduced and rail erosion becomes small. The railgun system consists of the pneumatic single-stage pipe-gun for the first stage and the railgun for the second acceleration stage. A laser is the YAG laser (0.9J, 6ns, 1064nm).

In this fiscal year, acceleration properties against various rail-materials and laminated-type rails were investigated. Pellets are a dummy pellet (lauan), 3mmϕx3mmL (10mg). Tested

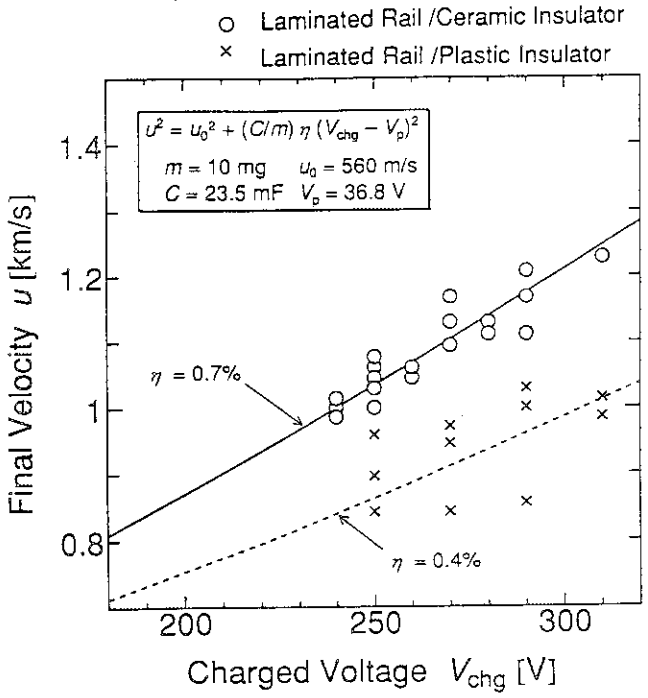

Fig.V.1.5-1 Dependence of the final speed of dummy pellets on charged voltage to capacitors. η is acceleration efficiency. u and u_0 are final and initial speeds of the pellets, m is the pellet mass, Vchg and Vp are the charged voltage and voltage drop in the plasma, C is capacity of the condenser.

materials of the rail are copper, tungsten-alloy, plastics and ceramics. The laminated-type rail consists of Cu and W-alloy (W-alloy faces a plasma armature). Plasma damage of rails used W-alloy is smaller than that of Cu rails. This W-alloy rail can be used more than 40 times without any maintenance. Also, it was found that a plasma production method by the laser is very useful to reduce rail damage near the initial-plasma formation region. There was no difference of acceleration properties (speed) between the laminated-type rails and W-ally rails. Figure V.1.5-1 shows the dependence of the final speed on the charged voltage to capacitors. Open circles are the case using the ceramic insulator (Al_2O_3) between rail conductors, and crosses are the case using the plastic insulator. Rail conductor is the laminated one. The acceleration efficiency in the ceramic insulator cases is about 1.8 times as large as that in plastic insulator cases. The efficiency is defined as the ratio of kinetic energy gained by pellets during acceleration by the railgun to input energy. Signals from magnetic probes to detect magnetic field generated by the plasma-armature current indicate that there is no separation of the armature during acceleration. These are due to low erosion of the ceramic insulator compared with the plastic one. It is very important to select materials of rails. These investigations have been done in the collaboration with Mitsubishi Heavy Industries, Ltd.

1.6 Fabrication and test of proto-type rotors with full pump blades for 25 m^3/s TMP

JAERI has been proposed a magnet-suspended, 25 m^3/s turbomolecular pump (TMP) for the ITER torus pumping system. The feasibility study and conceptual design of the 25m^3/s TMP [1.6-1] was started in 1992.

In this fiscal year, the prototype rotors were fabricated and tested as an ITER emergency task. That is, two types of rotor disks with full pump blades, 860 mm in diameter, were machined to examine the accuracy of manufacturing. Figure V.1.6-1 shows the fabricated rotors of 4th (disk B) and 6th (disk C) stage disks in a total of 14 stages from the inlet. An aluminum alloy (A2219T852) disk, roughly 1000 mm in

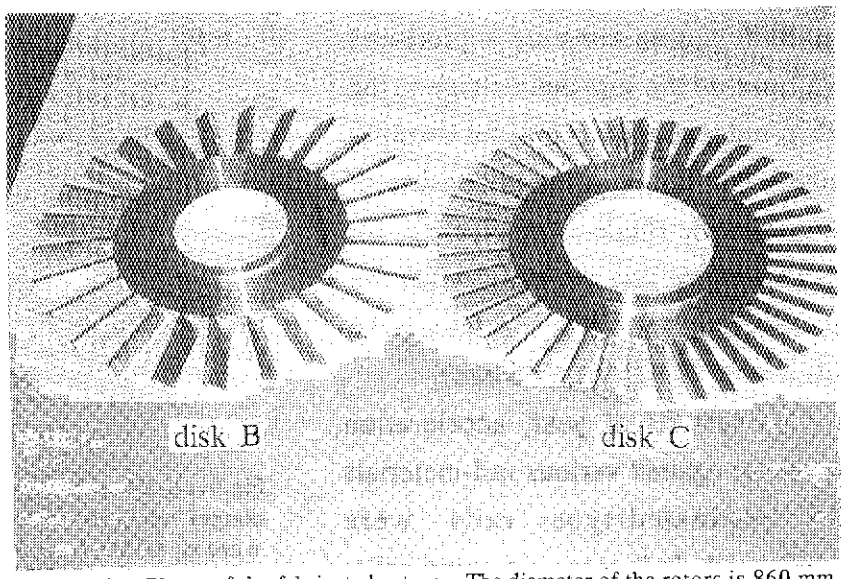

Fig.V.1.6-1 Photo of the fabricated rotors. The diameter of the rotors is 860 mm and the numbers of blades for disk B and C are 26 and 42, respectively.

diameter and 80 mm in thickness, was lathed to make a bare rotor disk, then the blades were formed on the rotor disk with a fraise. The forming accuracy of the lathe was the order of 10 μm , whereas that of the fraise was insufficient, i.e., the order of 0.1 mm. The thickness of the blades measured was 6.25 ± 0.02 mm for disk B and 3.90 ± 0.18 mm for disk C. The rotor unbalance which results from the scattering of the blade thickness was found especially in disk C, and the unbalance values for disk B and C were evaluated to be 286 g·mm and 2376 g·mm, respectively. It was concluded that the decrease in scattering of the blade thickness is a key to improve the rotor unbalance on disk C.

References

[1.3-1] Hiroki S., Abe T. and Murakami Y., Rev.Sci.Instrum.65, 1912 (1994).
[1.3-2] Hiroki S., Abe T., Murakami Y., et al., to be published in J.Vac.Sci.Technol.
[1.6-1] Annual Report of Naka Fusion Research Establishment, JAERI-M 93-193, 63 (1993).

2. Superconducting Magnet Development

2.1 Introduction

Under the ITER Program, JAERI is developing the superconducting magnet technology and cryogenic system technology required for the construction of ITER system. The test coils under fabrication are the Outer Module of the Central Solenoid Model Coil (CS Model Coil), CS Insert Coil and Nb_3Al Insert Coil. These Insert Coils will be tested placed at the inner bore of the CS Model Coil.

Major evolution from April 1993 to March 1994 are as follows:

(1) Advanced Nb_3Sn Strands that first satisfied the technical specification for the CS Model Coil were developed and their high performances were confirmed also by the benchmark test by the EC and US. They have highest critical current densities and lowest hysteresis pulsed operation loss among the international samples developed for ITER and tested in 1993.

(2) It was decided in the ITER Program that the US and Japan fabricate the inner and outer module of the CS Model Coil, respectively. Superconducting strands will be made in the Four Home Teams and they are put into Incoloy jacket by EC Home Team. The conductors thus made will be supplied to the US and Japan for winding of the CS Model Coil.

(3) Eleven contracts were established between JAERI and Japanese industries for the construction of the CS Model Coil Test Facility and fabrications of many apparatus have been started. Coordination and technical interface control between the industries are performed by JAERI team. Its construction will be completed by mid of 1995.

2.2 Central solenoid(CS) model coil

2.2.1 Design of coil

The purpose of the CS model Coil is to demonstrate the reliability of the design and the feasibility of the manufacture of the full size CS coil.

The CS model coil is composed of the inner module coil, the outer and the support structure, as shown in Fig. V.2.2.-1. Major parameters of these coils are listed in Table V.2.2-1. The structure which support their two modules from axial direction is divided in 18 sectors to reduce eddy current loss. The coil is designed with the same conductor and winding configuration as the full-size CS coil. The coil which has an inner diameter of 1.6 m, an outer diameter of 3.6 m and a height of 2 m, is fabricated with a layer winding method. The CS model coil consists of 18 layers which are manufactured by using a two-in-hand winding method and a wind-and-react technique. The coil is designed to generate 13 T at its current of 46 kA.

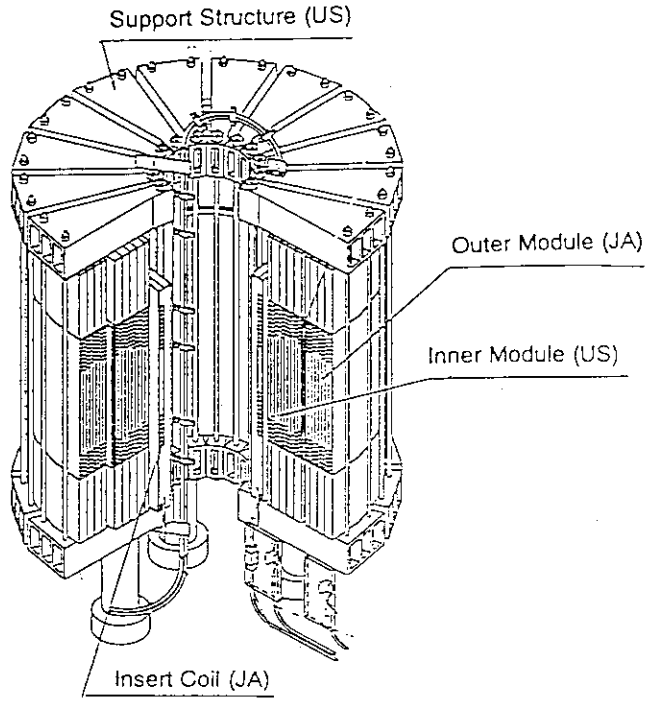

Fig. V.2.2-1 Concept of the CS model coil

Table V.2.2-1 Parameters of the CS model coil and the insert coil

	CS Model coil		Cs Insert Coil
	Inner Module	Outer Module	
Number of layers	10	8	1
Number of turns	328	272	30
Inner diameter (m)	1.6	2.7	1.4
outer diameter (m)	2.7	3.6	1.6
Height (m)	1.8	1.8	1.6
Rated current (kA)	46	46	40
Max. magnetic field (T)	13	6.6	13

The stored magnetic energy is about 600 MJ and this value is around 30 times as much as the value of the superconducting pulse coil which have been fabricated and operated until now. The winding pack is insulated with an insulator of 10 mm to withstand for 27 kV. Therefore, because

many sensors can not be attached to the winding pack of the CS model coil, the conductor of the CS model coil can not be tested in detail. The insert coil is fabricated with one layer to examine the conductor used for the CS model coil in detail. The insert coil will be installed into the CS model coil and will be tested. This coil system will be constructed with Japan-US cooperation, by using the superconductors which will be manufactured by four Home Teams. Japan is in charge of the outer module and the insert coil.

2.2.2 Development of high-performance Nb_3Sn strand

JAERI has progressed the development program of high-performance Nb_3Sn strand for the pulse high-field CS coil of the ITER since 1991 with Japanese industries, and high-critical-current-density but short-length strands were developed in 1992. The detailed specification of the strand and the amount of the strand necessary for the ITER model coils were fixed in the spring of 1993, as shown in Table V.2.2-2, and the schedule of the development work of the strand for the model coil was decided. The total amount of Nb_3Sn strand necessary for the ITER model coils was estimated to be 26 tons and the duty of each party was decided to be 6.5 tons. In this fiscal year, the development work of the strand which met the fixed requirements and the development of the technique for stable manufacturing were carried out. As the result, satisfactory high-performance mass-production-level Nb_3Sn strands were developed as shown in Fig. V.2.2-2 and its stable manufacturing techniques were established. During these development works, 1 tons of Nb_3Sn strand for the CS model coil was completed as was planned. The rest 5.5 tons of strand will be completed in the spring of 1995.

Table V.2.2-2 Nb_3Sn strand for the CS model coil.

Strand diameter	0.81 mm
Cu/non-Cu ratio	1.5
Unit length	>1500 m
Critical current density at 12T per non-Cu area	>550 A/mm^2
Hysteresis loss for 3T per non-Cu volume	<200 mJ/cm^3

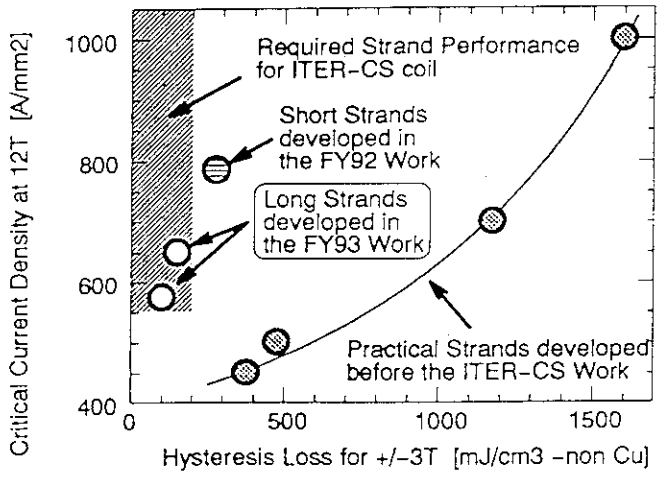

Fig. V.2.2-2 Performance of the Nb_3Sn strand developed in the FY93 work.

2.2.3 Development of large-current Nb_3Sn conductor

Full-size conductors, which are composed of about 700 Nb_3Sn strands and designed at the rated performance of a 40-kA current and a 13-T magnetic field, were manufactured for the CS model coil. The critical current measurements of the full size conductor were performed at JAERI. The measured critical current of this conductor is 80 kA, which is twice as much as the rated current. Current sharing temperature of full-size conductor at rated condition was measured at the Fusion Engineering International Experiments (FENIX) test facility in Lawrence Livermore National Laboratory (LLNL). According to this experimental results, it was confirmed that the developed full-size conductor met the design requirement for temperature margin, which is more than 2 K, as shown in Fig. V.2.2-3.

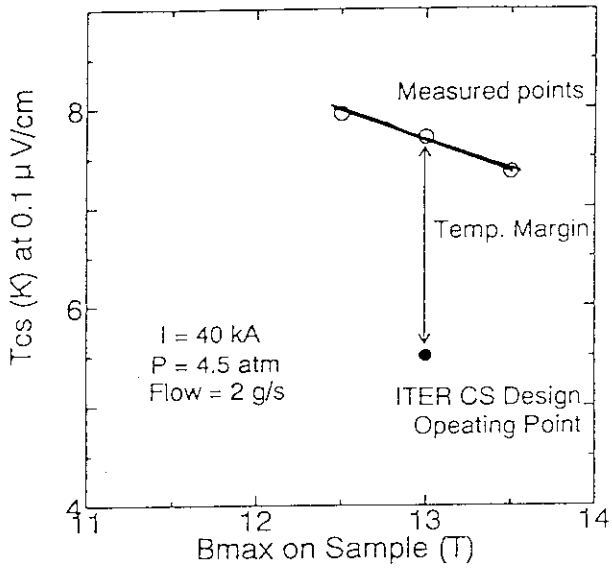

Fig. V.2.2-3 Results from Tcs measurements

2.3 Cryogenic system

2.3.1 Common test facility

A cryogenic system is one of the key systems in the common test facility, which is required to perform the following major criteria;

(1) To cool the CS model coil (around 150 tones) down within 20 to 40 days,

(2) To supply supercritical helium (0.6 MPa, 4.5 K) of 350 to 500 g/s to the CS model coils,

(3) To continue the pulse operation (10,000 cycle) of the coil for around 3 months.

In order to satisfy the above criteria, the capacity of the helium cryogenic system has been determined as the refrigeration capacity of 5 kW or the liquefaction rate of 800 L/h. This system is reliable by adopting Claude cycle with two turbines, liquid-nitrogen pre-cooling, and a double Joule-Thomson (JT) valve system as shown in Fig. V.2.3-1. The general configuration of the cryogenic system is shown in Fig. V.2.3-2. The coil cooling flow is hydraulically separated from the cold box as shown in the figure to avoid the transient heat induced by the coil on quench or rapid pulse operation. The hatched components are newly fabricated and the others are the re-installation components from the existing cryogenic system. Re-installation was carried out to consider whether an existing component is applicable for the required refrigeration operation of the CS model coils. The specification of the key components of the system are listed in Table V.2.3-1.

Table V.2.3-1 Specification of main components

Component	Specification
Cold box*	Claude cycle with double J-T valves Refrigeration power: 5 kW at 4.5K, Liquefaction rate: 800 L/h
Compressor*	Screw type, Oil injection Low press. stage: 3 units, High press. stage: 1 unit Mass flow rate: 750 g/s (max.) Isothermal efficiency: more than 55%
Liquid helium tank	20,000 liter
Buffer tank	700+200 m^3 at 2.06 MPa
Cryogenic pump unit	Centrifugal pump Mass flow rate: 500 g/s at 4.5K ,0.6 MPa,(rated) Pump head: 0.25 MPa (max.)
Gas purifier	Mass flow rate: 20 g/s

The superscript "*" means the new components. The others are the re-installation components.

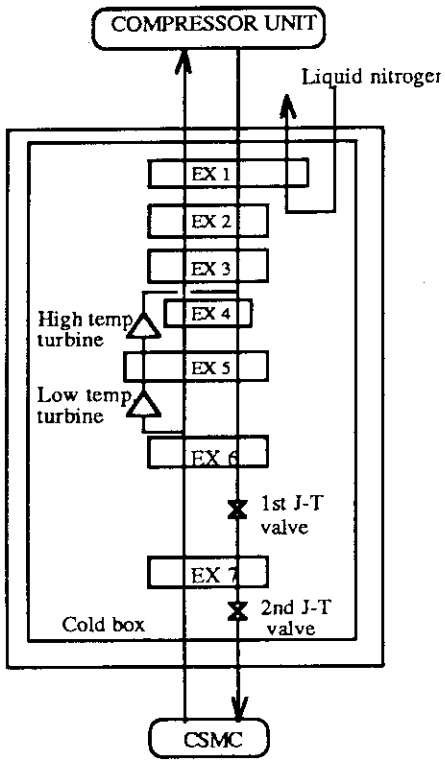

The superscript "*" means the new components.

Fig. V.2.3-1 Cold Box Process Diagram

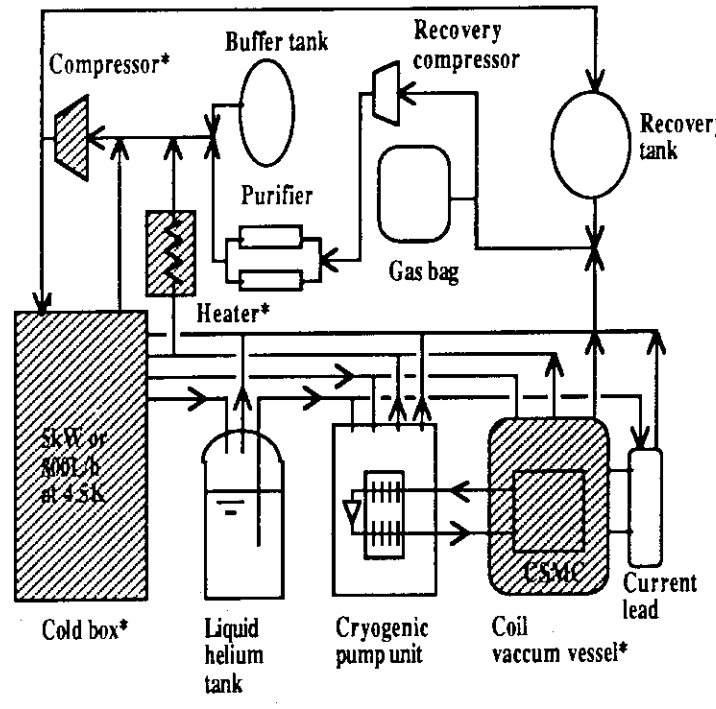

The others are the re-installation components.

Fig. V.2.3-2 General configuration

2.3.2 Vacuum chamber and vacuum pump system

A vacuum chamber and vacuum pump system in the common test facility have been installed in the experimental building as shown in Fig. V.2.3-3. The requirements for the vacuum chamber and vacuum pump system are as follows;

(1) To be exhausted to an order of 10^{-5} Torr within 7 days,

(2) To provide a cylindrical space (4.2m in diameter and 5m in height) for the CS model coil,

(3) To have a thermal radiation shield wall cooled at liquid nitrogen temperature.

The vacuum chamber consists of three parts divided in the vertical direction for transportation. It has about 6.5 m in diameter and about 9.5 m in height. The cylindrical space, which is about 5.5 m in diameter and 5 m in height, is available for the CS model coil. The configuration of the vacuum chamber and vacuum pumps are shown in Fig. V.2.3-4. Vacuum pumps are composed of a oil diffusion pump, a roots pump and two rotary pumps. The specifications of the pumps are listed in Table V.2.3-2. The vacuum chamber is equipped with 80-K thermal radiation shield wall composed of 99 panels with many of liquid nitrogen cooling channels. This wall is made of stainless steel and is separated into four sections in the circumferential direction to reduce the resistive heating due to eddy current.

Table V.2.3-2 The specifications of pumps

	Diffusion pump	Roots pump	No.1 Rotary pump	No.2 Rotary pump
Rated achieved Pressure (Torr)	210-7	510-4	510-3	510-4
Rated Exhaust velocity (Litter/sec)	4104	555.6	250	20

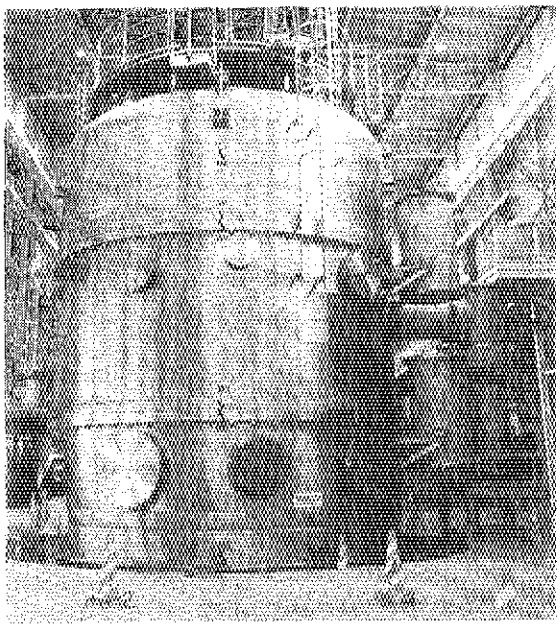

Fig. V.2.3-3 Vacuum Chamber installed in the Experimental Building

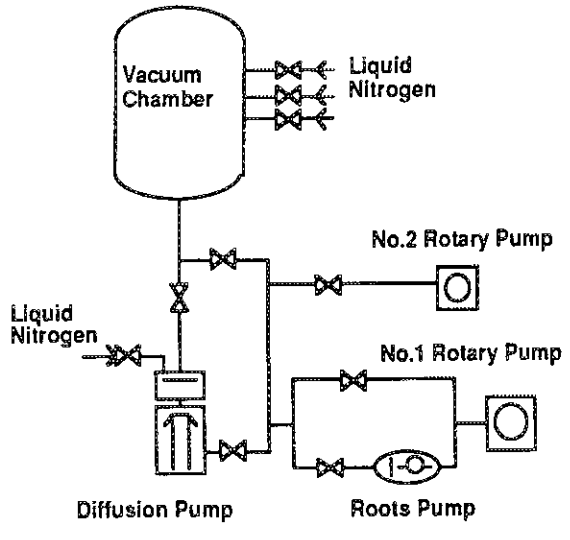

Fig. V.2.3-4 The configuration of the vacuum chamber and vacuum pump system

2.3.3 Power supply system

Power supply system for the common test facility is composed of newly fabricated components (50-kA and 30-kA DC supplies, a 50-kA, 10-kV DC circuit breaker, a 1-GJ discharging resistor, and 50-kA Aluminum busbars) and the existing components (30-kA DC power supply, JT-60 pulse power supplies, a 30-kA, 1.5-kV DC circuit breaker, a 110-MJ discharging resistor, and 30-kA Aluminum busbars). The outline of the electrical circuit and the power supplies are shown in Fig. V.2.3-5. Two electrical circuits, whose capacities are DC 50 kA and 60 kA at regular intervals, are prepared to energize the CS model coil and the insert coil individually. The installation and performance test of 50-kA and 30-kA power supplies will be completed as the first components in the common test facility at the end of July 1994.

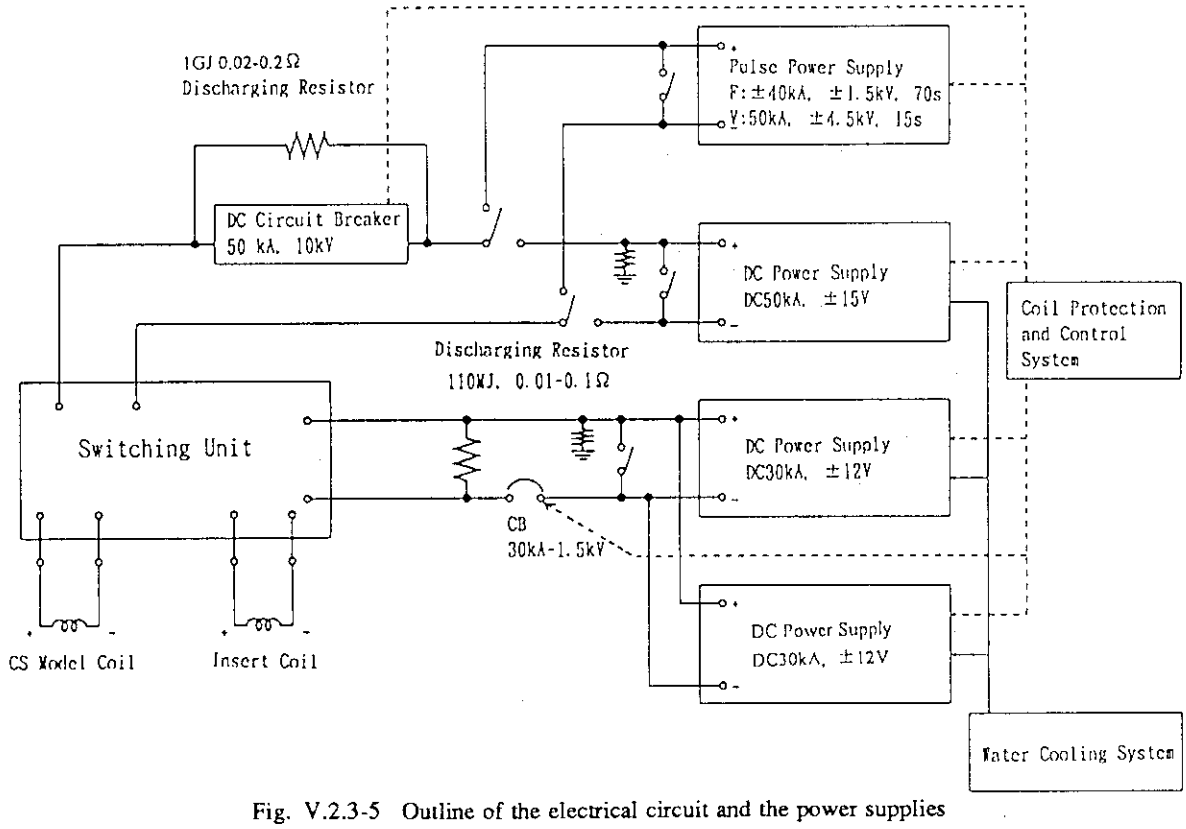

Fig. V.2.3-5 Outline of the electrical circuit and the power supplies

2.4 Development of advanced Nb_3Al conductor

Nb_3Sn strand is mainly used for present high-field superconductors. However, its critical current is very sensitive to a mechanical strain. In a tokamak fusion reactor, the conductors in a toroidal field coil are subjected to a strain due to very strong electromagnetic force during operation and due to different thermal expansion between strands and components of the coil during a cool-down. The Nb_3Sn strand has therefore difficulty in application to the toroidal field coil, because of large degradation of its critical current. On the other hand, Nb_3Al is not so sensitive to strain compared with Nb_3Sn. Typically, the degradation of the Nb_3Al strand is one-

fifth of that of the Nb_3Sn strand. Moreover, its intrinsic critical temperature and critical field are superior to that of Nb_3Sn. One problem of Nb_3Al is difficulty of its fabrication.

JAERI started to develop Nb_3Al strand from 1984, aiming at the application in the toroidal field coil. For the application to the magnet in a fusion reactor, long strand having a high critical current should be fabricated by overcoming the manufacturing difficulty. Figure V.2.4-1 shows a history of the development of the Nb_3Al strand in JAERI in the viewpoint of the critical current and strand length. 800 A/mm^2 non-Cu at 12 T in the critical current and 7 km in the strand length could be achieved. According to these results, it is demonstrated that Nb_3Al can match Nb_3Sn for the critical current performance and is applicable to a fusion machine.

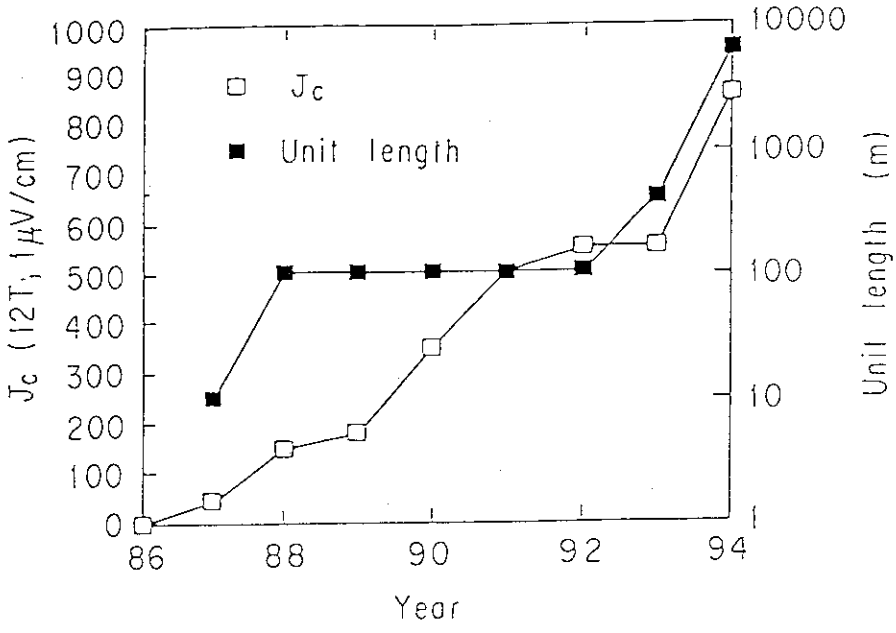

Fig. V.2.4-1 Developing history of Nb_3Al

2.5. Design of ITER coils

The following two design works were performed in this period.

(1) CS coil

The concept of International Thermo-nuclear Experimental Reactor (ITER) magnet system was proposed by the Joint Central Team (JCT). JCT also proposes that CS coil is fabricated by using the layer-winding method as shown in Fig. V.2.5-1. The layer-wound CS coil needed the investigation of the manufacturing feasible study and the cost estimation, because this type of large-size coil has not been fabricated until now. Other hand, Japan home team had designed the pancake-wound CS coil under the task agreement with the JCT in this period, in oder to compare with the layer-wound CS coil which is proposed by the JCT, as shown in Fig. V.2.5-1.

The stress level of both concepts, layer and pancake, was in the same level. From the view point of the maintenance of the coil system, however, the JCT selected the layer-wound CS coil.

(2) Fault analysis

Fault stress analysis was carried out to investigate the magnet safety. The finite element model, used in this analysis, is shown in Fig. V.2.5-2. Full Tokamak is modeled and consists of 24-toroidal field(TF) coils, CS coil, and a mechanical structure.

Two load conditions, during abnormal operation, were analyzed as follows;

(a)Short circuit mode: One TF coil is over current and can not be discharged.

(b)Open circuit mode: One TF coil is discharged.

These results are listed in Table V.2.5-1. In the short circuit mode, the maximum displacement of the TF coil is 130 mm from the position after cool down. This is found at the equatorial plane of the outer leg, and the direction of the displacement is in plane of the coil. In the case of the open circuit mode, the maximum displacement of the TF coil is 96 mm from the position after cool down. This is also seen at the equatorial plane of the outer leg. And the direction of the displacement is out of plane of the coil. Large stress appears in the TF coils, but this value is smaller than the yield strength of the structural material. Therefore, the failure will not occur in these conditions.

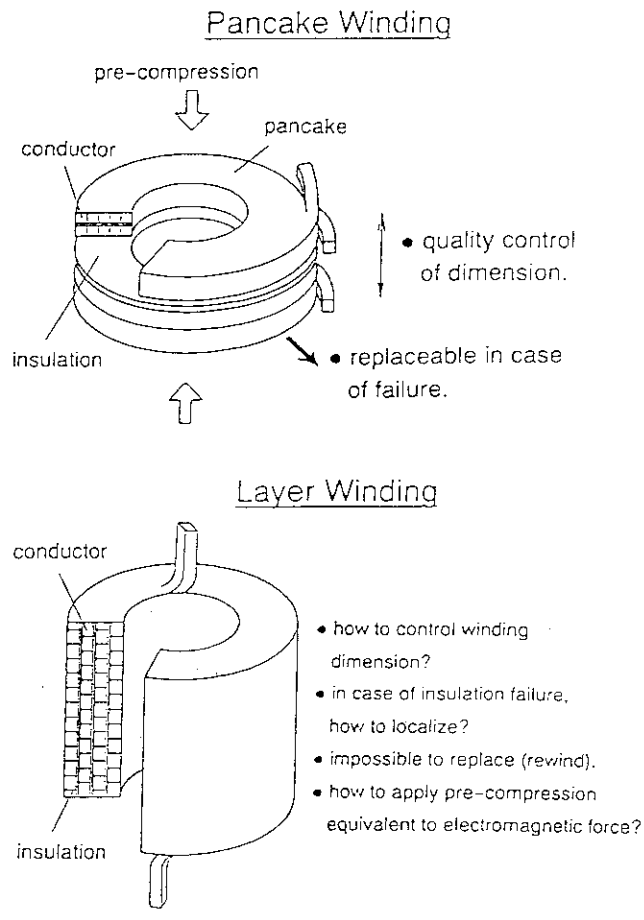

Fig. V.2.5.-1 Concept of Pancake winding and Layer winding

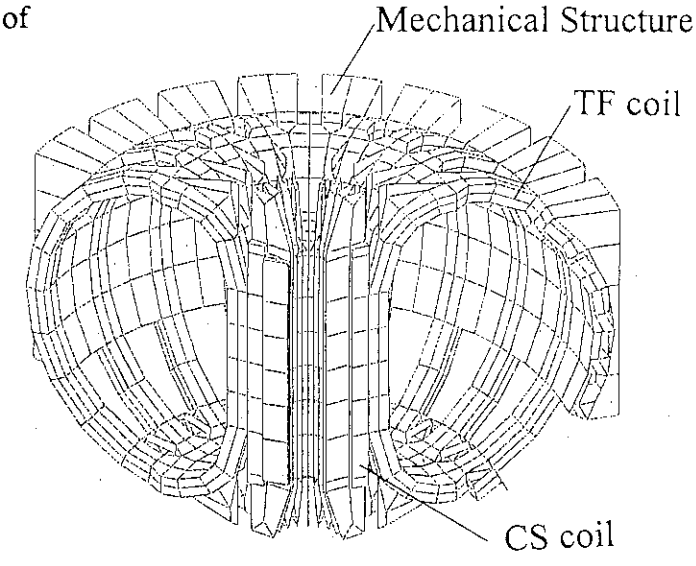

Fig.V.2.5-2 Finite element model for fault stress analysis

Table V.2.5-1 Results of the fault stress analysis

	Short circuit mode	Open circuit mode
Max. displacement -Position -Direction	130 mm from Cool down -Equatorial plane of the outer leg -In plane of the coil	96 mm from Cool down -Equatorial plane of the outer leg -Out of plane of the coil
Max. Tresca stress	922 MPa	652 MPa

3. Beam Technology

3.1 Introduction

A negative-ion-based neutral beam injector (N-NBI) system is one of the promising candidates for heating, current drive and current profile control device for fusion reactors such as JT-60U and ITER. R&D activities on negative ion sources producing high current, long pulse and high energy beams have been performed energetically to realize the system.

On the other hand, a high current low energy ion source and a high brightness ion source have been developed as applications of ion beam technology for neutral beam injectors.

3.2 Negative ion beam technology

3.2.1 Development of a negative ion source for the JT-60U N-NBI

(1) Manufacture and test of the negative ion source for the JT-60U N-NBI

The N-NBI system for JT-60U is under construction for experiments of current drive and heating of high density core plasma [3.2-1]. The system requires a high power negative ion source which can produce 500 keV, 22 A D^- ion beams for 10 s with a current density of 13 mA/cm^2 and a beam divergence of less than 5 mrad. The negative ion source has been designed and manufactured based on R&D results at JAERI [3.2-2].

A cross-sectional view of the ion source is shown in Fig.V.3.2-1. The overall size is 2 m in diameter and 1.7 m in height. D^- ions are produced in a Cs seeded multi-cusp plasma generator, which has a semi-cylindrical shape with

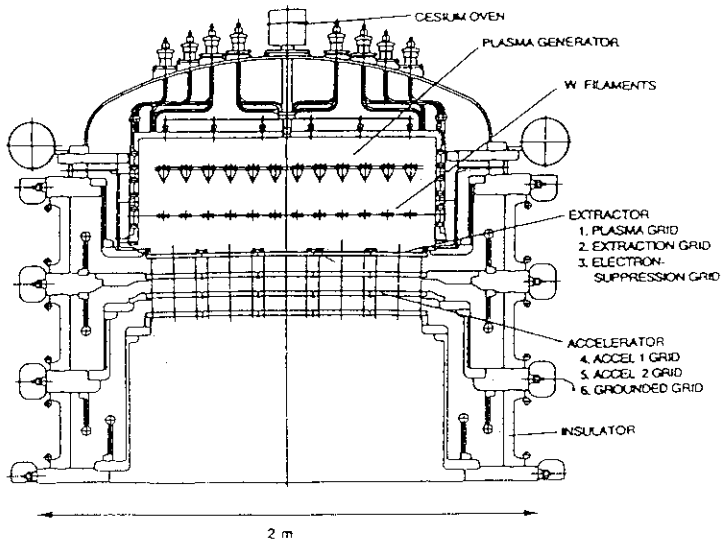

Fig.V.3.2-1 A cross-sectional view of the negative ion source for the JT-60U N-NBI

64 cm in diameter and 122 cm in length. A new type magnetic filter, called PG filter, is adopted to produce a uniform filter field within a large extraction area of 45 cm x 110 cm^2. The D^- ions are extracted in a multi-aperture extractor. The extractor consists of the plasma grid, the extraction grid and the electron suppression grid. Each grid is divided in five segments, each of which has 216 apertures of 14 mm in diameter.

The D^- ions are accelerated with a multi-stage, multi-aperture electrostatic accelerator. The accelerator has three acceleration stages. The gap length is 75 mm, 65 mm and 55 mm from the side of the extractor, respectively. The diameter of the aperture is 16 mm.

An initial test has been started since 1993 using the plasma generator and one segment of the extractor. It was confirmed that the source plasma is generated uniformly at a low operating pressure of 0.3 Pa, the design value of the JT-60U ion source. The negative ion beams were extracted with a good beam optics from the central segment. An overall test combining the plasma generator and the accelerator will start from the end of 1994.

(2) High energy acceleration of the negative ion

The beam acceleration experiment has been performed with the up-graded 350 keV three-stage electrostatic accelerator. Basic structures of the accelerator, such as the gap length, the aperture size and the number of acceleration stages are the same as those of the JT-60U ion source except for a number of apertures. A H^- ion beam of a current of 0.18 A was successfully accelerated up to 400 keV for 1s with a good beam optics of 6 mrad. The corresponding H^- current density is 13 mA/cm^2, which is almost the same level of the required current density of the JT-60U ion source.

3.2.2 Construction of a MeV test facility [3.2-3,4]

The most important issue to realize the NBI system for future fusion reactors such as ITER is the negative ion acceleration. A MeV Test Facility (MTF) is designed to accelerate ampere class ion beams up to the energy of 1 MeV, the beam energy required in the ITER NBI system. This is the only one facility in the world that can test a high energy acceleration of ampere class ion beams.

A bird's-eye view of the MTF is shown in Fig.V.3.2-2. The MTF is composed of a prototype accelerator, power supplies and auxiliary systems such as a cooling water system and a vacuum

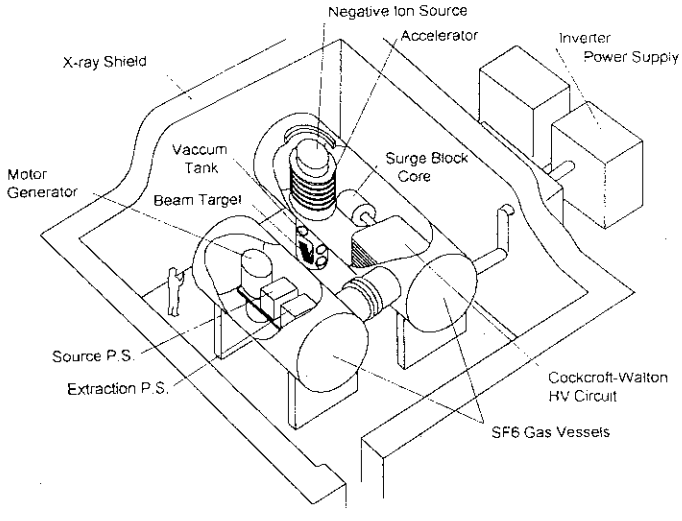

Fig.V.3.2-2 A bird's-eye of a MeV Test Facility

system. Most of them are located in the X-ray shield pit covered with concrete wall whose thickness is 80 ~ 100 cm. For the high voltage insulation, the power supply system and the prototype accelerator are installed in two pressurized tanks filled with SF_6 of 0.6 MPa.

The accelerator power supply is a Cockcroft-Walton type DC high voltage generator driven by a 3 kHz inverter system. A capacity of the DC generator is 1MV, 1 A, 60 s with a duty cycle of 1/60. Power supplies for negative ion generation and extraction are composed of a cathode, an arc, a bias, an ion extraction, and an electron suppression power supplies. These power supplies are mounted on a high voltage platform insulated from the ground, and driven by a motor generator of 100 kVA.

The prototype accelerator was designed to produce 1 MeV, 1 A hydrogen negative ion beams for 60 s with a current density of 13 mA/cm^2. Fig.V.3.2-3 shows a cross-sectional view of the accelerator. The accelerator is composed of a semi-cylindrical plasma generator, an extractor, and a five-stage electrostatic accelerator. Acceleration voltage of 200 keV is supplied in each acceleration stage. Each gap length is designed to be shorter in the downstream stages, so that the electrostatic fields are stronger in the downstream stages, which forms a focussing electrostatic lens.

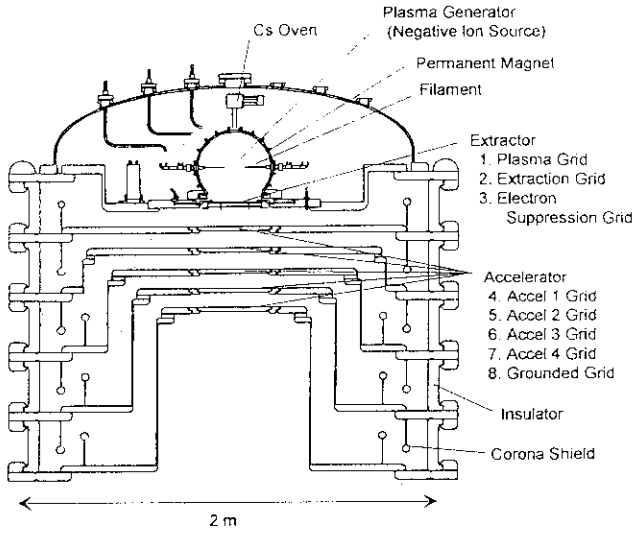

Fig.V.3.2-3 A cross-sectional view of the prototype accelerator

Construction of a control room and the X-ray shield pit was completed in January 1993. Manufacture of the power supplies, the accelerator, the vacuum system and the cooling system has been continued, and the MTF is scheduled to be functional in May 1994.

3.2.3 Development of multi-single type extractor / accelerator [3.2-4]

Two types of accelerators have been proposed for the ITER-NBI system by JAERI. One is a conventional "multi-multi" type extractor / accelerator, the other is "multi-single" type. A conceptual illustration of both types of extractor / accelerators is shown in Fig.V. 3.2-4. An experiment of the "multi-single" type extractor / accelerator was carried out under a US-Japan collaboration, where a JAERI ion source was combined with a LBL's ESQ (electrostatic quadrupole) accelerator. In the experiment, a merging system with an extractor composed of semi-spherical grids were used to merge multi-beamlet into a high current single beam to inject the ESQ accelerator. A merged H^- beam extracted from 19 apertures was successfully accelerated up to 200 keV in the ESQ accelerator with a current of 100 mA.

3.2.4 Study on a mechanism of negative ion production [3.2-6]

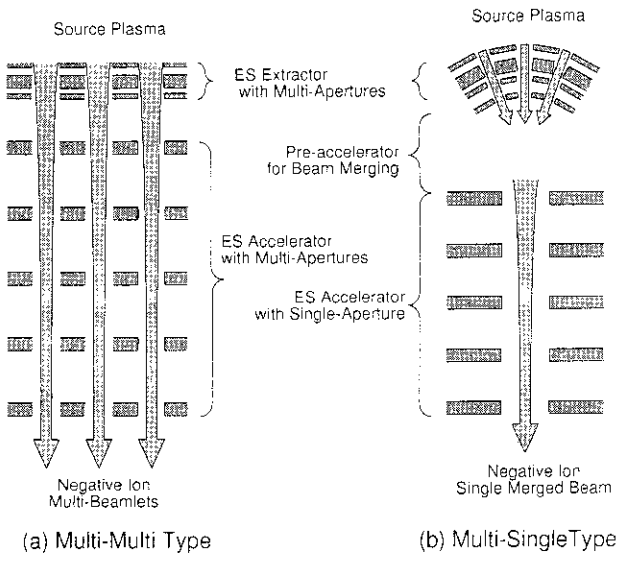

A negative ion yield in a volume-production-type source is enhanced by seeding Cs. This has been considered to be due to the surface production on a plasma grid that has a low work function because of the Cs coverage. To illuminate the mechanism of the negative ion yield enhancement, a correlation between a negative ion current and the work function was investigated. The work function was measured using Ar^+ laser. The negative ion current increased significantly when the work function decreases below 2 eV, which confirms the negative ion yield enhancement is due to the surface production.

References

[3.2-1] Kuriyama M., Akino N., Araki M., et al., in Proc. 15th Symp. on Fusion Engineering, Hyannis, USA, (1993) 470.
[3.2-2] Okumura Y., Hanada M., Inoue T., et al., in Proc. 15th Symp. on Fusion Engineering, Hyannis, USA, (1993) 466.
[3.2-3] Ohara Y., Hanada M., Inoue T., et al., Proc. 5th International Conference on Ion Source, Beijing, (1993) 1159.
[3.2-4] Inoue T., Hanada M., Maeno S., et al., "Design study of prototype accelerator and MeV test facility for demonstration of 1 MeV, 1 A negative ion beam production", JAERI-Tech 94-007 (1994).
[3.2-5] Inoue T., Miyamoto K., Mizuno M., et al., Proc. 15th Symp. on Fusion Engineering, Hyannis, USA, (1993) 474.
[3.2-6] Shinto K., et al., to be submitted for publication.

3.3 Application of high current ion beam technology

3.3.1 Development of a high current low energy ion source

An ion source producing high current ion beams at a low energy was developed for studies on plasma-surface interaction. Moreover, it is applicable to an industrial field such as the thin film formation or the semiconductor process.

A new type electrode producing high current density even at a low energy was designed. A schematic of the ion source is illustrated in Fig.V.3.3-1. This electrode is designed to be a slit structure to enhance the transparency. It is composed of 100 tungsten wires of 0.5 mm in diameter arranged at intervals of 1.0 mm. The space between two electrodes is 0.7 mm. Such a narrow space makes it possible to form the strong electrostatic field, and high current ion beams can be extracted even at a low energy of a few hundred volts. Each wire is pulled by springs to absorb the thermal expansion. A hydrogen ion beam of 100 ~ 300 eV, 1 A beam was produced using this electrode.

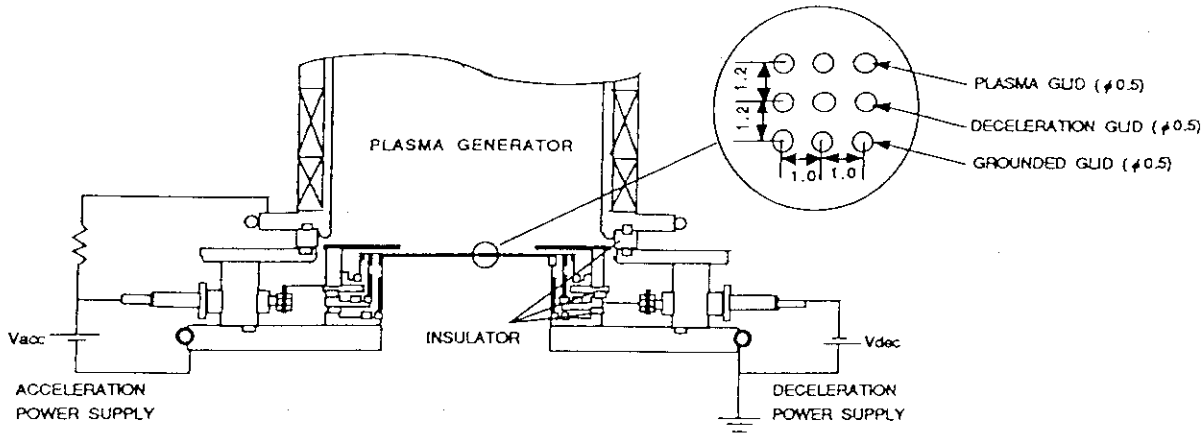

Fig.V.3.3-1 A schematic of the high current low energy ion source

3.3.2 Development of a high brightness ion source for the proton linear accelerator

A prototype ion source has been developed for the 10 MeV, 10 mA, CW proton linear accelerator called Basic Technology Accelerator (BTA) at JAERI. The required performances of the source are 100 keV, 120 mA and a normalized emittance of as low as 0.5 p mm.mrad (90%).

A 100 keV, 140 mA hydrogen beam was successfully produced using the ion source by 1992, followed by a test of beam acceleration combining the ion source and a RFQ (radio frequency quadrupole) accelerator. The ion source was operated very stably at 100 keV and a proton beam was successfully accelerated up to 2 MeV with a current of 51 mA by the RFQ

References

[3.3-1] Maeno S., Nakamura K., Okumura Y., et al., Proc. 4th Symp. on Beam Engineering of Advanced Material Syntheses Including Bio-Medical Materials and Treatments, Tokyo, (1993) 19.

4. RF Technology

4.1 Introduction

Radio-frequency (RF) wave is a key tool for heating and current drive of the tokamak fusion reactor. The R&D of RF technology is indispensable to establish the engineering base for ITER and next generation tokamaks. Developments of high efficiency RF source for Electron Cyclotron Heating (ECH) and Lower Hybrid Current Drive (LHCD), and high performance Launching system for LHCD and Ion Cyclotron Heating (ICH) are the main efforts of JAERI RF Technology. The major activities in FY 1993 are the development of high power gyrotron at 100GHz band aiming at 1 MW, CW gyrotron required in ITER, high efficiency 5 GHz klystron, Japan-France cooperative experiment on LH launcher module for the next generation tokamak, new concept ICRF antenna and cryo-window for ECH. The most significant achievement is the successful power generation of 410kW, 1.3 sec from the developed gyrotron at 110GHz.

4.2 High power gyrotron and ECH component

The gyrotron development started in JAERI from 7 years ago and key technologies for the high power long pulse gyrotron have been obtained one by one. They are whispering gallery mode cavity, mode convertor into the Gaussian like beam mode, beam sweeping collector and double disc window. The long pulse gyrotron was fabricated in 1992, which has the oscillation mode of TE22,2 whispering gallery mode at 110GHz with mode convertor. In 1993, the behavior of the electron beam was studied and the optimum operation condition was found. As a result, the pulse extension of a 110GHz gyrotron was successfully performed. In Fig.V.4.2-1, the output energy vs. the pulse duration is shown. The output energy increases linearly with the pulse duration, which indicates the very stable oscillation. The maximum output energy exceeds the 0.5MJ[4.2-1].

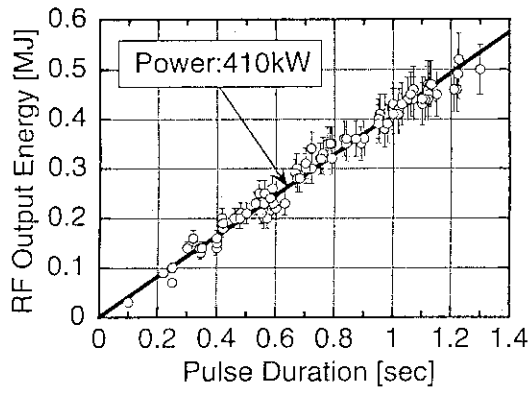

Fig.V.4.2-1 Output energy from the long pulse gyrotron

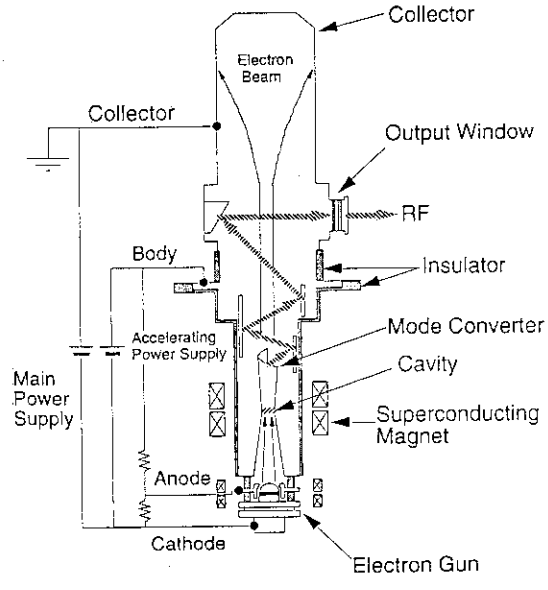

Fig. V.4.2-2 The principle of CPD gyrotron

One more key technology for ITER gyrotron is the efficiency enhancement using the energy recovery technique. By taking into account the experimental results, the gyrotron of 500kW level with the energy recovery system was designed and fabricated. In Fig.V.4.2-2, the conceptional picture of the gyrotron with the energy recovery system and the power supply system is illustrated. The oscillation mode is also TE22,2 mode, however, the cavity is improved to increase the efficiency. The body section is covered by the insulation jacket and the long ceramic insulator is installed between the body and the collector, which make it possible of the high voltage application up to 50kV. Then, the retarding voltage for the energy recovery appears between the collector and the body section(CPD: Collector Potential Depression). The decelerated electron beam energy is recovered by the power supply system electrostatically, which will bring a drastic improvement of the gyrotron efficiency. The initial oscillation experiment was performed, and the 750kW output at 1msec was attained. The efficiency was ~30%. The

simulation indicates that the efficiency of 30% is improved up to 50% by the application of CPD, which will be tested in the experiment of 1994.

The preliminary test of the high power RF injection into a cryogenic cooled window was done. The window material, sapphire, has characteristics that the RF absorption coefficient decrease significantly as the window temperature does. The sapphire was cooled to ~13degrees Kelvin using the cryogenic refrigerator. The RF power of ~400 kW was injected up to 1sec. The data seem to indicate that the RF absorption coefficient increases with the temperature. More detail experiment will be done in 1994.

4.3 LH development

LHCD has been showing the best performance of current drive and current profile control experiments in the present day tokamaks. Development of a launcher, however, is required for its application to a steady-state tokamak reactors, because the launcher must stand high-heat flux under the reactor environment and should radiate high-RF power stably. The simplification of the launcher system is a key to realize the reactor relevant launcher. For this purpose, a new concept LH module has been proposed. This module is made from dispersion strengthen copper which has high-mechanical property even in high temperature and high-thermal conductivity for heat removal. The module is featured by RF-power dividing in both directions as shown in Fig. V.4.3-1, RF-power is divided in the poloidal direction using mode converter technique and in the toroidal direction by E-plane multijunction technique. This feature allows to reduce RF-power density in front of plasmas due to large cross-section with large waveguides number, and leads to stable power injection. Moreover optimized spectrum is expected by changing adjacent phase between main waveguides and the spectrum is advantage to current profile control. The test of this new module is planned in Cadarache test stand under the collaboration between Japan and France.

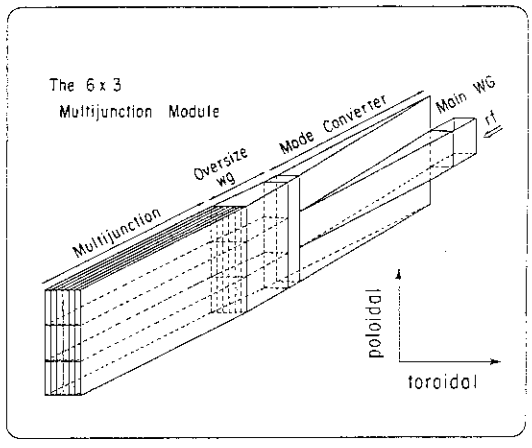

Fig. V.4.3-1 Poloidal mode convertor module

One of the key components of the LHRF system is the high power tube of 1 MW level at 5-10 GHz. The target of the tube in ITER CDA is the RF efficiency of more than 60 % and the RF output power of more than 700 kW with CW operation. As a first step to achieve this goal, the prototype klystron has been developed to evaluate the performance of the hollow beam for efficiency enhancement. RF efficiency of near 60% and RF output power of 700 kW is obtained.

4.4 ICRF launcher

Developments of antenna elements for the ion cyclotron range of frequencies (ICRF) have been performed on three items, that is, a traveling wave antenna, a back Faraday shield and all metal supports.

RF properties of the mock up spiral antenna has been tested at low power level, where the spiral antenna is a kind of traveling wave antenna for fast wave current drive (FWCD) experiments. VSWR of spiral antenna is pretty low (below 1.33) at the wide frequency range from 25 MHz to 201MHz. Back Faraday shield is a new concept element for decreasing heat load on Faraday shield and improving coupling properties of ICRH and FWCD antennas. FWCD antenna with back Faraday shields made of titanium have been installed in JFT-2M, for checking coupling properties and stand off voltage. All metal helical support and the ridge waveguide feeder support have been being developed, since neutron damage on the antenna in future machines demands all metal structure for antenna.

4.5 Millimeter wave free electron laser

A construction of 2MeV induction accelerator was completed.[4.5-1] Parameters of the induction linac are; beam energy: 2MeV, beam current: 5kA, and pulse width: 160ns.

Primary characteristic of the accelerator is that the pulse form is tunable by changing the capacitance of the pulse forming line. Fig.V.4.5-1 shows a schematic view of the tunable capacitor which is placed in the pulse forming line. Figure V.4.5-2 shows experimental cold test results of voltage wave form for each of the ramp-up, ramp-down , and normal case. With suitable choice of the voltage wave form will compensate the changeof the impedance of the electron beam during the pulse.Millimeter FEL experiment between 30GHz-300GHz will start in 1995.

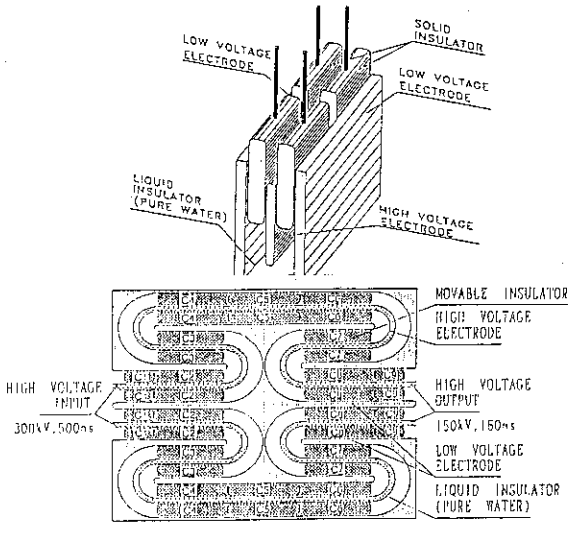

Fig.V.4.5-1 Detailed structure of the tunable capacitor

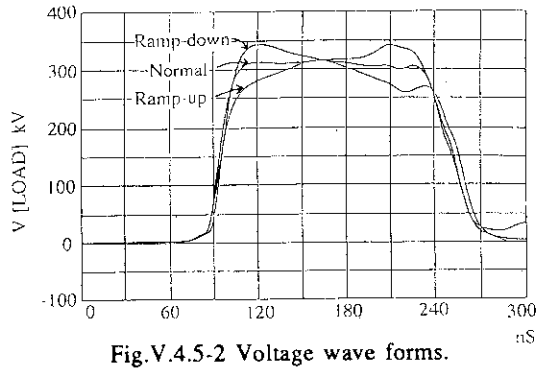

Fig.V.4.5-2 Voltage wave forms.

References

[4.2-1] Kasugai A., Sakamoto K., Tuneoka M., et al., in Proc. of 5th Int. Toki Conf., on Plasma Physics and Cont. Nucl. Fusion, Toki, 1993.

[4.5-1] Shiho M., Kawasaki S., Sakamoto K., et al., Nucl. Instr. Meth. in Phys. Res. A341(1994) 412

5. Tritium Technology

Continuous efforts were paid to the improvement of developed tritium technology in TPL. Additionally, some new and important activities were initiated in tritium processing technology and tritium safety & accountability technology in this year.

In the development of tritium processing technology, the plasma exhaust stream under non-steady tokamak operation was demonstrated by the developed system under collaboration between Japan and US/DOE (extended Annex IV). Experimental and design works on the tritium processing system, including the fuel cleanup system, isotope separation system, blanket tritium recovery system and tritiated water reprocessing system, were performed to meet with the requirement of the ITER specification.

In the development of tritium safety & accountability technology, the small scale gas separation perimeter module with polyimid membrane was fabricated and submitted to the preliminary experiments. Also, the metal bed type tritium transportation container was licensed and shipped to CRNL in Canada for loading of tritium. Other basic research experiments were performed on the tritium safety confinement, tritium and tritiated compounds concentration measurement and accounting, tritium - material interaction and tritiated waste treatment. Safe operation of TPL tritium facility, itself, is the on-sight valuable experience that proves the ability of safe handling of tritium. The annual environmental dose from TPL was less than 5×10^9 Bq/year that is extremely low release to the environment. The improvement effort was also paid to the safety system for achieving as safe tritium handling as possible, too.

5.1 Development of tritium processing technology under US-Japan collaboration

One of the major subjects of the extended Annex IV were to test the integrated tritium processing technology for non-steady operation of tokamak reactor. In the early stage of the fusion reactor, pulsed operation might be the practical operation mode. Various non-steady conditions for fusion fuel processing were simulated in the "non-steady experiments" using TSTA fuel processing loop[5.1-1]. Typically, pulsed operation of tokamak will involve : start up of process loop, pulsed fuel feed and exhaust with ramp up, flat-top, and ramp down, discharge cleaning and/or conditioning pulses and baking, shut down and recovery of tritium from the fuel processing system. TSTA loop was operated to simulate fuel processing in above modes with changing flow rates and composition, processing intermittent impurities and supply and recovery of tritium. Figure V.5.1-1 shows the basic experimental configuration of "non-steady" experiments at TSTA.

As the results of the simulated non-steady experiments, over-all the TSTA processing loop was found to be flexible to accept changing throughput, various impurity modes and producing various isotopic streams. Automatic control of ISS columns and effectiveness of side stream recycle for this purpose were verified. JFCU process demonstrated the versatile processing

modes and configuration to be suitable for various operation needs including avoiding generation of water. The results experimentally proves the advantages of ISS multi-column cascade configuration and JFCU palladium diffuser-catalyst-electrolysis combination in a practical fusion fuel loop under non-steady conditions with reactor relevant scale and quality.

Reference

[5.1-1] Konishi S., Yamanishi T., Enoeda M., et al., "Operation of a simulated Non-steady Tokamak Fuel Loop Using the Tritium Systems Test Assembly", 3rd Intl. Symp. Fus. Nucl. Technol., Los Angels, June 94.

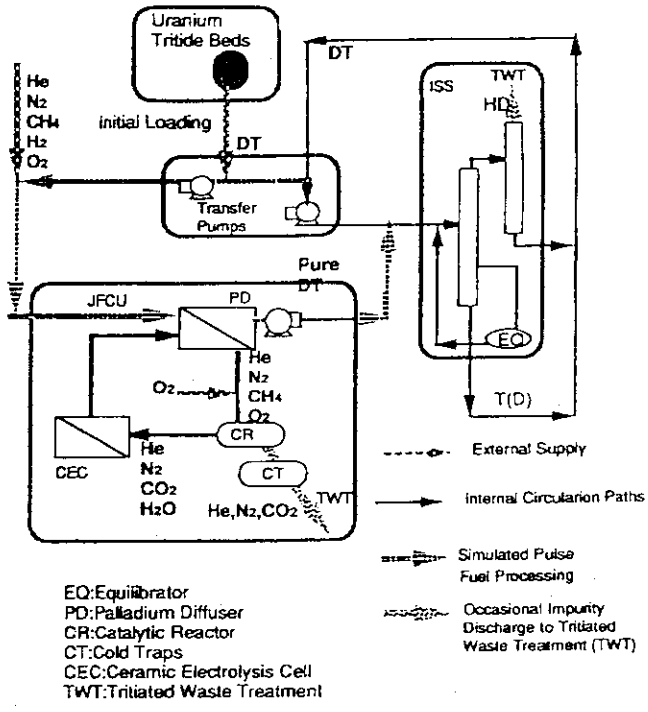

Fig. V.5.1-1 Basic Configuration of Non-Steady Experiments by TSTA Fuel Loop.

5.2 Development of tritium processing technology in TPL

The experiments on fusion fuel cycle, which are the fuel cleanup, isotope separation, and tritium recovery system from breeder blanket, have been carried out at the TPL.

In the fuel cleanup system, the ceramic electrolysis cell that decomposes water vapor (HTO), is one of the most critical components. The performance of the cell for the decomposition of the water was measured under various combinations of carrier gases and water vapor[5.2-1]. A modular type cell is also developed to make maintenance of the cell easy.

The system composed of four thermal diffusion columns has been operated to recover tritium from the hydrogen isotope mixtures used in the experiments at the TPL. One batch operation of the system needs a week, and three batch operations are required to get high purity tritium. Three batch operations are further required to obtain and exhaust the hydrogen isotopes that are essentially tritium free.

The operation method of the system was thus established. The separation factor of the thermal diffusion column can remarkably be increased by cooling the column wall with liquid nitrogen. In this fiscal year, some instruments such as a fumehood and an ion chamber were installed to initiate tritium experiments.

The Zr-Co compound developed by JAERI is presently used for the storage of hydrogen isotopes; it is sometime observed that the capacity of absorption of the hydrogen isotopes is decreased over iterative absorption and desorption. This phenomenon was investigated and fond

to be the reversible disproportionation. The new material composed of Zr-Co-Hf is developed and studied. It is expected to have improved characteristics against the disproportionation[5.2-2].

The R&D on the Breeding Blanket Tritium Recovery System was initiated with basic experiments with a bench-scale test stand. The Breeding Blanket Tritium Recovery System recovers tritium from the breeding blanket. In case of ITER/CDA, 117 kmol/h of helium purge gas flow with 0.1 % of H_2 is supplied to the breeder section, swamped . Tritium in the breeder is extracted to the purge gas flow by isotopic swamping from helium. Tritium concentration is estimated to be about 10 ppm in the purge gas. So the separation of hydrogen isotopes including tritium is the most important primary process in the breeding blanket tritium recovery system. There are several candidate processes for the separation of small amount of hydrogen isotopes from inert gas such as palladium membrane diffuser, metal bed scavenger and cryogenic molecular sieve bed (CMSB). However, the flow rate of the helium purge gas is extremely large and the concentration of hydrogen isotopes is relatively small compared to the torus exhaust gas flow. In such condition, CMSB process is more suitable than other candidate processes because of the simple operation and apparatus. This year, we focused on obtaining basic engineering data on adsorption of HT in excess H_2 (total 0.1 to 1 % of hydrogen isotopes, H/T= 1000) in bench scale (2 l/min) by using tritium. As shown in Fig. V.5-2-1, it is demonstrated that tritium was successfully recovered by CMSB. In this figure, dashed and solid lines represent H_2 and HT breakthrough curve, respectively. Computer simulation code was developed to evaluate the operation characteristics of CMSB. The developed code is regarded as the basic procedure for the design and operation analysis of CMSB in the breeding blanket tritium recovery system. Computer simulation analyses can give the values of separation factor and mass transfer coefficient of HT in H_2, which are very important basic parameters for the optimum design of CMSB process in the blanket tritium recovery system.

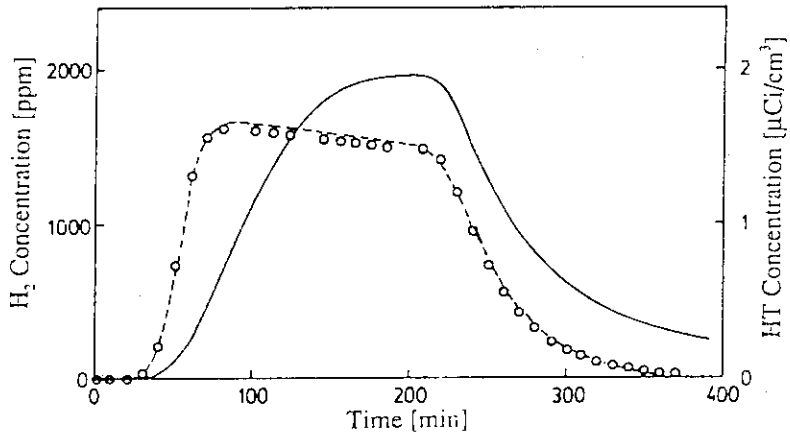

Fig.V.5.2-1 Example of Breakthrough Curve of H_2 and HT.

As the summary of this year's results, bench-scale apparatus for tritium experiment was established up to the flow rate scale of 2 l /min. The experimental value of the separation factor was obtained by tritium as 1.8 to 2.0[5.2-3]. Further study is necessary to obtain the dynamic characteristics of the CMSB. Additionally, scale up experiments will be necessary to confirm the basic experimental results.

References
[5.2-1] Hara M., Konishi S., Okuno K., et al., '94 Nihon Genshiryokugakkai
[5.2-2] Konishi, S., Nagasaki T., Okuno K., et al., "Improvement in ZrCo Based Tritium Storage Media.", 11th Topl. Mtg. Technol. Fus. Energy, June 94, New Orleans.
[5.2-3] Enoeda M., Kawamura Y., Okuno K., et al., "Recovery of Tritium by CMSB in BBI Condition", ibid.

5.3 Tritium system design and analysis

Development of computer simulation programs for the design of the fusion fuel cycle has been carried out. The simulation programs at the steady state operation have been provided for the major components of the fusion fuel cycle. A conceptual design of the fusion fuel cycle has been carried out by using the simulation programs. The designed system includes not only the main fuel cycle but also the tritium recovery from the breeder blanket and coolant. In addition, the designed system can process the exhaust gases from the plasma that is operated under various modes such as the pulse operations in a physics and a technology phase of ITER[5.3-1]. The next subject to be studied in the design of the fusion fuel cycle is clarified through this study.

Reference
[5.3-1] Okuno K., Konishi S., Yamanishi T., et al., "Conceptual Design of a Fuel Cycle Optimized for the Fussion Devices in Near Future.", 3rd Intl. Symp. Fus. Nucl. Technol., Los Angeles, June 94.

5.4 Development of tritium safety technology

In order to establish the public acceptable technology concerning the tritium safety for the D-T fusion experimental reactor, R&D activities were mainly focused and performed in this year on (1) the tritium removal & confinement, (2) the tritium accounting, (3) the tritium-material interaction and waste handling[5.4-1]. There were also carried out the development of tritium transport package and the design of a new caisson as a test stand of the global tritium safety demonstration.

The study of the compact tritium confinement system using gas separation membranes was continuously carried out in the TPL[5.4-2]. In order to search more effective gas separation membrane, the permeability and separation factor on the selected membrane such as polyimide and cellulose tri-acetate were measured with N_2, O_2, Ar, He, H_2, H_2/N_2 mixtures and water vapor. The effect of tritium exposure to the gas separation function was also investigated. Figure V.5.4-1 shows the temperature dependence of H_2 and N_2 permeation coefficients with the result after tritium exposure. Generally, the permeation coefficient of the above gases was large in the order of water vapor, He, H_2, O_2, Ar and N_2 through both membranes. From this figure, the permeability on cellulose tri-acetate was larger than that of polyimide. However, separation factor of H_2 from N_2 on polyimide was about 100 at 313 K and it was larger than that of cellulose triacetate (about 50). Concerning the tritium durability, the separation performance (permeation coefficient) of polyimide membrane did not decrease after the tritium exposure that corresponded

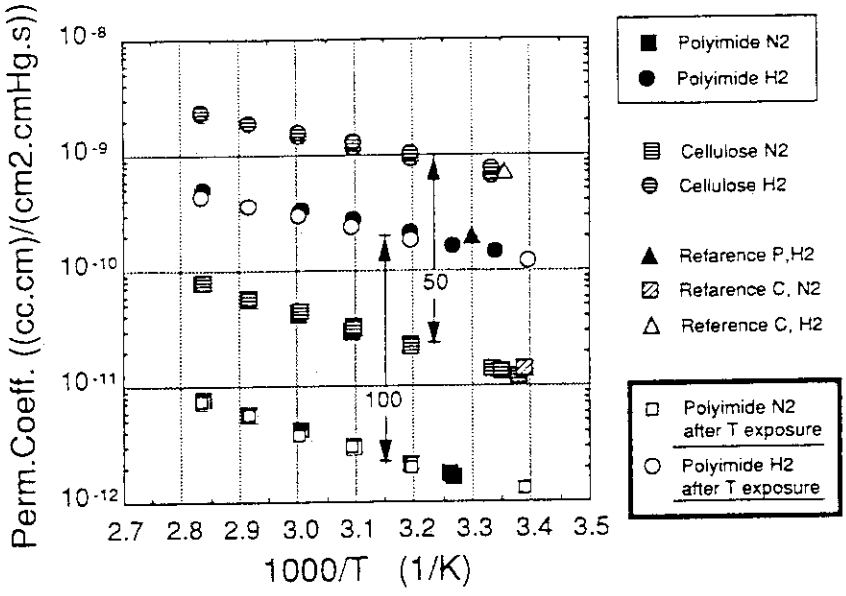

Figure V.5.4-1 H2 and N2 permeation coefficients with the result after tritium exposure (3000 Ci/m^3, 2 months)

to the maximum accumulated tritium exposure during the ITER life time. Therefore, polyimide membrane was more useful for the tritium confinement system.

Using the above result, a scaled gas separation membrane module, that made by hollow filament type polyimide, was fabricated and installed in a closed gas circulation loop for its gas separation performance test with tritium.

In order to develop more reliable and in-situ tritium inventory measurement technology, the study of in-bed gas flowing calorimetry was proceeded. A new experimental apparatus was installed as shown in figure V.5.4-2 and the cold test was started. This metal (ZrCo) bed has a storage capacity of 25 grams of tritium and the target tritium accounting sensitivity is 1 gram in the system.

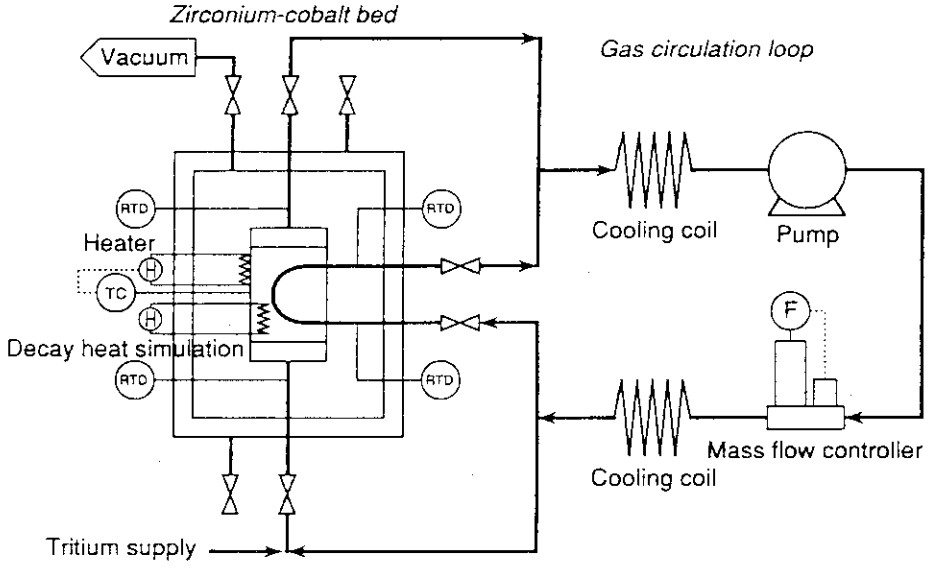

Fig. V.5.4-2 Schematic flow diagram of in-bed gas flowing tritium calorimetry system

As the research of the interaction between tritium and various materials and the research and development of recovery/ decontamination of tritium contaminated plasma facing material, some kinds of experiments have been carried out to accumulate data which will be used for safety evaluation of the ITER.

Using the apparatus for the tritium implantation/permeation experiments in the TPL, deuterium permeation experiments have been carried out. Permeation rates of deuterium implanted into V-alloy (V-5Cr-5Ti), Ti-Al and 316 stainless steel membranes were measured. Dependence of the permeation rate on temperature, incident ion beam flux and incident ion beam energy were investigated and the rate determining step of the respective permeation are resolved.

As the first step to develop techniques of tritium recovery/decontamination from the plasma facing materials, release behaviors of deuterium implanted by plasma exposure are investigated by thermal heating and photon irradiation methods to observe the chemical state and the release behavior of hydrogen isotopes in and from the plasma facing materials. The first series of experiments was one with high density isotropic graphite samples exposed to deuterium RF plasmas. Varying the sample temperature linearly with time from room temperature to 1473 K (temperature rising rate 5 - 100 K/min), the mass spectra of the released gas and those of deuterium (D_2) thermal deposition from the graphite samples were taken. According to the mass spectra obtained, the deuterium implanted into the graphite sample by plasma exposure was released in form of not only deuterium molecules (D_2) but also many sorts of hydrocarbons (C_nD_m). In the deuterium (D_2) thermal deposition spectra obtained by heating the sample, two kinds of peaks of the release rate were observed at different temperatures. From the temperature rising rate dependence of the peak shift, the activation energy for the state corresponding to each peak was calculated according to Redhead's theory of thermal deposition. The activation energies of the two different states obtained from the preliminary experiments are (1.90 Å} 0.15) eV for the peak around 800 K and (3.98 Å} 0.32) eV for that around 1250 K, respectively. Both desorption processes obeyed first-order kinetics apparently. The result shows that the rate-determining step of D_2 desorption from graphite is release of D atom/ion from a certain state in the bulk. And it can be said that the state with the lower activation energy corresponds to release of D from a trapped site and the other with the higher activation energy corresponds to that from a rather stable state which is likely to be a chemical bond between carbon and deuterium. As the next step, we are planing some experiments for decontamination of tritium, which is bonded weakly on the surface, by UV irradiation. And an ESCA spectrometer has been set up to get further detail information of the state of hydrogen isotopes in the plasma facing materials, and the preliminary experiments have started.

Using laser Raman spectroscopy, the research of reactions between tritium gas and various kind gases which may exist in the fusion reactor plant has been carried out. In case of the reaction of carbon monoxide and tritium investigated, the amount of tritium decreased at a half of initial one

after several hours while carbon dioxide increased, and solid fine particles of reaction product were observed.

In addition, concerning the development of tritium transport package (TPL-92Y-450K), a real shipping vessel was fabricated and the approval as a transport package was obtained from STA-Japan. The design of a new caisson was proceeded and the system concept was cleared as a test stand for the global tritium safety technology such as the compact tritium confinement system development and the studies on the behavior of tritium released into a room.

References

[5.4-1] Hayashi T. and Okuno K., Jour. Fus. Energy 12(1993)21-25.
[5.4-2] Hayashi T. and Okuno K., "Development of compacct tritium confinement system using gas separation membrane", 2nd Japan-China Symp. Mater. for Advanced Energy System aand Fission and Fusion energy, June 5-8 1994, Tokyo Japan.

5.5 Operation of tritium safety system

The safety system at TPL has been in tritium service since 1988 without any off-normal tritium release. The Glove box Gas Purification System (GPS) has been operated for 8,300 hours. The Effluent Tritium Removal System processed about 1000 m^3 of tritiated gas and recovered 1.6 x 10^{13} Bq of tritium this year. Also, the Air Cleanup System was operated for cleaning up 16,500 m^3 of the air during maintenance works. Newly installed "tritiated methane recombiner" was tested by using tritiated methane and gave more than 10^6 of decontamination factor. Figure V.5.5-1 shows the monthly environmental release record from TPL in this year. Total tritium release was less than 5 x 10^9 Bq which shows the very safe tritium handling technology of TPL.

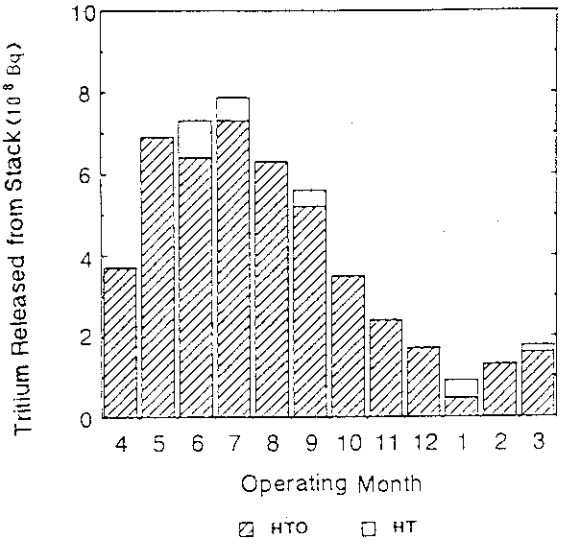

Fig. V.5.5-1 Monthly Release of Tritium from TPL in FY1993

6. High Heat Flux Technology

JAERI has been actively researching and developing plasma facing components (PFCs) for ITER (International Thermonuclear Experimental Reactor) and JT-60. The roles of the PFCs such as divertor plates and a first wall are to remove thermal loads from a fusion plasma and to protect in-vessel components against the high thermal loads. The PFCs are subjected to a high heat flux and a particle flux. In particular, the divertor plates are considered to be subjected to a severe heat flux of around 5 MW/m^2 in the EDA phase of ITER.

6.1 R&D's on divertor plates for ITER and JT-60 [6.1-1], [6.1-2], [6.1-3]

The ITER divertor plate is required to satisfy with the following design specifications;

1) The plasma facing surface of the divertor plates is covered with low-Z materials to minimize impurity content into the plasma.
2) The divertor plates are required to withstand a stationary heat flux of more than 5 MW/m^2 for the heated length of around 1 m.
3) The thickness of the armor tiles is typically 10 mm.

To remove the steady-state heat flux of 5 MW/m^2, the armor tiles have to be metallurgically bonded to the water cooled substrate of the divertor plate. One of the most important issue for developing the divertor plates is to establish the bonding technique between armor tiles and a metal substrate. Based on the experimental results in existing tokamak machines, a carbon based material is considered to be one of the most promising materials because of its lower atomic number and its refractory characteristic. Especially, carbon fiber reinforced carbon composite (CFC) materials are candidate for surface materials of PFCs because of their higher thermal conductivity and the superior mechanical strength comparing to reactor grade graphite materials. Residual stresses of the various CFC/metal bonded structures have been analyzed by the numerical method. A material combination of a unidirectional CFC with high thermal conductivity and a tungsten-copper (W-Cu) composite was found to be a promising structure with less residual stress after bonding. A W-Cu flat plate divertor module has been manufactured and tested. In the heating test of the module, the maximum surface heat flux of 15 MW/m^2 was applied. Some armor tiles failed off from the W-Cu substrate, which was caused by the initially lack of braze material at the bonded interface and by the thermal stress during the heating period.

The divertor plates in ITER are also required to be restrained thermal deformation towards the main plasma. In the CDA phase of ITER, the thermal deformation of the divertor plates next to each other should be restrained less than 0.5 mm. Therefore, the divertor plate should be equipped with a support structure which can restrain its thermal deformation. 1 m long divertor modules with a sliding support structure has been successfully made. Figure V.6-1 shows a photo of the 1m long divertor module. Two types of the support structures were used; one was a pin type support structure and the other was a rail type support structure (see fig. V.6-2). Both of the modules had a monoblock divertor structure. The armor tiles were made of 2-D CFC material. The cooling tube of the modules had a twisted tape to enhance its heat removal capability; the tape twist ratio (required tape length to turn 180° / inner diameter) was 3. Heating experiments of these divertor modules were performed at a peak heat flux of 15 MW/m^2; a heating

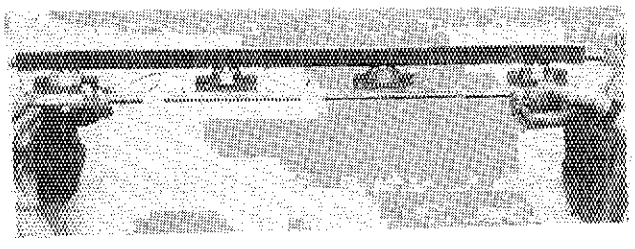

Fig. V.6-1 1 m long divertor module
(Rail type support structure)

duration of 30 s was selected so that the modules could reach their thermal steady-state. During the heating period, we confirmed the upward deformation of the module with a pin type support was found to be less than 0.5 mm.

A flat plate divertor module with parallel cooling channels has also been manufactured and tested in collaboration with the JT-60 group. Figure V.6-3 shows a photo of the module. The metal substrate was made of OFHC copper and the armor tiles were made of a unidirectional CFC material. To simplify the structure, the flat plate design was selected; the maximum dimension of the armor tile was 50 mm x 50 mm x 6 mm^t. Thermal cycling experiment was conducted at a heat flux of 10 MW/m^2 with a heating duration of 10 s, which corresponded to the design values of the JT-60 divertor plate. After 1,000 thermal cycles, the divertor module could keep its thermal performance; no degradation of the thermal response was found throughout the experiment. Moreover, a screening experiment was also performed at a heat flux of up to 13 MW/m^2; the inlet coolant pressure of 1.3 MPa and the flow velocity of 5 m/s were selected to simulate the JT-60 divertor conditions. The permissible surface heat flux at this divertor module was found to be 13 MW/m^2. To adopt an actively cooled divertor structure for JT-60, a divertor structure with better thermal performances should be modified for safety margin point of view.

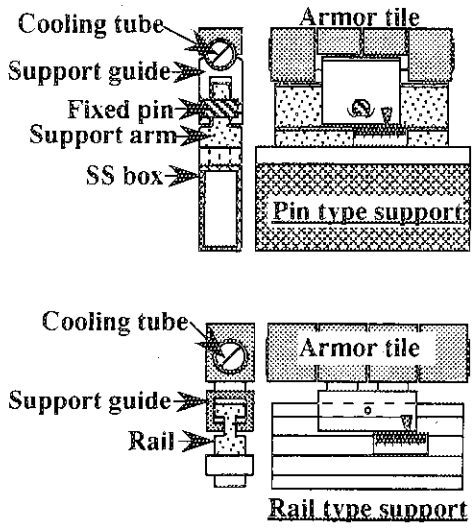

Fig. V.6-2 Sliding support structures for 1m long divertor modules

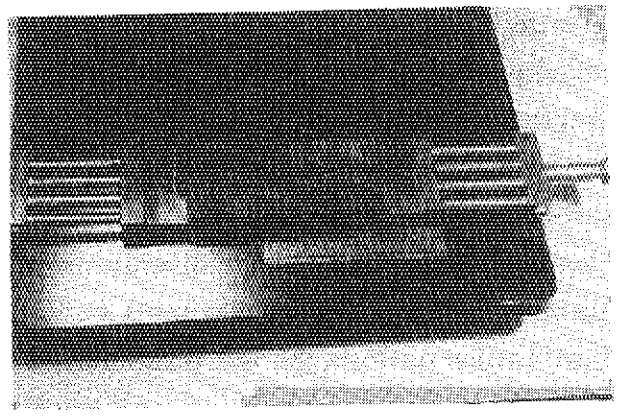

Fig. V.6-3 Flat plate divertor module with parallel cooling channels for JT-60

References

[6.1-1] Cardella A., Akiba M., Duwe R., et al., "Thermo-mechanical tests of a CFC divertor mock-up", J. of Nucl. Mat., 209 (1994) 117-121

[6.1-2] Nakamura K., Akiba M., Suzuki S., et al., "HIGH HEAT FLUX EXPERIMENTS OF PLASMA FACING COMPONENTS FOR NEXT FUSION DEVICES", Proc. of 15th Symp. on Fusion Engineering, (1993)

[6.1-3] Smid I., Akiba M., Araki M., et al., "MATERIAL AND DESIGN CONSIDERATIONS FOR THE CARBON ARMORED ITER DIVERTOR", JAERI-M 93-149 (1993)

6.2 R&Ds on heat removal technology [6.2-1]

Plasma facing components for fusion machines, in particular the divertor plates, are subjected to high heat loads with heating on one side. Since the nucleate boiling region is partially expected in the cooling tube of the divertor plate, a swirl tube is used as the cooling tube because of its high performances not only in heat transfer but also in burnout compared with those in a straight tube. To design the divertor plate, it is very important to evaluate heat transfer coefficients for tubes with and without a twist tape. Up to now, studies on heat transfer mechanisms have been done in the world. However most of their studies have been performed under a uniform heating condition and have been established by few data at transient to boiling region. Furthermore, none of the confirmations has been done whether or not these existing heat transfer correlations are applicable for one-sided heating condition. To establish heat transfer correlation under one-sided heating conditions, we have performed heat transfer experiments on smooth circular and swirl tubes in regions from non-boiling to high subcooled partial nucleate boiling using an hydrogen ion beam test facility at JAERI.

As results, it is confirmed that the existing heat transfer correlations can be applicable at only non-boiling region. In the subcooled partial nucleate boiling region, a new heat transfer correlation has been established and proposed because of the difficulty of applying the existing correlations for one-sided heating conditions.

Reference

[6.2-1] Ikeda S., Araki M., Ogawa M., et al., JAERI-M 893-070, (March 1993) and also see Araki M., Akiba M., Watson R.D., et al., to be published for Atomic and Plasma-Material Interaction Processes in Controlled Thermonuclear Fusion, Vol. 5 (1994).

6.3 Study of plasma surface interaction [6.3-1], [6.3-2]

The surface of the PFCs is suffered from ion sputtering by plasma ions and from thermal shocks at the plasma disruptions. It is essential to estimate the erosion characteristic of plasma facing materials and to develop new materials that can stand these loads from a fusion plasma.

6.3.1 Sputtering erosion

The ITER divertor plates will be subjected to a high particle flux of 4×10^{23} ion/m^2/s. However, the particle flux obtained in the existing test facilities is limited to 10^{19} ion/m^2/s at an energy of around 100 eV. JAERI has newly developed an ion source which can produce higher flux at lower energy, using the neutral beam technology. The maximum hydrogen ion flux reached 10^{21} ion/m^2/s at an energy of 50 - 100 eV. Sputtering erosion test for carbon based materials was carried out. At an energy of 100 eV, sputtering yield by deuterium was found to be twice as high as that by hydrogen.

6.3.2 Disruption erosion

The maximum surface temperature of the ITER divertor plates during operation will be about 1,000 °C. The disruption simulation experiments should be conducted at an elevated temperature. The disruption simulation experiments at up to 1,000 °C were performed at JEBIS. The maximum surface heat flux to the sample was 1,800 MW/m^2. Figure V.6-4 shows the results from the experiments for carbon based materials. As shown in this figure, the erosion rate at the elevated temperature was twice or three times higher than that at a room temperature.

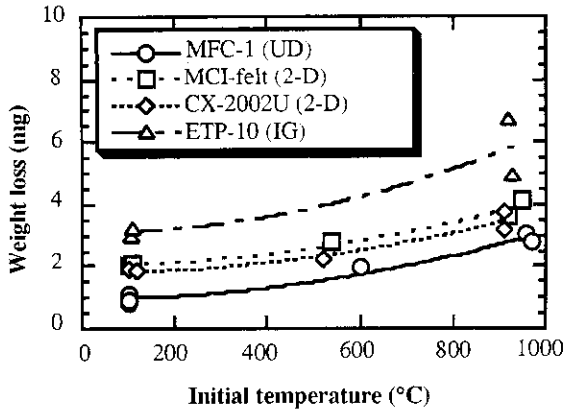

Fig. V.6-4 Disruption erosion of various carbon based materials at elevated temperatures

Various B_4C overlaid CFC materials have been manufactured and tested to evaluate an erosion rate against thermal shocks. These B_4C materials tested were made by the low-pressure plasma spray method, by the CVD method and by the conversion method. The thickness of the B_4C layer varies from 100 μm to 1 mm with respect to the manufacturing processes. As a result, B_4C converted CFC material had better adhesion between B_4C layer and CFC substrate; the less erosion rate was found in B_4C overlaid CFC material.

References

[6.3-1] Nakamura K., Akiba M., Suzuki S., et al., "Erosion of CFC and W at high temperature under high heat loads", J. of Nucl. Mat. (to be published)

[6.3-2] Akiba M., Araki M., Nakamura K., et al., "Thermal Response Tests on Plasma Facing Components", Proc. of IAEA TCM on ATOMIC AND MOLECULAR DATA FOR FUSION REACTOR TECHNOLOGY, (1993) 99-109

7. Reactor Structure Development

7.1 Introduction

The reactor structure of a tokamak machine is composed of a vacuum vessel, tritium breeding blanket, divertor system and a cryostat for the superconducting magnet system. These components will inevitably be massive and large, and should withstand severe loads of neutron irradiation, electromagnetic force and heat. Also each component must be compatible with full-remote maintenance/exchange. The major tasks of R&Ds for the reactor structure include establishment of the manufacturing technology and the remote assembling/disassembling technology. In this fiscal year, R&D efforts were focused on development of major components such as non-circular bellows, fail-safe first wall, FGM insulation joints, full-scale in-vessel manipulator, CO_2 bore tooling and radiation hard components.

7.2 Reactor structure development

7.2.1 Large-rectangular Bellows

In a fusion experimental reactor, large-sized non-circular bellows are needed for port penetrations to absorb the relative displacement due to different operating temperature. Since the bellows should have high reliability as a tritium boundary under the various loading conditions such as internal/external pressure and electromagnetic forces as well as relative displacement, the structural integrity must be assured. For this purpose, a rectangular bellows with a cross-section of 1,426 x 1,026 mm and a thickness of 3 mm was fabricated in hydraulic press process, as shown in fig.V.7.2-1. It is demonstrated that there is no failure in a cyclic test over 5 x 10^3 cycle with a displacement of ±15 mm and the helium leakage is less than He detectable value of 10^{-10} Torr•l/sec. FEM analyses to assess the structural integrity of this bellows were performed under the loading conditions of internal pressure and relative displacement. The analytical results are in good agreement with the experimental results. Further investigation on double boundary bellows and buckling characteristics of rectangular bellows is being conducted.

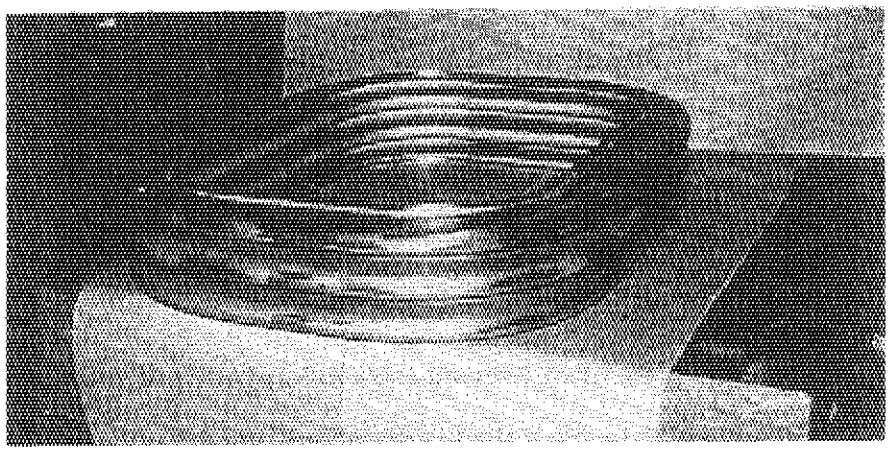

Fig.V.7.2-1 Fabricated 3 gathers rectangular bellows

7.2.2 Double-walled structure for fail-safe

The first wall of ITER is a water-cooled component so as to cool the maximum surface heat load of 0.5 MW/m^2 and nuclear heating of 20 MW/m^3. The leakage of water into the reactor is one of the most critical problem in connection with the cooling of in-vessel component and plasma condition. To solve this problem, a system to be able to monitor the water leakage continuously during reactor operation was developed and applied to first wall structure. In general, the structure is not fail-safe if the critical crack is so small that it can not be detected. However, the first wall with the double-wall concept can be made fail-safe by the application of the multiple load path (MLP) and leak-before-break (LBB) concepts.[7.2-1] When the fail safe strength is well defined, subcritical crack growth in the damaged wall can be permitted. This enables to detect stable leak rate of a coolant with good accuracy. In this year, fabricability of double-walled panel was confirmed and its basic thermal and mechanical characteristics were obtained.

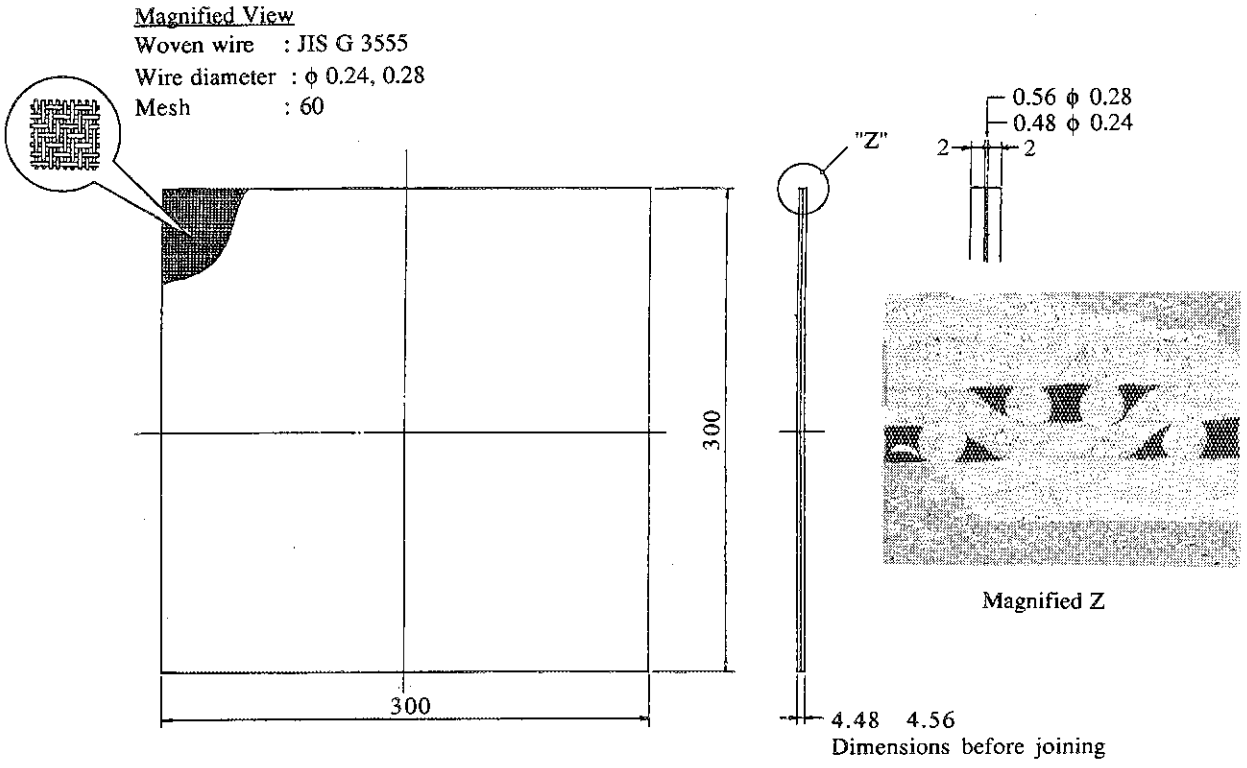

Fig.V.7.2-2 Fabricated double-walled panel and the section of mesh region

The sample of double-walled structure is 30 cm x 30 cm with 0.4 mm thickness mesh region sandwiched between 2 mm thickness stainless steel panels as shown in fig.V.7.2-2. The fabrication was implemented by hot press (HP) and hot isostatic pressing (HIP).

Bending and tensile tests show that the strength of double-walled structure depends on the panel region. Heat conductivity was reduced 17~41% by the mesh region.

From these results, applicability of double-walled structure to first wall of ITER are demonstrated. Detectability of leakage and feasibility of quilting structure are being examined for further assessment.

7.2.3 Functionally Gradient Material for electric insulation

In a fusion experimental reactor, coupling of eddy current induced by a plasma disruption and magnetic field for plasma sustaining causes severe magnetic force to structural components or cooling pipes. This force possibly damages the components. As a solution of this problem, it is essential to provide high resistance part in components and cooling pipes so as to reduce the induced current. On the other hand, conventional methods for insulation break such as mechanical joint and brazing of ceramic/metal interfaces have less reliability for high vacuum/pressure environment required in the fusion reactor. The Functionally Gradient Material (FGM) is an attractive method to solve these problems with their continuously graded ceramic/metal

compounds. The FGM joint with pure ceramics at center, pure metal at both ends and graded region between them has been developed.

It has higher reliability as vacuum/pressure boundary compared with directly bonded joint of ceramic/metal because of capability to be metallurgically welded to metallic pipes. For constituent material, partially stabilized zirconia with 20wt% Al_2O_3 (PSZA) is chosen as an electrical insulation due to its excellent mechanical strength, electrical resistance and low-temperature sinterability for a ceramic/metal macro-heterogeneous structure.

Fig.V.7.2-3 shows the FGM joint, which is 30 mm in diameter and 38 mm in length, fabricated by sintering with pure ceramics at center, type 430 stainless steel at both ends.

As a result, the fabrication method of FGM pipe for electrical insulation is successfully developed, and the radiation hardness and scale-up capability are the further issues.

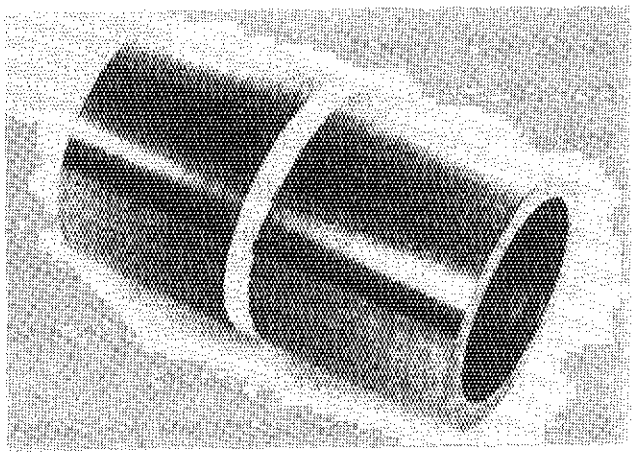

Fig.V.7.2-3 FGM sample of type 430 stainless steel

Reference

[7.2-1] Shibui M., Nakahira M., Tada E., et al, "Fail-Safe First Wall for Preclusion of Little Leakage", JAERI-M 94-074 [1994].

7.3 Remote maintenance development

7.3.1 Full-scale in-vessel manipulator

The rail-mounted vehicle maintenance system was selected for the scheduled maintenance components such as plasma facing components. In this system, the rail is expanded sequentially and supported by four arms from the respective 90-degree horizontal ports so as to provide stable and reliable operation.[7.3-1] Following one-fifth scale model tests, the full-sized model of a divertor handling manipulator with telescopic arm and rotational mechanism, which is a key component of the system, has been developed. In this year, a setup of full-scaled manipulator mock-up has been completed as shown in fig.V.7.3-1 and the combination test with the full-scale mock-up of divertor plate is being conducted.

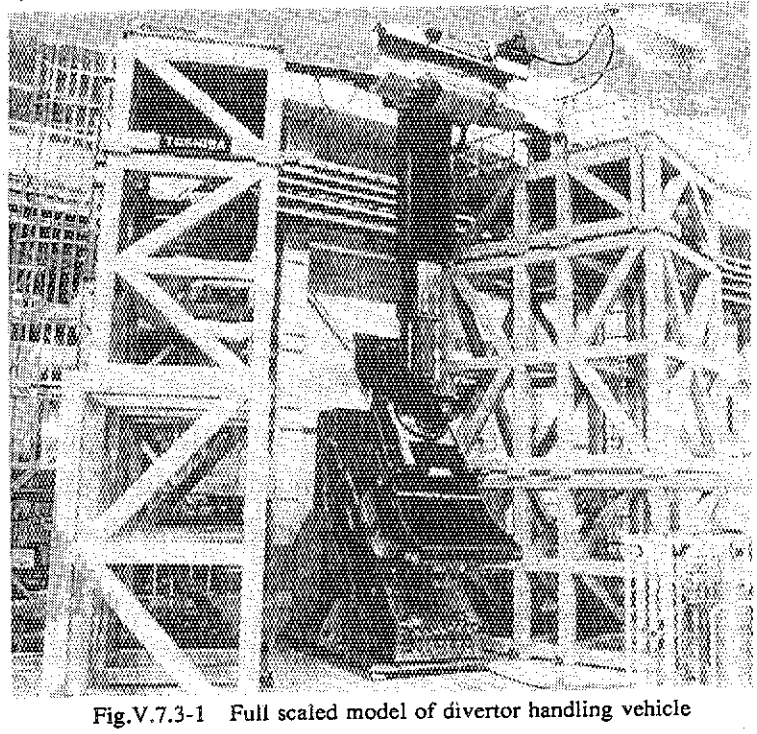

Fig.V.7.3-1 Full scaled model of divertor handling vehicle

7.3.2 CO_2 laser bore tooling

In the design of fusion experimental reactor, cooling pipes are connected to the divertor plate through a narrow port space, so that the external space of the pipes is not sufficient to allow an access of the ordinary TIG welder or mechanical cutter. A new maintenance system of bore tooling based on a CO_2 laser beam has been developed for the cooling pipe welding/cutting as shown in fig.V.7.3-2.[7.3-1] Key features of this system are as follows :

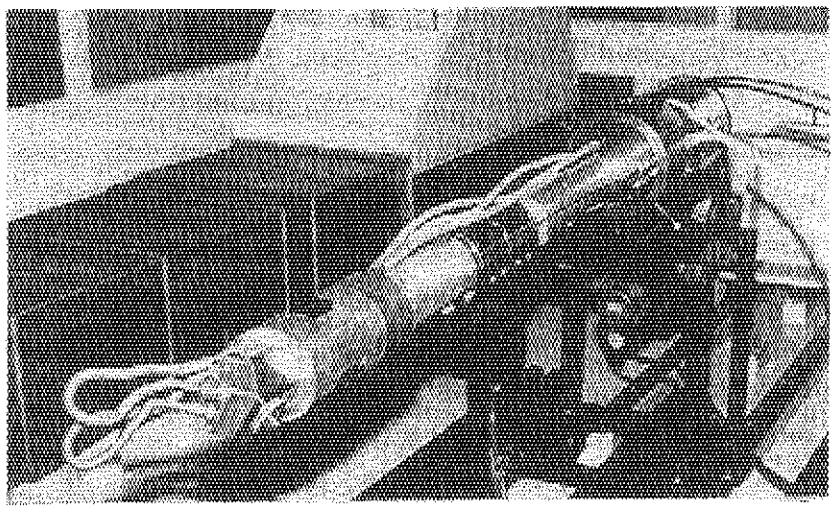

Fig.V.7.3-2 CO_2 laser bore tooling

(1) The cooling pipes are cut/welded from the inner surface from a view point of high space performance for welding/cutting.

(2) Welding and cutting operations are carried out using a common head and the laser power is adjustable to be optimized for both welding and cutting.

In this year, two types of laser processing heads have been fabricated and the feasibility of a newly developed internal access pipe welder/cutter has been successfully demonstrated for the 100-A pipe. In particular, the adjusting mechanism composed of a guide roller and a pneumatic support is found to give precise centering performance within +0.13mm and stable rotation of the laser processing heads are achieved. The guide roller provides accurate tracing of the inner wall of the pipe to be welded and cut. In addition, the optical transmission performance was examined under gamma-ray radiation and radiation hardness was demonstrated up to ~10^9 rad.

7.3.3 Radiation hard component

In fusion experimental reactors such as ITER, remote handling equipments have to withstand radiation condition of more than 10^6 R/h. For this purpose, irradiation tests on a number of critical components for the remote handling system have been extensively conducted under similar radiation conditions. As a result, radiation-hard-component development has been progressed and it has been demonstrated that critical elements such as motor, lubricant, optical lens and mirror, and force sensor can be available for more than 10^9 R.

Reference

[7.3-1] Kondoh M., Shibanuma K., Kakudate S., et al, "Design and Development of Remote Maintenance System for ITER-CDA In-vessel Components", JAERI-M 93-066 [1993]

8. Blanket Technology

8.1 Introduction [8.1-1] [8.1-2]

The blanket is a component which protects the vacuum vessel and the super conducting magnet from radiation, generates tritium as the fuel gas of a thermonuclear reaction, and changes the kinetic energy of neutrons to thermal energy, and is one of the key components for energy-producing fusion reactors. In experimental reactors, the blanket is mainly utilized for the radiation shielding and the tritium breeding, while DEMO reactor blankets must fulfill the above three functions.

In this fiscal year, R&D efforts were focused on the development of box structure for ITER shielding blanket and the out-of-reactor testing of ITER breeding blanket. As for the development of box structure, mechanical properties of HIP bonded structure were examined. As for the out-of-reactor testing, the effective thermal conductivity of beryllium sphere packed bed was studied.

The construction of the blanket loop test facility was completed. Together with the existing cooling water test loop, a sweep gas loop was newly installed in this fiscal year. Two kinds of test mockups ; the mockups for the mass transfer test of the lithium oxide pebble bed and that for the pressure drop test of the first wall cooling channel were prepared.

Design work has been also continued on the layered pebble bed solid breeder concept, on the alternative solid breeder concept ,e.g., the pin-type concept and on the shielding blanket concept made of steel and water.

References

[8.1-1] Kurasawa T., Takatsu H., Sato S., et al., Ceramic Breeding Blanket Development for Fusion Experimental Reactor in JAERI, to appear in 3rd ISFNT Los-Angeles, (1994).

[8.1-2] T. Kurasawa, Takatsu H., Sato S., et al., Design and R&D Activities on Ceramic Breeder Blanket for Fusion Experimental Reactors in JAERI, to appear in 18th SOFT Karlsruher, (1994).

8.2 Fabrication of the blanket box structure integrated with first wall [8.2-1]

The blanket structure integrated with first wall and shield is a candidate configuration of the ITER shielding blanket. The box wall has a thickness of 15 - 30 mm to withstand the enormous electromagnetic load (about 10 MN/m). The first wall must have cooling channels in it to remove nuclear heating (about 20 MW/m^3) and surface heat (about 0.5 MW/m^2). An advanced technique was applied to the fabrication of the first wall-panel, i.e. diffusion bonding of rectangular tubes with two flat plates by HIP (Hot Isostatic Pressing) bonding. It has the advantages of small deformation, small residual stress and good physical and mechanical properties similar to the base metal.

In order to obtain mechanical properties and evaluate the soundness of the elements made by the HIP process, mechanical tests were conducted using test specimens made by the HIP process

under the conditions of 1000 - 1100 °C, 1500 atm and 2 - 4 hours. Test blocks were fabricated by HIP bonding two flat plates of 316SS for providing test specimens. Mechanical tests conductedby this study were tensile tests, Charpy impact tests, fatigue tests, Vickers hardness tests, metallurgical examination, non-destructive examination and creep tests.

Fatigue data is shown in Fig.V.8.2-1 together with the published data of the base metal [8.2-2]. Tensile and fatigue tests showed final fracture was observed in the base metal, and tensile and fatigue strengths are nearly equal to those of the base metal. And it can be concluded that the hipped joints have almost the same mechanical properties as those of the base metal.

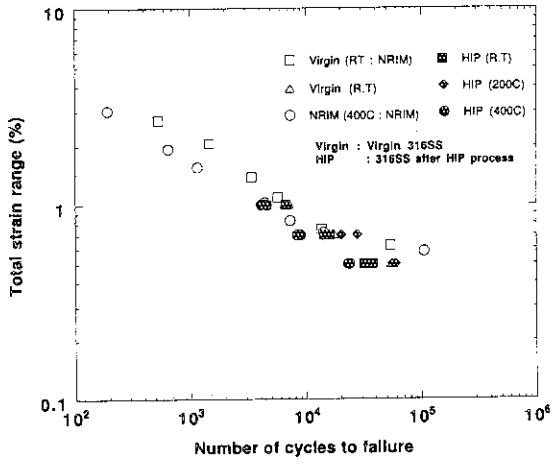

Fig.V.8.2-1 Relation between strain amplitude and fatigue life of hipped 316 SS samples

In addition to toroidal segmentation from assembly/maintenance point of view, the blanket is poloidaly divided into modules due to the capacity of the available HIP facility, so the poloidal modules divided need to be bonded by using a welding technique except HIP bonding. In order to verify the feasibility of poloidal joining technique for the first wall equipped with cooling channels joining of the first wall partial model was tried by using laser welding from both sides. Macrosections of the laser-welded first wall is shown in Fig.V.8.2-2. The configurations of the cooling channels were not deformed at all, and the poloidal joint of the first wall was successfully completed. Radiation Testing satisfied the first grade requirement of JIS (Japanese Industrial Standard).

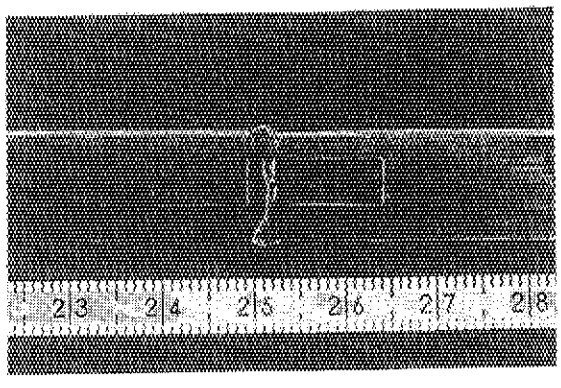

Fig.V.8.2-2 Macrosections of the laser-welded first wall

References

[8.2-1] Sato S., Takatsu H., Hashimoto T., et al., to be published as JAERI-M (1994).
[8.2-2] NRIM Fatigue Data Sheet No. 15, National Research Institute for Metals (1979).

8.3 Out-of-reactor testing

8.3.1 Effective thermal conductivity of beryllium sphere packed bed

The effective thermal conductivity of the packed bed was measured with Be spheres with diameters of 1 to 3 mm. The test was performed by using a cylindrical cell whose diameter is about 100 mm. The test cell has a water cooling tube at the center and was heated from outside by infrared image furnace (Fig.V.8.3-1) up to 450°C as the average bed temperature. Helium gas

pressure was about 0.1 MPa as the stagnant environment. The amount of the sphere examined was around 1000 g, which was increased twice of the previous experiment to reduce heat loss in the axial direction. Two kinds of Be spheres (1 mm diameter) were tested. Some were fabricated by the rotating electrode method, and another were the sub-product in the course of the magnesium reduction, which have diameters of 1, 2 and 3 mm. In this experiment, the dependence of the effective thermal conductivity on the temperature and sphere diameter was investigated by measuring the temperature gradient within the packed bed. Experimental data can be described as the linear function of the temperature for practical use of the design works.

$k=(1.57\pm 0.03)+(2.02\pm 0.10) \times 10^{-3} T$

for 1 mm Be sphere

$k=(1.67\pm 0.04)+(2.42\pm 0.12) \times 10^{-3} T$

for 2 mm Be sphere

$k=(2.18\pm 0.06)+(1.73\pm 0.20) \times 10^{-3} T$

for 3 mm Be sphere

,where k is the effective thermal conductivity in W/m°C and T is the temperature in °C. Fig.V.8.3-2 shows the obtained effective thermal conductivity of Be sphere at 60 % packing fraction with an average temperature of the packed bed. Because of negligible difference between two kinds of Be products, data of both products are not necessary to be distinguished each other.

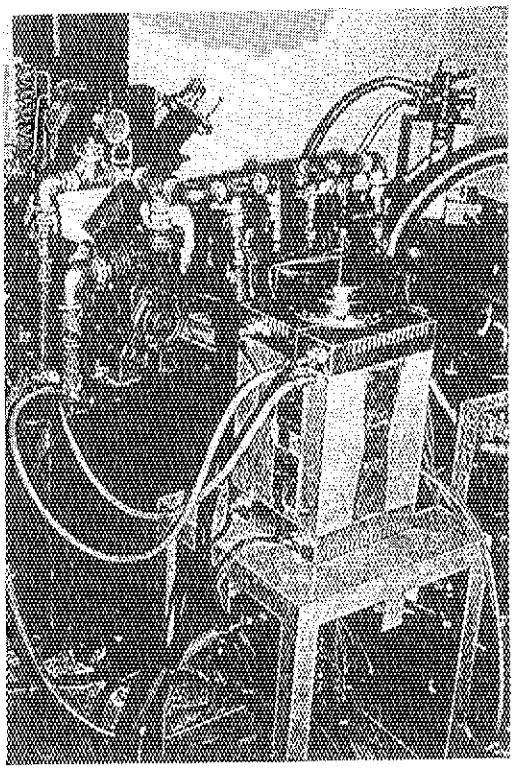

Fig.V.8.3-1 Appearance of the test cell

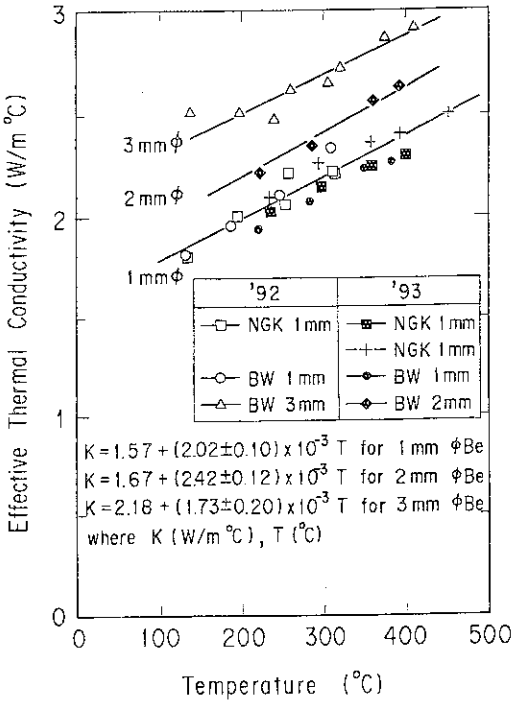

Fig.V.8.3-2 Effective thermal conductivity of Be sphere packed bed

8.3.2 Preparation of medium scale blanket loop test facility

A small scale sweep gas loop was installed as a part of medium scale blanket loop test facility. This gas loop installed has enabled to be used for atmospheric adjustment during various thermo-hydraulics tests of medium scale blanket mockup unit, and also can be utilized to perform the test

of mass transfer for the layered lithium oxide pebble bed blanket. The schematics layout of this medium scale thermal-hydraulic test facility is shown in Fig.V.8.3-3.

In addition, to clarify the hydraulic performance of the first wall cooling channel, the pressure drop test mockup of one 1/1-scaled and one 1/2-scaled cooling channel were prepared, and the preliminary pressure drop test is being conducted by using the blanket loop test facility.

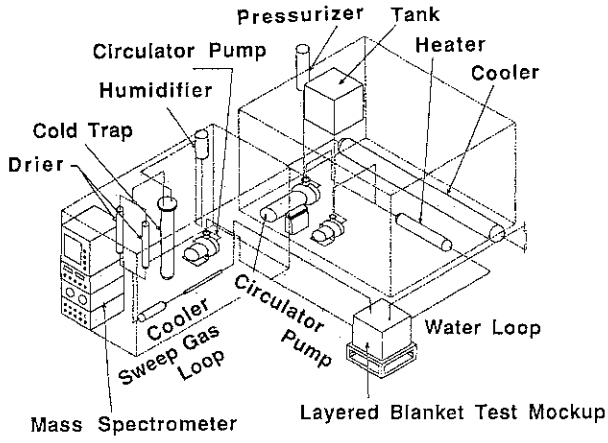

Fig.V.8.3-3 Schematics layout of thermal-hydraulic test facility

8.4 Design of tritium breeding blanket [8.4-1]

An analytical study was continued to refine the layered pebble bed blanket proposed for ITER. Thermo-mechanical analyses of the first wall of the ITER breeding blanket were performed, by using a local model shown in Fig.V.8.4-1, under the transient and steady state over-power conditions [8.4-2]. Typical results are shown in Fig.V.8.4-1 for the case of the steady state condition, where fusion power of 1.5 GW corresponds to the reference conditions. The tritium inventory in the breeding and multiplier region was evaluated.

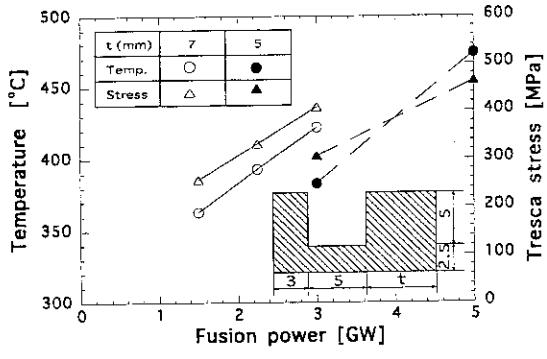

Fig.V.8.4-1 Maximum temperature and stress of the first wall under over power conditions

A design study of the ITER alternative breeding blanket was also performed. A pin-type concept [i.e. breeder-in-tube type] and a tube-in-shell concept [breeder-out-of-tube type] were studied, together with a convertible concept, in which a non-breeding shield blanket is able to be converted to a breeding blanket without the exchange of the box structure. As for a pin-type and a tube-in-shell concept, the concepts were examined by conducting neutronics, thermal and hydraulic analyses, and taking fabrication and assembly process into account. As for a convertible concept, a preliminary concept was developed by studying the filing up method of the breeding material.

A design study of the ITER non-breeding shield blanket was also performed. Two kinds of blanket ; the blanket integrated with the first wall and the blanket with the separate first wall were studied. A preliminary design of the blanket with the separate first wall was completed by conducting stress analyses due to the thermal stress, the internal pressure and the electro-magnetic

force, and studying the fixing method, the jointing method of the toroidal segmentation of the blanket module and the coolant configuration.

A neutronics analysis of the liquid lithium breeding blanket, which is one of the ITER alternative breeding blankets, was performed [8.4-3]. Shielding effectiveness of the liquid lithium breeding blanket on the super conducting magnet was evaluated, and the configuration to satisfy the shield design target was clarified.

References

[8.4-1] Takatsu H., Hashimoto T., Sato S., et al., to be published as JAERI-M (1994)
[8.4-2] Kuroda T., Sagawa H., Shimakawa S., et al., to be published as JAERI-M (1994)
[8.4-3] Sato S., Mori S., Takatsu H., et al., to be published as JAERI-M (1994)

VI. INTERNATIONAL THERMONUCLEAR EXPERIMENTAL REACTOR (ITER)

1. Introduction

ITER Engineering Design Activities (EDA) Agreement and Protocol 1 were signed on July 21, 1992 by the four Parties, the European Atomic Energy Community, the Government of Japan, the Government of the Russian Federation and the Government of the United States of America. The overall programmatic objective of ITER, which guides the ITER EDA, is to demonstrate the scientific and technological feasibility of fusion energy of peaceful purposes. According to the ITER EDA Agreement, the four parties conduct jointly the ITER EDA to produce a detailed, complete, and fully integrated engineering design of ITER and all technical data necessary for future decisions on the construction of ITER. The ITER EDA, being conducted under the auspices of the IAEA, will have a duration of six years.

The organization prescribed by the ITER EDA Agreement for this purpose is outlined in Fig.VI-1. The ITER Council is responsible for the general direction of the ITER EDA and exercises overall supervision of its execution. The ITER Director shall direct and coordinate the performance of all activities pertinent to the ITER EDA and organize, direct and supervise the Joint Central Team (JCT). The Technical Advisory Committee (TAC) and the Management Advisory Committee (MAC) shall advise the ITER Council in technical matters and management matters, respectively. Two Special Working Groups (SWG) were established. SWG-1 was charged to review the detailed technical objectives of the project. SWG-2 was mainly charged to develop the draft of Protocol 2 and guidelines for the implementation of task assignments to the Home Teams. The JCT is located at the Joint Work Sites: Garching near Munich, Naka (Ibaraki), and San Diego (California). Home Teams, each

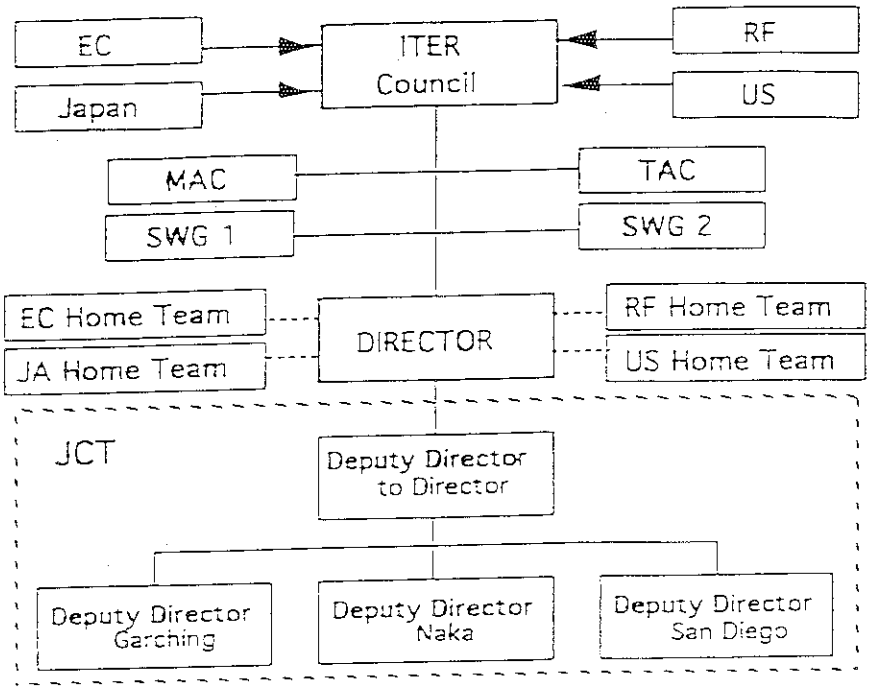

Fig.VI-1 ITER EDA Organization

party establishes and organizes, perform the tasks assigned to them in accordance with the ITER EDA Work Programme.

The organization of the Japanese Home Team is outlined in Fig.VI-2. JAERI established a new task force, named JAERI ITER Project to form a core of the Japanese Home Team for the efficient execution of ITER tasks. It consists of five teams, and each team is also subdivided into some units.

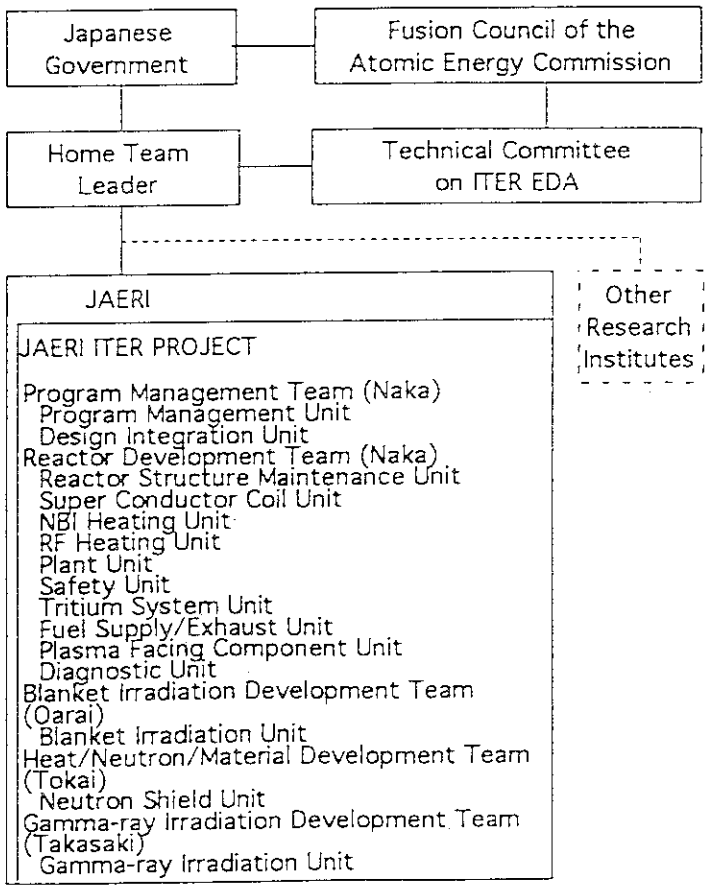

Fig.VI-2 Organization of Japanese Home Team

2. ITER Engineering Design Activities (EDA)

2.1 Development of the Outline Design

Following the recommendation by TAC, the ITER Council requested the ITER Director and the JCT to complete the Outline Design to integrate requirements of cost, technical guideline, and performance margin in the third and fourth ITER Council Meetings, on April and September 1993, respectively. The work incorporated the priorities of the ITER Council and achieved within the JCT by adding the cooperation of the Parties and the contributions of the Home Teams. In accepting the Outline Design Report in the fifth ITER Council Meeting, on January 1994, the ITER Council considered it constitutes an acceptable basis for consideration by the Parties to proceed toward the Protocol 2.

Figure VI-3 and Table VI-1 show the bird-eye view and brief specifications of the Outline Design of ITER device, respectively. The Design Tasks of super conducting coils, plasma controls and others were shared into Japanese Home Team. Improved Plan of the Outline Design from Japanese Home Team was produced from the view point of total concept including construction and maintenance and plant system, and was contributed to complete the ITER Outline Design Report. The basic concepts of site selection, safety design, and safety evaluation of fusion experimental reactor were summarized for safety assessment.

Following the recommendation by TAC, the Council requested the Director and the JCT

to conduct a sensitivity analysis to determine the optimum way to achieve a reduction in cost while minimizing the impact on the performance margin. The Council requested TAC to assess the results of the sensitivity analysis to be carried out by the Director and the JCT. This assessment should be carried out as soon as the sensitivity study is completed, which is expected to be the case in about six months.

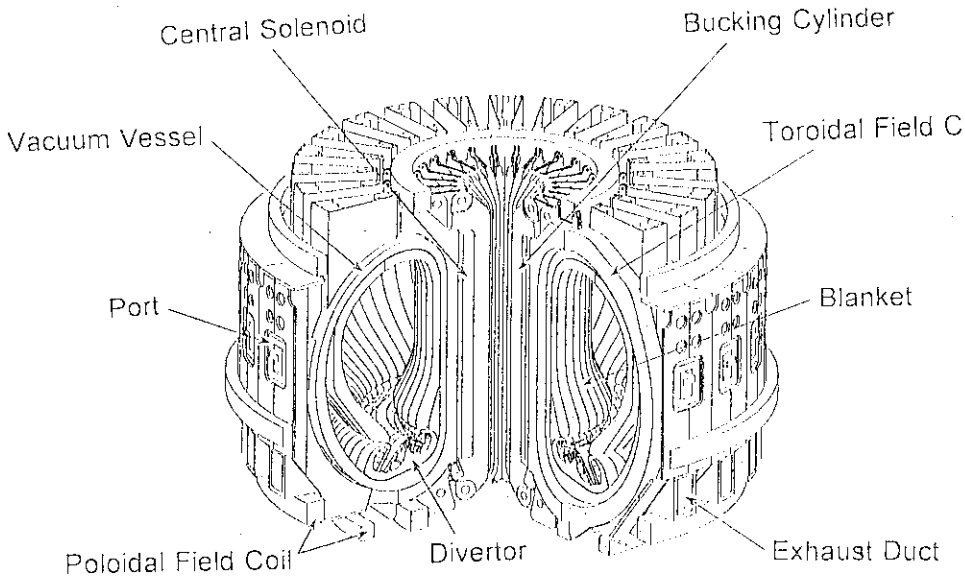

Fig.VI-3 Bird-eye View of ITER Device in the Outline Design

Major Radius	7.7	m
Minor Radius	3.0	m
Elongation	1.6	
Plasma Current	24	MA
Toroidal Magnetic Field	6	T
Burn Time	1000	s
Fusion Power	1.5	GW

Table VI-1 Brief Specifications of the Outline Design of ITER Device

2.2 Milestones

The ITER Council approved the Director's prepared ITER EDA Milestones as revised on the basis of the TAC and MAC recommendations in the fifth ITER Council Meeting, in January 1994. Figure VI-4 shows the chart of the ITER EDA Milestones. The planning is based on the assumption of a site selection in mid-1996. Guidance concerning this assumption is needed. The ITER Director has started that two years is the minimum required period following site selection to accomplish site specific design, negotiate a site agreement and

complete the site specific safety evaluation. All this would be required before access to the site and initiation of site construction would be possible.

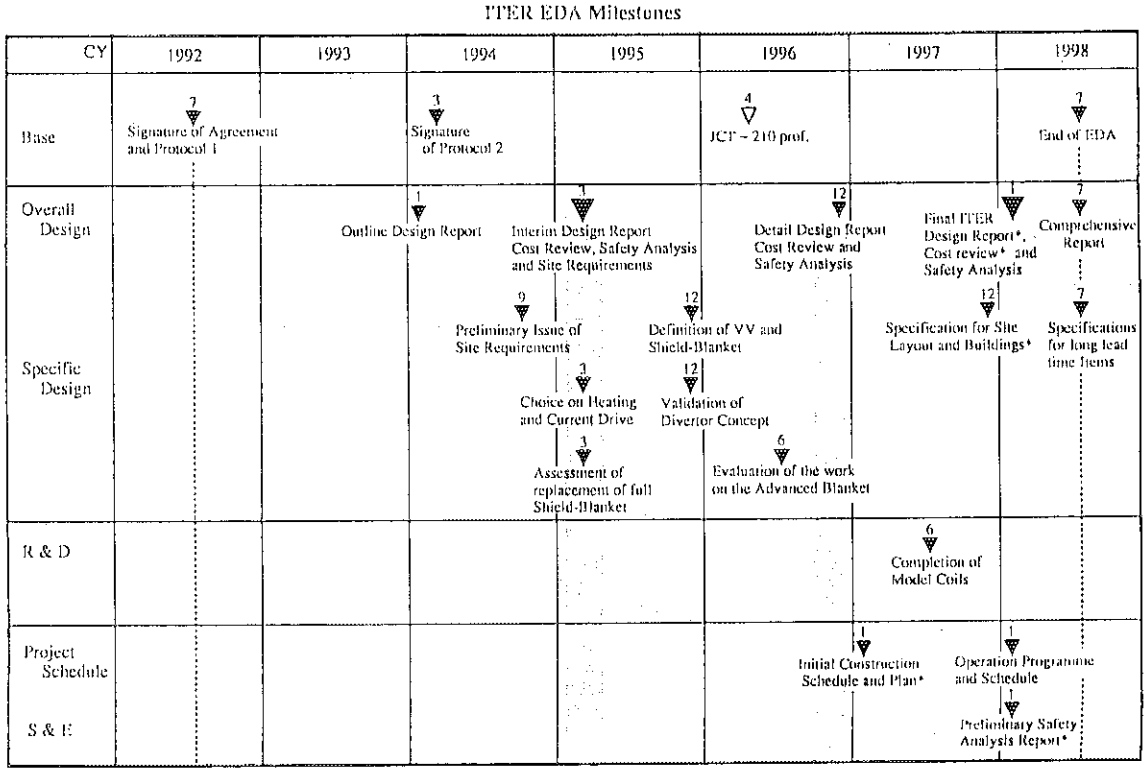

Fig.VI-4 Chart of the ITER EDA Milestone

The proposed interim design report needs to include a conceptual level definition and cost estimates of all elements of the construction phase of the project. It is proposed to have an in-depth TAC review of the cost at the time of this report. It is MAC's understanding that industry will be asked to develop cost estimates for most of the Tokamak components.

2.3 Signing of ITER EDA Protocol 2

In accordance with the schedule agreed upon by the ITER Parties, Protocol 2 of the ITER EDA Agreement has been signed in Vienna on 21 March 1994. Protocol 2 specifically covers the detailed technical work up to the end of the Agreement. Protocol 1, which was the first step of the implementation of the Agreement, ended the day before. Under Protocol 2, which will cover efforts of the ITER Director and the JCT through the end of the Agreement on July 20,1998, the ITER Director and the JCT will complete an engineering design of ITER.

2.4 Technology R&D and Design Tasks

In addition to the comprehensive Task Agreements, work has continued in formulating Task Agreements following the standard procedures. As of the end of December 1993, the ITER

Director had issued 82 Task Agreements. The total value of technology R&D credits granted, proposed or imminent now exceeds 300 KIUA (1 IUA = 1000 US$ in 1989). The items in charge of technological R&D in Japanese Home Team are the construction of the common test facility for super conducting coils, the development of the central solenoid (CS) model coil, and the component developments of the reactor structure and others. The technology design credits, which are already distributed among four Parties, is about 50 % of whole resources. Japanese Home Team's shares of Design Tasks are designs of first wall, heating and current drive and so on. The concrete results of the ITER Technology R&D and Design are described in the chapters V and VII.

VII FUSION REACTOR DESIGN AND FUSION SAFETY

1. Introduction

Fusion reactor design activities are conducted to construct an attractive concept of fusion reactor power plant . The DREAM (DRastically Easy Maintenance) tokamak reactor concept was improved regarding utilization of low activation materials and improvement of thermal efficiency by using a combination of gas turbine and steam turbine cycles.

Fusion safety related research activities were conducted to secure and enhance the safety of fusion power reactor. The plasma and thermalhydraulic behaviors at accidental situations were investigated by analytical and experimental methods.

2. Fusion Reactor Design

To improve the availability of the Steady State Tokamak Reactor(SSTR),. an innovative reactor concept called DREAM was proposed. For easy maintenance of in-vessel reactor, plasma configuration with high aspect ratio(with slender doughnut shape) around 6 and a small number of torus sectoring of 12 are introduced to extract the 1/12 sector of the torus by a single straight radial motion through the space between the adjacent toroidal field coils. The toroidal field coil system is embedded in the reactor building and in time of need repaired independent of the torus structure. The detailed procedure and time of maintenance were evaluated and the feasibility as a power reactor was confirmed .

Silicon carbide composites(SiC/SiC) was investigated as low activation material for structural application of DREAM reactor internals such as divertor and blanket. The feasibility was confirmed if the thermal conductivitty of silicon carbides is expected to be more than 60 W/m/K. This value could be realized in the future by improvement of silicon carbides by additives such as beryllium oxide.

Helium-solid(SiC particles) suspension flow was investigated to obtain a high thermal efficiency. A combination of gas turbine cycle and steam turbine cycle was proposed. The condition of heat utilization system was clarified to attain thermal efficiency over 40%. The overview of the DREAM concept is shown in Fig.VII.2-1.

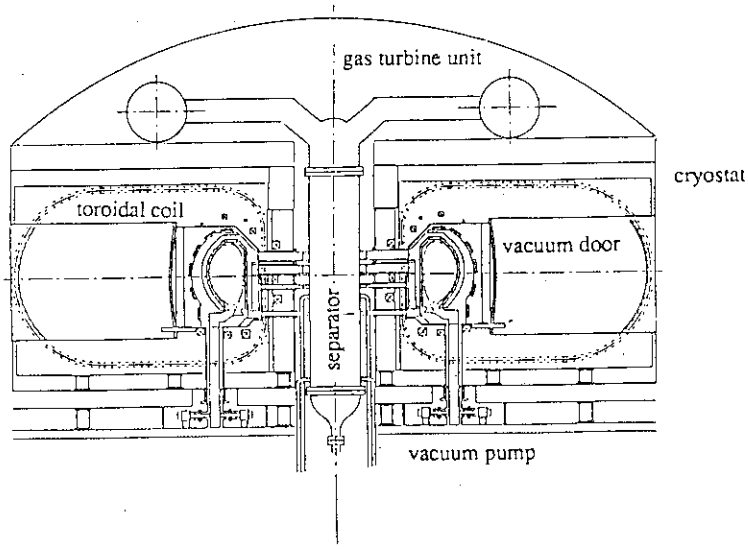

Fig.VII.2-1 Sideview of DREAM reactor

3. Fusion Safety

The comprehensive safety evaluation methodology has been developed to clarify accidental sequences resulting in the release of radioactivity. This development has been carried out under the framework of the IEA Implementing Agreement on International Co-operation of Environmental, Safety and Economics Aspects of Fusion Power which was signed June 4,1992. A simplified point model plasma transient analysis code has been developed and combined with a one dimensional thermalhydraulic analysis code. The thermal behavior of structures in a vacuum vessel at plasma disruption, and the thermal behavior of components and dynamic behavior of plasma at loss of coolant accident were evaluated in fiscal year 1993. The anlyses show that plasma can be passively shut down for small sized break(1%) LOCA, but cooling tubes were at large break(200%) LOCA in the divertor cooling system.

In addition, the thermalhydraulic behavior at ingress of coolant event was analyzed using TRAC-BD1 code. The pressure transients for Ingress of Coolant Event(ICE) during burn were calculated under ITER-CDA condition. The analyses show that the pressure can be kept below design pressure by using the remainig cooling systems free from channel break.

The experimental apparatus for loss of vacuum accident and ingress of coolant event was constructed. Preliminary experiments were done. The experimental apparatus is shown in Fig.VII.3-1.[3-1]

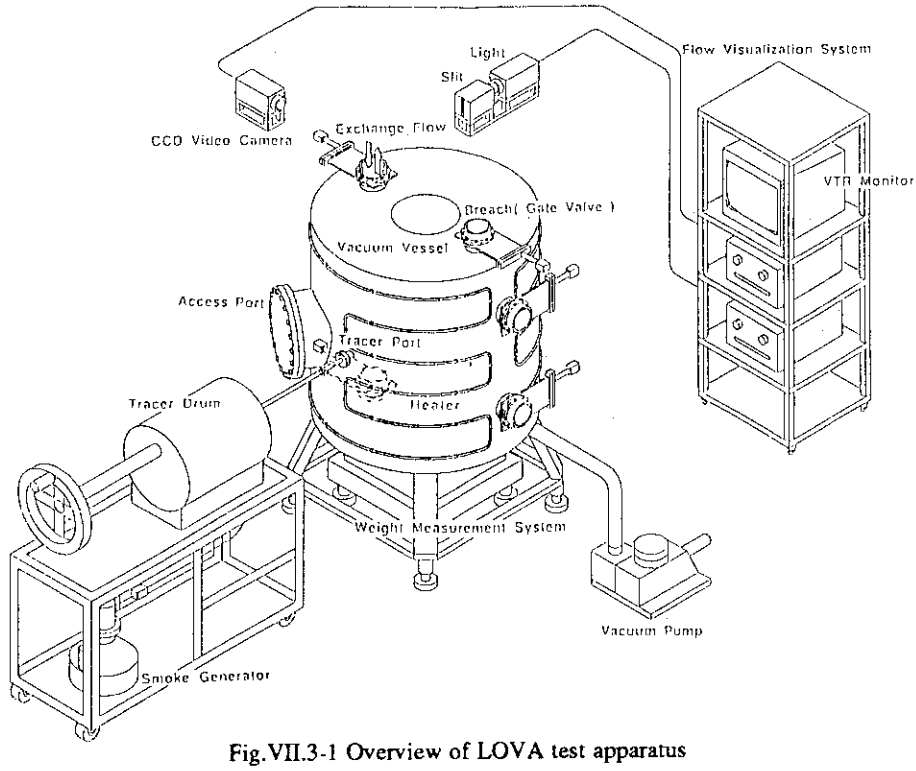

Fig.VII.3-1 Overview of LOVA test apparatus

Reference

[3-1] Ogawa M. and Kunugi T.,Private Communication.

APPENDICES

A.1 Publication List (April 1993 - March 1994)

A.1.1 List of JAERI-M reports (Fusion Facility)

1) Tokuda S., Kumakra T., Yoshimura K., "Numerical Experiment on Finite Element Method for Matcing Data", JAERI-M 93-075 (1993) (in Japanese).
2) Konishi S., Hayashi T., Inoue M., et al., "JAERI Fuel Cleanup System (J-FCU) Stand-Alone Tritium Test at the TSTA -First J-FCU Test with One Gram of Tritium on June 1991-", JAERI-M 93-080, April 1993.
3) Hayashi T., Nakamura H., Konishi S., et al. "Joint Operation of the TSTA with the J-FCU under the Collaboration between JAERI and U.S.-DOE - The First Integrated tritium Test Between J-FCU and ISS on Oct. 1991-", JAERI-M 93-081, April 1993.
4) Hayashi T., Nakamura H., Konishi S., et al.,"JAERI-Fuel Cleanup System (J-FCU) Stand-Alone Tritium Test at the TSTA -JFCU Tritium Test with Full Impurities on Feb. 1992-", JAERI-M 93-082, April 1993.
5) Hayashi T., Nakamura H., Konishi S., et al., "Joint Operation of the TSTA with the J-FCU under the Collaboration between JAERI and U.S.-DOE - TSTA Extended Loop Operation with 100 grams of Tritium on April May 1992-", JAERI-M 93-083, April 1993.
6) O'hira S., Konishi S., Okuno K., et al., "Test of the Cold traps in the JAERI Fuel Cleanup System in the Tritium Systems Test Assembly", JAERI-M 93-087, April 1993.
7) Konishi S., O'hira S., Hayashi T., et al., "Test of the Palladium Diffuser in the JAERI Fuel Cleanup System in the Tritium Systems Test Assembly", JAERI-M 93-088, April 1993.
8) Konishi S., O'hira S., Hayashi T., et al., "Test of the JAERI Fuel Cleanup System at the Tritium Systems Test Assembly -JFCU Stand Alone Deuterium Test -", JAERI-M 93-089, April 1993.
9) Konishi S., Yoshida H., Naruse Y., et al., "Tritium Test of the Tritium Processing Components under the Annex III US-Japan Collaboration -Annex III Final Report-", JAERI-M 93-090, April 1993.
10) Hayashi T., Konishi S., O'hira S., et al., "Test of the Scroll Pump in the JAERI Fuel Cleanup System in the Tritium Systems Test Assembly -JFCU Scroll Pump Test and Result-", JAERI-M 93-094, April 1993.
11) Kasugai A., Sakamoto K., Maebara S., "Mode Analysis of Gyrotron Oscillation using a k-spectrometor",JAERI-M 93-101
12) Yoshida H., Naruse H., Ohkawa Y., et al., "Design Study of Fusion Experimental Reactor Tritium Plant (I) Tritium Safety Systems for Reactor Building", JAERI-M 93-107 (in Japanese).
13) Okazaki T., Seki Y., Inabe T., et al.,"A Method of Safety Assurance for Experimental Reactor",JAERI-M 93-112(in Japanese).
14) Elevant T., Hoek M., Nishitani T., "Design Study of a Time-of-Flight Neutron Spectrometer for JT-60U", JAERI-M 93-123.
15) Moriyama K., Nishino T., Seki Y., et al"Improvement Study of the Divertor Configuration of the Steady State Tokamak Reactor(SSTR)", JAERI-M 93-130 (in Japanese).
16) Tanaka M., Hanada M., Inoue T., Okumura Y., "Production of High Current H^- Beams in a Cesium Seeded Volume Negative Ion Source Equipped with PG Filter", JAERI-M 93-132, (1993).
17) Yoshida H., Naruse H., Ohkawa Y., et al., "Design Study of Fusion Experimental Reactor Tritium Plant (II) Tritiated Water and Radioactive Solid Waste Processing Facilities", JAERI-M 93-136 (in Japanese).
18) Zimin S., Takatsu H., Mori S., et al., "Two Dimensional Over-all Neutronics Analysis of the ITER Device", JAERI-M 93-141, (1993).
19) Yamanisihi T., and Okuno K., "Effect of Helium on Separation Performance of Cryogenic Distillation Column Cascade for Fusion Reactor", JAERI-M 93-145, July 1993.
20) Smid I., Akiba M., Araki M., et al., "Material and Design Considerations for the Carbon Armored ITER Divertor", JAERI-M 93-149 (1993)
21) Totsuka T., "Development of a VME and CAMAC Based Data Acquisition and Transfer System for JT-60 Control", JAERI-M 93-158 (1993) (in Japanese).
22) Yamanisihi T., and Okuno K., "Design Concept of Control System for Cryogenic Distillation Columns of Fusion Reactor", JAERI-M 93-162, Aug. 1993.
23) Mori S., Zimin S. and Takatsu H., "Multi-group Helium and Hydrogen Production Cross Section Libraries for Fusion Neutronics Design", JAERI-M 93-175, (1993).
24) Yamanishi T., Hayashi T., Nakamura H., et al., "Separation Characteristics of Cryogenic Distillation Column Having Feedback Stream Separation Experiment with H-D System", JAERI-M 93-188, Oct. 1993.
25) Horiike H., Kuroda T., Murakami Y., et al., "Comparison Between a Steady-state Fusion Reactor and an Inductively Driven Pulse Reactor", JAERI-M 93-208, (1993).

26) Nelosn.R.J.,Takahashi Y.,Isono T., et al., "AN INVESTIGATION OF A.C. LOSSES IN TWO SUB-SIZE CONDUCTORS FOR THE ITER", JAERI-M 93-219, (1993)
27) Kurita G., Tuda T., Azumi M., Takeda T., "Simulation of Tearing Mode Stabilization by Using ECH", JAERI-M 93-224 (1993).
28) Yagyu J., Arai T., Ogiwara N., et al., "Evaluation of In-situ Coated Boron Film in JT-60U (Portable Sample Stage System and Its Application to Evaluate the Coated Boron Film)", JAERI-M 93-249 (in Japanese).
29) Hoek M., Nishitani T., Ikeda Y., et al., "Initial Results from Neutron Yield Measurements by Activation Technique at JT-60U", JAERI-M 94-002.
30) Ogawa T., Oasa K., Hoshino K., et al., "Fusion-neutron Diagnostic on the Microwave Tokamak Experiment", JAERI-M 94-021 (1994).
31) Aikawa H., "A Proposal to Introduce a Turbulence Factor into a Diffusion Coefficient of a Tokamak Plasma", JAERI-M 94-035 (1994).
32) Maeno M., Ogiwara N., Ogawa H., et al., "Development of a Fast Response Polarimeter for a Faraday Rotation Measurement", JAERI-M 94-039 (1994).
33) Aoki I., and Seki Y.,"Design of Fusion Safety Data Base", JAERI-M 94-044 (in Japanese).
34) Arika M.,"Development of Safety Analysis Methodology for Fusion Systems [I]- System Model of General Fusion System for Safety Analysis-", JAERI-M 94-045 (in Japanese).
35) Ishizuka H., Nakahara Y., Kawasaki S., " Emmitance Measurement of ultra high intensity micro-wave beam" JAERI-M 94-047
36) Hamamatsu K., Azumi M., " Numerical Analysis of ECRH on JT-60U and JFT-2M" JAERI-M 94-062 (1994) (in Japanese)
37) NBI Facility Division and NBI Heating Laboratory "Design Study of a Negative-ion Based NBI System for JT-60U",JAERI-M,94-072(1994)

A.1.2 List of papers published in Journals

1) Seki, Y., "Fusion Power Reactor Studies in Japan", Proc. 10th Topical Meeting Technology of Fusion Energy, Boston, June 7-12, 1992, Fusion Technology, 21 (1992) 1707
2) Takase, T., Hasan, M. Z., Kunugi, T., "Heat Transfer in Plasma Facing Components on Fusion Reactors: Non-MHD Laminar Flow in Rectangular Channels", ibid. 1840
3) Ogawa, M., Kunugi, T. and the ITER/FER Safety Group, "Experiments on Exchange Flow through Two Breaches during Loss of Vacuum Accident in Nuclear Fusion Experimental Reactor", ibid. 2036
4) Yamauchi, M., Seki, Y., Kobayashi, S., Kasahara, F., "Comprehensive Safety Evaluation Methodology for Fusion Reactor", ibid. 2056
5) Itoh S-I., Itoh K., Fukuyama A. et al. , "Theory of Anomalous Transport in H-mode Plasmas", Phys. Rev. Lett. 72 (1994) 1200
6) Allen S.L., Brown M.D., Byers J.A., et al., "Nonlinear Absorption of High Power Free-Electron Laser-Generated Microwaves at Electron Cyclotron Resonance Heating Frequencies in the MTX tokamak", ibid. 1348.
7) Sato M., Ishida S., Isei N., "Relativistic Broadening Effect on Application of Electron Cyclotron Emission Measurements to High Temperature Tenuous Tokamak Plasma", J. Phys. Soc. Jpn., **62** (1993) 3106.
8) Itoh K., Itoh S-I., Fukuyama A. et al. , "Prandtl Number of Toroidal Plasmas", ibid. 4269
9) Yagi M., Itoh K., Itoh S-I. et al. , "Current Diffusive Ballooning Mode in Low Shear and Negative Shear Regions of Tokamaks", J. Phys. Soc. Jpn., 63 (1994) 10
10) Saidoh M., Ogiwara N., Shimada M., et al., "Initial Boronization of JT-60U Tokamak Using Decaborane", Jpn. J. Appl. Phys. **32** (1993) 3276.
11) Yamage M., Ejima T., Saidoh M., et al., "Wall Temperature Dependence of Boronization Using Decaborane and Diborane", ibid. 3968.
12) Kawashima H., Trukhin V.M., Lohr J., et al., "X-Ray Energy Analysis for Radio Frequency Current Drive Experiments in the DIII-D Tokamak", ibid. 3975.
13) Kikuchi M., "Prospect of a Stationary Tokamak Reactor", Plasma Phys. Control. Fusion **35** (1993) B39.
14) Naito O. and JT-60 Team, "Steady State Plasma Performance on JT-60U", Plasma Phys. Control. Fusion, **35** (1993) B215.
15) Kimura H., Fujii T., Saigusa M., et al , "High-harmonic ICRF Heating Experiments in JT-60", ibid. 845.
16) Itoh K., Itoh S-I., Fukuyama A. et al. "Confinement Improvement in H-mode like Plasmas in Helical Systems", Plasma Phys. Control. Fusion, 36 (1994) 123
17) Itoh K., Itoh S-I., Fukuyama A. et al. , "Self-sustained Turbulence and L-mode Confinement in Toroidal Plasmas I", ibid. 279
18) von Blokland A.A.E, Azumi M., Kikuchi M. et al., " Impact of the Magnetic Field Ripple on H-mode Performance", ibid. 925

19) Fukuyama A., Itoh k., Itoh S-I. et al. , "Isotope Effect on Confinement in DT Plasmas", Comments on Plasma Phys. Controlled Fusion, 15 (1994) 309
20) Fukuyama A., Itoh K., Itoh S-I. et al. , "Nonresonant current drive and Helicity Injection by Radio-freqency Waves", Phys. Fluids B5 (1993) 539
21) Yagi M., Wang J.P., Kim Y.B. et al. , "Ion-temperature-gradient-driven modes in Neoclassical Regime", Phys. ibid. 1179
22) Hosogane N., "Confinement and Divertor Studies in Japan Tokamak JT-60 Program", ibid. 2412.
23) Yagi M., Itoh K., Itoh S-I. et al. , "Analysis of the Current-diffusive Ballooning Mode", ibid. 3702.
24) Naito O., Yoshida H. and Matoba T., "Analytic Formula for Fully Relativistic Thomson Scattering Spectrum", ibid. 4256-4258.
25) Ida K., Itoh K., Itoh S.-I., et al., "Thickness of the Layer of High Shear Radial Electric Field in JFT-2M H-mode Plasmas", Physics of Plasmas 1 (1994)116.
26) Yamagiwa M., "Effects of Radio-frequency-induced Radial Diffusion on Triton Burnup", ibid. 205.
27) Yagi M., Horton W., "Reduced Braginskii Equations", ibid. 2135
28) Ueda N., Suzuki Y., Tanaka M., et al., "Review of the Present Status of Consistent Scrape-off Layer Modeling by Codes", Contrib. Plasma Phys. **34** (1994) 350.
29) Tanaka M., Ueda N., Suzuki Y., "Numerical Simulation of Carbon Impurities in JT-60U Experiment", ibid. 460.
30) Matsuoka M. et al.,"Production of a Negative Radial Electric Field in Tokamak Edge Plasmas by Perpendicularly Injected Low Energy Neutral Beams", Nuclear Fusion, **33**,No.1(1993)
31) Kurihara K., "Tokamak Plasma Shape Identification on the Basis of Boundary Integral Equations", Nuclear Fusion **33**, No.3 (1993) 399-412.
32) Saigusa M., Yamamoto T., C.C.Petty., "Analysis of the coupling properties of the toroidal antenna array in JFT-2M by a code considering the solid septa", ibid. 421
33) Tani K., Takizuka T., Azumi M., "Ripple loss of alpha particles in a tokamak reactor with a non-circular plasma cross-section", ibid. 903.
34) Ozeki T., Azumi M., Tokuda S. et al. , "Effects of a Hollow Current Profile on the Ideal MHD Stability of High bp Plasmas in a Tokamak", ibid. 1025.
35) Kubo H., Sugie T., Shimada M., et ai., "Study of Impurity and Radiative Losses in Divertor Plasmas with Absolutely Calibrated VUV Spectrometers in JT-60U", ibid. 1427.
36) Yoshino R., Neyatani Y., Hosogane N., et al., "The Softening of Current Quenches in JT-60U", ibid. 1599.
37) Nagashima K., Sakasai A., Fukuda T., "Gas Puff Modulation Experiments on JT-60U", ibid. 1677.
38) Thomsen, Campbell D.J., Cordey J.G., et al., "ITER H-mode confinement database update", Nucl. Fusion 34(1994)131.
39) Nagashima K., Koide Y., Shirai H., "Experimental Determination of Non-diffusive Toroidal Momentum Flux in JT-60U", ibid. 449
40) Wang J.P., Azumi M., Callen J.D. et al. , "Momentum and Heat Friction Forces between Fast Ions and Thermal Plasma Species", Nuclear Fusion (in press)
41) Sakamoto K., Kobayashi T., Kawasaki S., "Millimeter wave amplification in a free electron laser with a focusing wiggler" J. Appl. Phys. Vol.75,No.1, P.36-42
42) Tokuda S., "Analysis of Unstable Modes in Tokamaks", Simulation **12** (1993) 119 (in Japanese).
43) Suzuki S., Crawford J. F., Bradley J. T., et al., "Experimental study of pulse plasma heat flux adsorption and ablation during the simulation of a tokamak plasma disruption", J. of Nucl. Mat., 200 (1993) 265-269
44) Cardella A., Akiba M., Duwe R., et al., "Thermo-mechanical tests of a CFC divertor mock-up", J. of Nucl. Mat., 209 (1994) 117-121
45) Suzuki S., Akiba M., Araki M., et al., "High heat flux experiments of saddle type divertor module", J. of Nucl. Mat., (to be published)
46) Akiba M., Madarame H., "Effects of plasma disruptions on structural and plasma facing materials", J. of Nucl. Mat. (to be published)
47) Nakamura K., Akiba M., Suzuki S., et al., "Erosion of CFC and W at high temperature under high heat loads", J. of Nucl. Mat. (to be published)
48) Araki M., Sasaki M., Kim S. W., et al., "Thermal response experiments of SiC/C and TiC/C functionally gradient materials as plasma facing materials for fusion application", J. of Nucl. Mat. (to be published).
49) Ishiyama S., Akiba M., Eto M., Irradiation Damage Analysis on Relevant Divertor Structures for ITER, J. of Nucl. Matr. (to be published).
50) Akiba M., Watson R. D., "Thermo-hydrodynamic coupling with coolants", Atomic and Plasma-Material Interaction Processes, (1993) 455-480
51) Kuriyama M., Akino M., Araki M., et al., "Construction of a 500 keV Negative-Ion-Based NBI System for JT-60U", J. Fusion Eng. Des., **22**, (1993) 217.
52) Araki M., Akiba M., Sugihara M., et al., "Analytical and experimental evaluations of simulated sweeping heat load on the divertor plate for ITER", ibid. 217-227

53) Zimin S., "Empirical-analytical Formulae for Shield Effectiveness Examination for an Experimental Thermonuclear Reactor", ibid. 229.
54) Takatsu H., Yamamoto M., Shimizu M. and Ohta M., "Stress Analysis Method of U-shaped Bellows and its Experimental Verification", ibid. 239.
55) Saidoh M., Hiratsuka H., Arai T., et al., "A Boronization System in the JT-60U Tokamak - Application of a New Method Using a Less Hazardous Substance -", ibid. 271.
56) Maki K., Takatsu H., Seki Y., et al., "Radiation Shielding for Superconductive Toroidal Field Coils around the Neutral Beam Injector Duct in the ITER Design", ibid. 423.
57) Zimin S., "Simplified Method for Estimation of 3T Production in Boronized Shielding Materials and Li Burn Up in Breeder Blankets", J. Fusion Eng. Des., 23(1993)1.
58) Nishio S., Sugihara M., Shimomura Y., "Feasibility studies on plasma vertical position control by ex-vessel coil in ITER-like tokamak fusion reactor", ibid. 17-31.
59) Ikeda Y., Seki M., Maebara S., et al., "Development of a Diffusion Bounding Method for Fabrication of Lower Hybrid Current Drive Grills", ibid. 33.
60) Mizuno M., Hanada M., Inoue T., et al., "Conceptual Design of a 2MeV Neutral Beam Injection System for the Steady State Tokamak Reactor", ibid. 49.
61) Matsukawa M., Ushigusa K., Neyatani Y., et al., "Estimation of the JT-60 U Vessel Current by a Magnetic Fitting Code", ibid. 341.
62) Zimin S., "Cross-section Sensitivity Study for the Toroidal Field Coil Shielding Parameters in the ITER/OTR Design", J. Fusion Technol., 24(1993)168.
63) Murakami Y. and Sugihara M., "Optimization of Steady-state and Hybird Operations in a Tokamak Fusion Reactor by Using Divertor Scaling Models", ibid. 375.
64) Nishitani T.**), Takeuchi H.**), Itoh T., et al.,"Absolute Calibration of the JT-60U Neutron Monitors Using a ^{252}Cf Neutron Source", Rev.Sci.Instrum.63(11) , November 1992
65) Mizuno M., Ohara Y., "Design of an Electrostatic Magnetic Quadrupole Accelerator", Rev. Sci. Insturm., 64 (1993) 477.
66) Ishizuka H., Nakahara Y., Kawasaki S., et al., "Design Study of mm to nm Diameter Electron Beams for Sub Millimeter-wave to X-ray Free-electron Lasers", Nucl. Instrum. and Meth. in Phys. Res. **A331** (1993) 577.
67) Arai H., Kimura H., Fujii T., "A Ceramic-Free Waveguide for ITER Ion Cyclotron Wave System", IEEE Transaction on Plasma Science **21** (1993) 265.
68) Iwaki G.,Sasaki S.,Kamata K., et al., "Development of Bronze-Processed (NbTi)3Sn Superconducting wires for Central SolenoidModel coil of ITER", IEEE TRANSACTIONS ON APPLIED SUPERCONDUCTIVITY. **2**, 998-1001 (1993).
69) Ono M.,Wachi Y.,Shimada M., et al., "Charging Test results of the DPC-TJ a High-Current-Density Large Superconducting coil for Fusion Machines", IEEE TRANSACTIONS ON APPLIED SUPERCONDUCTIVITY, **3**, 480-483 (1993).
70) Ando T.,Nakajima H.,Hiue H., et al., "The Effect of Ti Conduit on the Critical Current in (NbTi)3Sn Cable-in-conduit Conductors", ibid. 492-495.
71) Ando T.,Takahashi Y.,Sugimoto M., et al., "Development of Nb3Al Cable-in-Conduit Fusion Superconductors", ibid. 492-495.
72) Isono T.,Hosono F.,Koizumi N., et al., "Development of a(NbTi)3Sn Strand for the ITER CS Scalable Model Coil", ibid. 496-499.
73) Sasaki T.,Koizumi N.,Nishi M., et al., "Stability Performance of the DPC-TJ Nb3Sn Cable-in-Conduit Large Superconducting coil", ibid. 523-526.
74) Sugimoto M.,Hosono F.,Isono T., et al., "Test Results of the Toroidal Model Pancake for ITER/FER Toroidal Field coils", ibid. 531-534.
75) Hosono F.,Sugimito M.,Tsukamoto H., et al., "AC Loss of the Toroidal Model Pancake(TMP)", ibid. 535-538.
76) Konn M.,Yasukawa Y.,Sasaki K., et al., "Superconducting Magnet System for high power Gyrotron", ibid. 551-554.
77) Okuno K.,Takahashi Y.,Tsuji H., et al., "Ac loss performance of 1-m-bore, large-current Nb3Sn Superconducting coils in JAERI Demo Poloidal Coil project", ibid. 602-605.
78) Takahashi Y.,Koizumi N.,Wadayama Y., et al., "Experlmental Results of Stability and Current Sharing of NbTi Cable-in-conduit conductor for the Poloidal Field Coils", ibid. 610-613.
79) Nishi M.,Ando T.,Tsuji H., et al., "Development of high current density, large superconducting coil for fusion machines: the DPC-TJ Program", Cryogenics **33**, 573-580 (1993).
80) Aoki M.,Ogaki T.,Noguchi K., et al., "Fabrication of superconductor for the DPC-TJ coil", ibid. 581-585.
81) Ono M.,Mukai H.,Shimada M., et al., "Test results of the DPC-TJ: electromagnetic performance", ibid. 586-591.

82) Koizumi N.,Yoshida K.,Isono T., et al.,"Test results of the DPC-TJ: stability performance", ibid. 592-596.
83) Wachi Y.,Mukai H.,Ono H., et al., "Test results of the DPC-TJ: mechanical performance", ibid. 603-608.
84) Iwabuchi A.,Iida S.,Yoshino Y., "Frictional properties of structureal steel JN2 at cryogenic temperatures in a vacuum", ibid. 1110-1115
85) Koizumi N.,Okuno K.,Takahashi Y., et al., "Experimental results on instability caused by non-uniform current distribution in the 30 kA NbTi Demo Poloida Coil (DPC-U) conductor", Cryogenics, **34**, (1994) 155-162,
86) Kohzaki, Y., Seki, Y. Motoshima, O. et al., "Prospects of Fusion Energy System", J. Atomic Energy Soc. Japan, **35** (1993) 3 (in Japanese)
87) Matsukawa M., Horie T., Horiike H., et al., "Stress Analysis of Poloidal Field Coil Support in JT-60U", ibid. 561 (in Japanese).
88) Okumura Y., ibid. 1049. (in Japanese)
89) Ioki K., Onozuka M., Akiba M., et al., "Development of Unidirectional C/C Composite with High Thermal Conductivity and Its Application to Plasma Facing Materials", J. of the Atomic Energy Society of Japan, **36**, (1994) No.3 239-244 (in Japanese)
90) Ogiwara N., Shiho M., Ueda Y., "A Mass Filter with a Cold Cathode", Vacuum **44** (1993) 661.
91) Obara K., Kakudate S., Tada E., et al., "Development of AC servo motor with Ceramic insulated-wire used for Severe environment" , J. Vacuum Soc. Jpn., **37** (1994) 124-127
92) Abe T., Hiroki S., Murakami Y., et al., "Performance test of a ceramic turbo-viscus pump", ibid. 161 (in Japanese)
93) Sugihara M., "Major Issues and R&D Tasks for ITER Divertor", J. of Plasma and Fusion Research, **69**(1993)1150 (in Japanese).
94) Watanabe K., Itoh T., Matsuoka M., "Surge Suppression in a Power Supply of a Neutral Beam Injector", ibid. 1229. (in Japanese)
95) Akiba M., "High Heat Flux Components and Thermal Conditions in Fusion Reactors", ibid. 1444-1449 (in Japanese)
96) Itoh K., Itoh S-I., Fukuyama A. et al. , "Confinement Improvement by the Current Profile Control", ibid. 1524 (in Japanese)

A.1.3 List of papers published in conference proceedings

1) Hasan, M. Z., Takase, K., "Aspect Ratio Effects on Heat Transfer in Non-MHD Laminar Flow Through Rectangular Channels in the Plasma Facing Components of Fusion Reactors", Proc. 17th SOFT (Sept. 14-18, 1992, Roma) 1369.
2) Shimada M. and JT-60 Team, "JT-60U High Power Heating Experiments", Proc. of 14th Int. Conf. on Plasma Phys. Control. Nucl. Fusion, Vol. 1 (1993) 57.
3) Kikuchi M., Shirai H., Takizuka T., et al., "H-mode and L-mode Confinement in JT-60U", ibid. 189.
4) Ishida S., Matsuoka M., Kikuchi M., et al., "Enhanced Confinement of High Bootstrap Current Discharges in JT-60U", ibid. 219.
5) Nishitani T., Tobita K., Tani K., et al., "Beam-Injected and Fusion-Produced Particle Studies in JT-60U", ibid. 351.
6) Itami K., Shimada M., Asakura N., et al., "Heat Transport and Electric Current in Tokamak Boundary Plasmas of JT-60U", ibid. 391.
7) Sakasai A., Kubo H., Shimada M., et al., "Impurity Generation Mechanism in JT-60U", ibid. 495.
8) Kamada Y., Takizuka T., Kikuchi M., et al., "Effect of Current Profile on MHD Characteristics and Plasma Performance in JT-60U", ibid. 507.
9) Ushigusa K., Imai T., Ikeda Y., et al., "Confinement and Transport of Energetic Electrons during Lower Hybrid Current Drive", ibid. 601.
10) Koide Y., Tuda T., Ushigusa K., et al., "Spontaneous Plasma Rotation of Nearly Perpendicular NBI and LHCD Plasmas in JT-60U", ibid. 777.
11) Ozeki T., Azumi M. Tsunematsu T. et al. , "Profile Control for Stable High- Beta-Poloidal Tokamak with Large Bootstrap Current", Proc. of 14th Int. Conf. on Plasma Phys. Control. Nucl. Fusion, Vol. 2 (1993) 187.
12) Fukuyama A., Itoh K.,Itoh S-I. et al. , "Stochasiticity-driven Disruptive Phenomena in Tokamaks", ibid. 363.
13) Itoh K., Itoh S-I., Fukuyama A. et al. , "Model of L-mode Confinement in Tokamaks", ibid. 381.
14) Yoshino R., Hosogane N., Neyatani Y., et al., "Disruption and Stable Plasma Shutdown in JT-60U", Proc. of 14th Int. Conf. on Plasma Phys. Control. Nucl. Fusion, Vol. 3 (1993) p. 405.
15) Fukuda T., Kikuchi M., Kiode Y., "H-mode Transition Physics Studies in JT-60U: The Role of Shear Flow, Turbulent Fluctuation and Edge Ion Collisionality", Proc. 20th European Conf. on Control. Fusion and Plasma Phys., Vol. I (1993) 31.

16) Sakasai A., Koide Y., Nakamura H., et al., "Helium Transport During H-mode in JT-60U", ibid. 67.
17) Van Blokland A.A.E., Azumi M., Koide Y., et al., "Effect of the Magnetic Field Ripple on H-mode Performance in JT-60U", ibid. 71.
18) Tanga A., Yoshino R., Hosogane N., et al., "Effects of Plasma Compression in JT-60U", ibid. 175.
19) Kikuchi M., Sato M., Koide Y., et al., "Hot Ion H-mode Characteristics in JT-60U", ibid. 179.
20) Neyatani Y., Kamada Y., Ozeki T., et al., "MHD Behavior in High bp and bN Discharges in JT-60U", ibid. 215.
21) Ikeda Y., Ushigusa K., Naito O., et al., "Lower Hybrid Current Drive Experiment in JT-60U", Proc. of 20th European Conf. on Control. Fusion and Plasma Phys., Vol. III (1993) 909.
22) Ushigusa K., Matsuoka M., Kamada Y., et al., "Current Profile Control by Non-Inductive Current Drive in JT-60U", ibid. 913.
23) Matsuoka M., Ishida S., Kamada Y., et al., "Beam-driven and Bootstrap Currents in JT-60 Upgrade", ibid. 929.
24) Ryter F., Kardaun O.J.W.F., Stroth U., et al., "An Examination of the ITER H-mode Power Threshold Database", 20th EPS Conference on Controlled Fusion and Plasma Physics, Lisbon,Vol.17C (1993)15.
25) Kardaun O.J.W.F., Ryter F., Stroth U., et al., "Analysis of the ITER H-mode Confinement Database", ibid. 15.
26) Sakasai A., Koide Y., Nakamura H., et al., "Helium Transport during H-mode in JT-60U", ibid. 67.
27) von Blokland A.A.E, Azumi M., Koide Y. et al., " Effect of the Magnetic Field Ripple on H-mode Performance in JT-60U", ibid. 71
28) Annaratone B.M., Yamauchi T., Maeda H., "Measurement of Electrostatic Turbulence in the Scrape off Layer of JFT-2M by Langmuir Probes", ibid. 311.
29) Yamauchi T. and TVTS Team, "Te and Ne Profiles on JFT-2M Plasma with the Highest Spatial Resolution TV Thomson Scattering System", ibid. 1195.
30) Itoh S.-I., Itoh K., Fukuyama A., et al., "Theory of L-mode, L/H transition and H-mode", ibid. 1427.
31) Matsuoka M. et al.,"Beam-Driven and Bootstrap Cuurents in JT-60 Upgrade", ibid.
32) Ikeda Y., Ushigusa K., Naito O., et al., "Lower Hybrid Current Drive Experiments in JT-60U ", Proc. of 20th EPS Conf. n Controlled Fusion and Plasma Physics (1993) III-909.
33) Saigusa M., Kimura H., Fujii T., et al., "Recent Progress in ICRF Heating Experiments on JT-60U ", ibid. III-989.
34) Yagi M., Azumi M., Wang J.P. et al " Eta-i Mode in Neoclassical Regime and Neoclassical Closure", Proc. 1994 International Sherwood Fusion Theory Conference (Dallas, 1994) 1D-11
35) Yagi M., Itoh K., Itoh S-I. et al., " Nonlinear Simulation of the Current Diffusive Interchange Mode", ibid. 3B01
36) Ninomiya H. and JT-60 Team, "Recent Progress and Future Prospect of the JT-60 Program", Proc. of 15th Synp. on Fusion Engineering, Vol. 2 (1994) 779.
37) Tajima T., Kishimoto Y., LeBrun M.J., et al., "Transport in the Self-Organized Relaxed State of Ion Temperature Gradient Instability", in Ion Temperature Gradient Driven Turbulent Transport, AIP Conference Proceeding **284** (1994) 255.
38) Kimura T., "VME and Network Applications to the JT-60U Control System", in Proc. of International Conf. on Accelerators and Large Experimental Physics Control Systems, Berlin, 1993, to be published in Nuclear Instruments and Methods.
39) Kimura H., Fujii T., Sato M., et al., "Sawtooth Stabilization Experiments by ICRF Heating Alone and its Combination with NBI or LHCD in JT-60U", 10th Conf. on Radio Frequency Power in Plasmas (Boston, 1993).
40) Tuccillo A.A., Ide S., FTU Team, "First Results of the 8GHz LH Experiment in FTU", ibid.
41) Fujii T., Ushigusa K., Saigusa M., et al., "Lower Hybrid Current Drive and ICRF Heating Experiments on JT-60U", Proceeding of 10th Topical Conference on RF Power in Plasma, Boston, (1993) 99.
42) Hoshino K., Mori M., Yamamoto T., et al., "Suppression of Disruptions with ECH on JFT-2M", ibid. 149.
43) Seki M., Ikeda Y., Ushigusa K., et al., "Characteristic of a Large Multijunction Launcher for High Power LHCD Experiments on JT-60U ", ibid. 319.
44) Ohara Y., Hanada M., Inoue T, et al., "Development of High Power Negative Ion Source for Fusion Researches at JAERI", in Proc. of 5th Int. Conf. on Ion Sources, Beijing, China, (1993) 1159.
45) Kuriyama M., Akino N., Araki M., et al., "High Energy Negative Ion Based NBI System for JT-60 U", in Proc. of 5th Int. Toki Conf. on Plasma Physics and Controlled Nucl. Fusion, Toki, Japan, (1993) 470.
46) Ohara Y., "Progress of NB R&D for Plasma Heating and Current Drive at JAERI", ibid.
47) Okumura Y., Hanada M., Inoue T., et al., "Development of a 500 keV, 22A D^- Ion Source for the JT-60 U Neutral Beam Injector", ibid.
48) Matsuoka M. et al.,"Non-Inductive Current Drive Experiments in JT-60", ibid.

49) Mizumoto M., Hasegawa K., Okumura Y., et al., "Development of Proton Linear Accelerator and Transmutation System", in Proc. of Int. Conf. and Technl. Exhibition on Future Nuclear System GLOBAL '93', Seattle, (1993).

50) Ogiwara N., Jimbou R., Saidoh M., et al., "The Reaction of H_2O, O_2 and Energetic O_2^+ on Boron Carbide", Proc. of 6th Intern. Conf. on "Fusion Reactor Materials", (Stresa, 1993).

51) Kawasaki S., Ishizuka H., Sakamoto K., "Design and Operation of Inductive Acceleration Modules for FEL with Controlled Voltage Ramp" Proc. IEEE Part. Accel.Conf. '93, Washington DC

52) Ishizuka H., Nakahara Y., Kawasaki S., "Ultrahigh-Brightness Microbeams: Considerations for Their Generation and Relevance to FEL", ibid.

53) Sakamoto K., Shiho M., Watanabe A., "Study of Wave guide Mode Identification in FEL Experiment", 15th Int. FEL Conf. 1993, Hague, Netherland

54) Kawasaki S., Takahashi M., Ishizuka H., "Analysis and optimal design study of tapered FEL amplifiers on the border of Raman and Comptonregimes", ibid.

55) Shiho M., Kawasaki S., Sakamoto K., "Design and Construction of Induction Linac For MM Wave Free Electron Laser For Fusion Research", ibid.

56) Nishio S., Murakami Y., Adachi J., et al.,"A Concept of Drastically Easy Maintenance(DREAM) Tokamak Reactor", 7th Int. Conf. on Emerging Nucl. Energy Systems, Makuhari,20-24,Sept,1993

57) Matsuoka M., Araki M., Direct EnergyRecovery with AC Electric Power Output, in Proc. of 7th Int. Conf. on Emerging Nucl. Energy Systems, (1993) 527.

58) NaKajima H.,Sasaki T.,Ando T., et al., "Effects of Cyclic Pulsed Operation on the Coil Performance in the Nb3Sn Demo Poloidal Coil (DPC-EX)", MT-13, (1993)

59) Nishi M.,J.R.Armstrong.,Koizumi N., et al., "Effect of Strand Diameter on the Stability of the Cable-in-Conduit Conductor", ibid.

60) Takahashi Y.,Sugimoto M.,Isono T., et al., "Experimental Results fo 40-kA Nb3Al Cable-in-conduit Conductor for Fusion Machines", ibid.

61) Nishi M.,Yamamoto K.,Sasaki T., et al., "Effect of the Vold-Fraction on the Property of the Nb3Sn Cable-in-conduit Conductor", International Cryogenic Material Conference, (1993)

62) Nyilas A.,Obst B.,Nakajima H., "TENSILE PROPERTIES, FRACTURE, AND CRACK GROWTH OF A NITROGEN STRENGTHENED", 3rd International conference on High Nitrogen Steels "HNS 93", KIEV UKRAINE, (1993)

63) Kurasawa T., "The VOM/JRR-2 Experiment; Performance of In-site Tritium Release from the Lithium Ceramics", in Proc. of 6th Int. Conf. on Fusion Reactor Materials, Stresa, 1993.

64) Okuno K., "Model Coil for the International Thermonuclear Experimental Reactor (ITER) Magnet Systems", 13th International Conf. on Magnet Technology, Victoria, (1993)20.

65) Kurihara K., Kimura T., Kawamata Y., et al., "Tokamak Plasma Shape Identification Based on Boundary Integral Equations and the Real-time Shape Visualization System", in Proc. of the 17th Symp. on Fusion Technology, Rome, 1992, Volume I, 1993, North-Holland, pp.860-866.

66) Okumura Y., Hanada M., Inoue T., et al., "Development of a Large D^- Ion Source for the JT-60 U Negative-Ion-Based Neutral Beam Injector", in Proc. of the 15th Symp. on Fusion Engineering, Hyannis, 1993, 466.

67) Inoue T., Miyamoto K., Mizuno M., et al., "Merging Beam Experiment of Intense Negative Ions for Advanced Compact Neutral Beam Injectors", ibid. 474.

68) JT-60 Team presented by I. Kondo, "Status of Machine Operation of JT-60", ibid. pp. 826-829.

69) Nakamura K., Akiba M., Suzuki S., et al., "High Heat Flux Experiments of Plasma Facing Components for Next Fusion Devices", ibid. 830.

70) Kitamura K., Nagata K., Akiba M., et al., "Optimization Studies on Interfacial Mechanical Strength in the Graphite-Copper Bonded Structure for a Divertor Application", ibid. 863.

71) Matsuzaki Y., et al., "Direct Current Interrupting System Using an Iron Core for Quench Protection of the Superconducting Coil", ibid. pp. 889-892.

72) Sherman R. H., Taylor D. J., Yamanishi T., et al., "Application of Sidestream Recycle to the Separation of Hydrogen Isotopes by Cryogenic Distillation", ibid..

73) Konishi S., Yamanishi T., Hayashi T., et al., "Extended Operation of Reactor-Scale Fusion Fuel Loop under US-Japan Collaboration", ibid..

74) Ando T., Kodama K., Matsukawa M., et al., "Material Behavior of JT-60U Plasma Facing Components and Installation of B_4C-converted CFC/Graphite Tiles", ibid.

75) Kuriyama M. at el., "Construction of A 500keV/Negative-Ion Based NBI System for JT-60U", ibid.

76) Oka K., Shibanuma K., Tada E, et al., "Critical Element Development of Internal-access Pipe Welding/ Cutting Equipment", ibid.

77) Sasaki N.$^+$, Ogawa H.$^+$, Obama M.$^+$, et al. "Development of the 1/5 Scale Model of Articulated Boom System for In-vessel Remote Maintenance of Fusion Experimental Reactor", ibid.

78) Takase K., and Hasan M.Z., "Heat Transfer in MHD Laminar Flow through a Rectangular Channel in the Plasma Facing Components of Fusion Reactor", ibid.
79) Sato S., Takatsu H., Hashimoto T., et al., "Fabrication of a Blanket Box Structure Integrated with the First Wall for a Fusion Experimental Reactor", ibid.
80) Enoeda M., Sato S., Kurosawa T. and Takatsu H., "Measurement of Effective Thermal Conductibity of Lithium Oxide and Beryllium Sphere Packed Bed", ibid..
81) Willms R. S., and Okuno K., "Recovery of Hydrogen from Impurities Using a Palladium Membrane reactor", ibid.
82) Nishi M.,Nakajima H.,Ando T., et al., "Ramp-Rate Limitaion Test Results of the Nb3Sn Demo Poloidal Coil (DPC-EX)", ibid.
83) Maeno S., Nakamura K., Okumura Y., et al., "Development of the Super Low Energy Ion Source (SLEIS) Producing 300 eV, 1 A Ion Beams", in Proc. of 4th Symp. on Beam Engineering of Advanced Material Syntheses Including Bio-Medical Materials and Treatments,Tokyo, Japan, (1993) 19.
84) Linke J., Akiba M., Ando T., et al., "Protective Coating for Plasma Facing Components in Thermonuclear Reactors", in Proc. of 13th Int. PLANSEE seminar '93, vol. 1 (1993) 112.
85) Deschka S., Akiba M., Breitbach G., et al., "High Heat Flux Tests on Brazed Divertor Components in Electron and Ion Beam Test Facilities", ibid. 1053-1067
86) Kurasawa H.,O.D.Slagie,R.A.Verrall,et al., "Tritium Recovery Characteristics of Lithium Oxide in BEATRIX-Phase and radiation", 6th ICFRM, Ispra, Italy, (1993).
87) Cheng T. and Saji G., "Activation and Waste Management Consideration of Fusion Materials", ibid.
88) Koizumi K., Tada E., Shibanuma K., et al., "Development Program of Tokamak Fusion Experimental Reactor and the Latest Progress of Reactor Structure Technology", The 5th Electromagnetics Symposium Proceedings, Hitachi, Japan 1993 (in Japanese).
89) Saji G., "ITER Technical Challenges and Opportunities", Canadian Fusion Symposium, Toronto, 1993.
90) Yonomoto T., Kukita Y., Ogawa M., et al., "Loss-of-coolant Accident Analysis for ITER Divertor System", 6th Internat. Topical Meeting on Nuclear Reactor Hydraulics, Grenoble, (1993).
91) Tsunematsu T., "ITER and Strategy of Fusion Reactor Development", NIFS Symposium, Nagoya, (1993) (in Japanese).
92) Itami K., Asakura N., Tsuji S., et al., "Heat and Particle Transport in the Boundary Plasmas during H-mode in JT-60U", IAEA TCM on H-mode Physics (Naka 1993).
93) Koide Y., Kikuchi M., Ishida S., et al., "Formation of Internal and Edge Transport Barriers in JT-60U", ibid.
94) Kamada Y., Ushigusa K., Naito O., et al., "ELMy H-mode with High-bN and High-bp in JT-60U", ibid.
95) M. Mori and JT-60 Team and JFT-2M Team, "Overview of Experimental Results on JT-60U and JFT-2M", ibid.
96) Fukuda T., Kikuchi M., Koide Y., et al., "H-mode Properties of JT-60U Discharges in Different Collisionality Regimes", ibid.
97) Yoshino R. and JT-60 Team, "Pellet Injection Study in JT-60U", IAEA TCM on Pellet Injection (Naka 1993).
98) Yoshino R., "Pellet Experiments", ibid.
99) Saidoh M., Jimbou R., Ogiwara N., et al., "Characteristics of B/C Materials as Plasma Facing Materials", Proc. of the IAEA Tech. Comm. Meet. on "Atomic and Molecular Data for Fusion Reactor Technology", (1993) p.88 (Cadarache, 1992).
100) Saigusa M., Moriyama S., Fujii T., "New Conceptual Antenna with Spiral Structure and Back Faraday Shield for FWCD" IAEA Technical Committee Meeting on Radio-Frequency Lannchers for Plasma Heating and Current Drive (Naka, Japan)
101) Akiba M., Araki M., Nakamura K., et al., "Thermal Response Tests on Plasma Facing Components", Proc. of IAEA TCM on Atomic and Molecular Data for Fusion Reactor Technology, (1993) 99.
102) Seki Y., Saito M., Aoki I.,et al, "Overview of Fusion Safety Environmental R&D Tasks in Japan", Proc. IAEA TCM on Development in Fusion Safety, June 7-11, Tronto, Canada(1993) J. of Fusion Energy, Vol.12, Nos.1/2 (1993)11.
103) Seki Y., Saitoh M., Aoki I., et al., "Fusion safety and environmental R&D tasks in Japan", ibid. 14.
104) Ogawa M., Kunugi T., and Seki Y., "Basic Experiments During Loss of Vacuum Event(LOVE) in Fusion Experimtal Reactor", ibid. 77.
105) Seki Y.,"Fusion Reactoru Design and Technology Programme in Japan", Proc. IAEA-TCM WS on Fusion Eng.Design.
106) Yamazaki S., Miura H., Koike H., et al., "Design Study of Helium-Solid Suspension Cooled Blanket and Divertor Plate for a Tokamak Power Reactor",Proc.IAEA=TCM WS on Fusion Reactor Design and Technology, Sept. 13-17 (1993), to be published in Fusion Eng.Design.
107) Shirai H., Takizuka T., Azumi M., "Transport Properties and Transport Simulation of JT-60 Plasmas", Proc. of International School of Plasma Physics "Local Transport Studies in Fusion Plasmas" (Varenna, Italy, 1993) 33

108) Nagashima K., Koide Y., Shirai H. et al., "Toroidal Momentum Transport Experiments on JT-60U", ibid. 75
109) Tuda T., "The effect of External Helical Field on Tokamak Plasma", 3rd International Youth School on Plasma Physics and Controlled Fusion (St.Petersburg, Russia).
110) Asakura N., Tsuji S., Itami K., et al., "Particle Recycling and Impurity Transport in Divertor on JT-60U", 35th Annual Meeting, APS Division of Plasma Physics (Missouri, US 1993).
111) Sato M., Kikuchi M., Kimura H., et al., "Temperature and Current Profiles in Hot Ion H-mode and Sawtooth Stabilized JT-60U Plasmas", ibid.
112) Kondoh T. and JT-60 Team, "High Performance and Current Drive Experiment in JT-60U", ibid.
113) Nishitani T., Isida S., Kikuchi M., et al., "Fusion Reactivity of High Poloidal Beta Plasma in JT-60U", ibid.
114) S. Ishida, Y. Koide, T. Nishitani, T. Fujita, M. Mori, et al., "Achievement of H-mode Confinement in the JT-60U High-bp Experiments", ibid.
115) Ozeki T., Azumi M., Tokuda S., et al., "Ideal Beta Limits in JT-60U High bp Discharges", ibid.
116) Shimomura Y., "Overview of International Thermonuclear Experimental Reactor (ITER) Engineering Design Activities", ibid.
117) Fukuda T., Sato M., Koide Y., et al., "Turbulence Diagnostics on JT-60U High-bp H-mode Discharges", US-Japan Workshop on Profile and Turbulence Diagnostics for High-β Plasma and Internal Magnetic Field Measurements (Prineton, 1993).
118) Kubo H., Fujita T., Isei N., et al., "Present Status and Plan of Motional Stark Spectroscopy on JT-60 Upgrade", ibid.
119) Ide S. and JT-60 Team, "Heating and Current-Drive Results from JT-60U and the Perspective for Long Pulse Operation", US/Japan Workshop on Physics Issues from Steady-state Tokamaks (Naka 1993).
120) Ozeki T., Azumi M., Tokuda S., et al., "Ideal Beta Limits in JT-60U High bp Discharges", US-Japan-Australia Workshop on New Concepts in MHD (Ena 1993).
121) Tanaka S., "Design of ITER Plasma Facing Components", US-Japan Workshop on High Heat Flux Components and Plasma Surface Interactions for Next Devices, San Diego, (1994).
122) Ando T., "PFCs and PSI in JT-60U", ibid.
123) Hamamatsu K., Azumi M., Tani K., "Neoclassical Effects on Slowing down Alphas in Tokamak Plasmas", Proc. of US-Japan Workshop on "Physics of High Energy Particles in Toroidal Systems" (Irvine, USA,1994) (in press)
124) Fukuda T., Mori M., Shrai H., "Evalution of the Local Transport via Turbulence Diagnostics", US-Japan Workshop on mm and Sub-mm wave Diagnostics (Tsukuba 1994).
125) Sato M., "ECE Measurements in JT-60U", ibid.
126) Fujita T., "Bootstrap Current in High Performance/High bp", US-Japan Workshop on Plasma Profile Control for High Power Performance Operation and Non-inductive Current Drive (Naka 1994).
127) Ide S., "Current Drive and Profile Controle by LHCD in JT-60U", ibid.
128) Kamada Y., "Impact of Profile Control in Bootstrap Current Dominant Discharges in JT-60U", ibid.
129) Ishida S. and JT-60 Team, "JT-60U High-bp Discharges and thier Scalings", TFTR/JT-60U Data Discussion for Supershot and High-bp Discharges (Princeton 1993).
130) Kamada Y. and JT-60 Team, "Steady State High Performance in JT-60U", Workshop of Three Large Tokamak on Termination of High Performance (Abinton 1993).
131) Saidoh M., Ogiwara N., Jimbou R., et al., "Application of B/C Materials for the First Wall in JT-60U", Proc. of 6th Intern. Workshop on "Carbon Materials", (Juelich, 1993).
132) Miyamoto K., Hanada M., Inoue T., et al., "A 350 keV, 0.2 A Negative Ion Source", in Proc. of the Third Workshop on Negative Ion Formation and Beam Handling, KEK, Japan, (1993) 1. (in Japanese)
133) Shinto K., Hanada M., Maeno S., et al., "Correlation between Negative Hydrogen Ion Production and Work Function of Plasma Grid", ibid. 135.
134) Nagashima T. and ITER Joint Central Team, "High-power RF Heating and Current Drive Experiments Planned for ITER", 2nd Int. WS on Strong Micrwaves in Plasmas, Novgorod, Russia, (1993)15.
135) Sakamoto K., Kasugai A., Tuneoka M., "Development of a high power gyrotron for fusion application in JAERI", ibid.
136) Suzuki T., Kikuchi Y., Akiba M., et al., "Development of Plasma Facing Material in Hitachi Chemical", Proc. of 6th Carbon Workshop, (1993).
137) Miya K., Muto Y., Takatsu H., et al., "Research on Structural Design Guideline for the Experimental Fusion Reactor", 2nd Internat. Workshop on Electromagnetic Forces and Related Effects on Blankets and Other Structures Surrounding the Fusion Plasma Torus, Tokai, (1993)15.
138) Neyatani Y., Ushigusa K., Matsukawa M. and Ninomiya H., "Effect of Electromagnetic Forces during Disruption in JT-60U Vacuum Vessel", ibid..
139) Mohri K., Sato K., Yamada T., et al., "First Wall/Blanket Fabrication Technology - Fabrication of Blanket Box Structure -", FAPIG, 135(1993)18 (in Japanese).

140) Fujisawa N., Weslay J. and the ITER Physics Unit, "ITER Physics Needs for Disruptions", ASDEX/DOE Workshop on Disruptions in Divertor Tokamaks, (1993).
141) Sugihara M., "Disruption Effects on ITER Divertor Design", ibid..
142) Tokuda S., "Resistive MHD Stability Analysis by Asymptotic Matcing Method", Proc. 1993-Workshop on MHD Computations (Institute of Statistical Mathematics, 1994) 85 (in Japanese).
143) Nakamura Y., "Position Control Analyses of Fusion Plasmas - Axisymmetric Tokamak Simulation -", ibid. 97.
144) Hoshino K. and JFT-2M Group, "Control of Plasma Disruptions by Electron Cyclotron Heating", ibid. 111.
145) Kurita G., Tuda T., Azumi M., Takeda T., "Simulation of Tearing Mode Stabilization by Using ECH", ibid. 123.
146) Takeda T., "Application of Neural Network to Nuclear Fusion Research", ibid. 221 (in Japanese).
147) Tsunematsu T., "Overview of Japanese Presentations and Codes", ITER/EDA Tech. Meeting on Plasma Equilibrium and Control, Naka JWS, 1993.
148) Shinya K. and Tsunematsu T., "Equilibrium Analysis Code with Virtual Stabilization Circuit", ibid..
149) Shinya K. and Tsunematsu T., "Comment on EDA Plasma and PF Configuration", ibid..
150) Nishio S., "Position Control Code", ibid..
151) Nishio S., "Control of Plasma Position on ITER", ibid..
152) Matsukawa M., "Preliminary Evaluation of the Power Supply Capacity for ITER EDA Magnetic Configuration", ibid..
153) Sugihara M., "Requirements for Plasma Equilibrium and Control Based on Preliminary Considerations of Divertor Geometry for EDA ITER", ibid..
154) Tsunematsu T., "Summary of Code Session", ibid..
155) Takatsu H., "Electromagnetic Issues Related to the ITER Structural Design Code", ITER/EDA Tech. Meeting on Design Standard and Remote Handling, San Diego JWS, 1993.
156) Takatsu H., "Summary and R&D Proposals", ibid..
157) Shibui M., "Japanese Activities on Development of Standard Components for ITER", ibid..
158) Shibui M., "Recommendation on Standard Processes for Component Fabrication", ibid..
159) Takatsu H., Shibui M. and Hada K., "Leak Before Break in the Overall Safety Approach", 2nd Tech. Meeting on Safety, Environment and Regulatory Approval, San Diego JWS, (1993).
160) Inabe T., "Japanese Regulatory Process, Schedule and Requirements", ibid..
161) Yamamoto H., Katagiri H. and Kobayashi H., "Japanese Criteria for No-evacuation Emergency Planning, Dose/Release Limits", ibid..
162) Oikawa T., "Japanese Approach to Global Assessment Methodology and Safety Functional Classification", ibid..
163) Oikawa T., "Japanese Criteria on DBA, Event Classes, Safety Classes", ibid..
164) Yamamoto H., "Summary of Radioactive Waste Land Disposal in Japan", ibid..
165) Matoba T., "Overview of Japanese Home Team", Technical Meeting on Radiation Effects on In Vessel Components, Garching JWS, (1993).
166) Iida T. and Oyama Y., "D-T Neutron Irradiation Facility in Japan -FNS and OKTAVIAN-", ibid..
167) Kakuta T., "Status of Existing Database in Japan", ibid..
168) Shikama T., "In-situ Type Irradiation Studies of Electrical Property of Ceramic Insulators in Japan", ibid..
169) Kakuta T. and Shikama T., "Development of Radiation Resistant Optical Fibers", ibid..
170) Iida T. and Oyama Y., "D-T Neutron Irradiation Experiments on Optical Window Materials", ibid..
171) Matoba T., "Irradiation Test Plan of Reflector/Mirrors and Windows in JMTR", ibid..
172) Matoba T., "Irradiation Test Plan of Magnetic Coils and Bolometers for Technology R&D in Japan", ibid..
173) Matoba T. and Ramsey A., "Summary on Reflectors and Mirrors", ibid..
174) Takizuka T., Tsuji S., "Comments on the Basic Equations and Main-plasma Boundary Conditions in Divertor Simulation Codes", Technical Meeting and Workshop on ITER Divertor Physics Design, Garching, Feb. (1994).
175) Shimizu K., Takizuka T., "Impurity Transport Code Based on Monte Carlo Techniques (IMPMC)", ibid..

A.1.4 List of other reports

1) Shimada M., "Plasma-material Interaction Data Needs for Impurity Control in Next Step Devices", Atomic and Plasma Material Interaction Processes in Controlled Thermonuclear Fusion, R.K. Janev and H.W. Drawin (ed) (1993) 319.
2) Nishitani T., et al., "Confinement and Heating of a Deutrium-Tritium Plasma", PPPL Report PPPL-2977.
3) Nishitani T., et al., "Fusion Power Production from TFTR plasm Fueled wit Deutrium and Tritium", PPPL Report PPPL-2978.

4) Yagi M.,Itoh K., Itoh S-I. et al. , "Analysis of Current DiffusiveBallooning Mode", National Institute for Fusion Study Report NIFS-216
5) Itoh K., Itoh S-I., Fukuyama A. et al. , "Self-sustained Turbulence and L-mode Confinement in Toroidal Plasmas", National Institute for Fusion Study Report NIFS-219
6) Itoh K., Yagi M., Fukuyama M. et al. "Comment on 'A Mean Field Ohm's Law for Collisionless Plasmas", National Institute for Fusion Study Report NIFS-229
7) Itoh K., Itoh S-I., Fukuyama A., et al. , "Prandtl Number of Toroidal Plasmas" , National Institute for Fusion Study Report NIFS-234
8) Miura Y., Okano F., Suzuki N., et al., "Ion Heat pulse after Sawtooth Crash in the JFT-2M Tokamak", NIFS-240 (1993).
9) Ida K., Miura Y., Matsuda T., et al., "Observation of non diffusive term of toroidal momentum transport in the JFT-2M Tokamak", NIFS-241 (1993).
10) Yagi M.,Itoh K., Itoh S-I. et al. , "Current Diffusive Ballooning Mode in Second Stability Regime of Tokamaks", National Institute for Fusion Study Report NIFS-246
11) Itoh K., Itoh S-I., Fukuyama A. et al. , " Confinement Inprovement by the Current Profile Control", FURKU Report 93-03(03)
12) Fukuyama A., Itoh K., Itoh S-I. et al. , "Theory of Improved Confinement in High Beta-p Tokamaks", FURKU Report 93-05(05)
13) Itoh S-I., Itoh K., Fukuyama A. et al. , "Partition in Power Transfer and Dissipation rate in Self-sustained Turbulence", FURKU Report 93-06(06)
14) Tajima T., Kishimoto Y., LeBrun M.J., et al., "Transport in the Self-Organized Relaxed State of Ion Temperature Gradient Instability", IFSR#612 (1993).
15) Kim, J.Y., Kishimoto Y., Horton W. and Tajima T., "Kinetic Resonance Damping Rate of the Toroidal Ion Temperature Gradient Mode", IFSR#623 (1993).
16) Yagi M., Horton W., " Reduced Braginskii Equations", Institute Fusion Studies Report IFSR#632
17) Falter H., Ciric D., Akiba M., et al., Testing of Plasma Facing Materials for Divertors in the JET Neutral Beam Test Bed, JET-report, JET-P(93)53.
18) Yamagiwa M., "Effects of Radiofrequency-Induced Radial Diffusion on Triton Burnup", JET-P(93)98 (1993).
19) Falter H., Araki M., Ciric D., Massmann P., Test of One Dimensional MFC-1 CFC Tiles Brazed to a OFHC Heat Sink, JET-report, JET-DN-C (93)115.
20) Sato S.,Oka K., "Development of the In-vessel Component and the Remote Handling Technique for Fusion Experimental Reactor", Atomic Energy Society of Japaa, Fusion Engneering, Newsletter Vol.1, No.2 (1993) 6-7
21) Seki, Y., "Path to Fusion Power Reactors", Nuclear Power Industries, Vol.39 (1993) 51 (in Japanese)

A.2 Personnel and Financial Data

A.2.1 Change in number of personnel and annual budget (FY1987-1993)

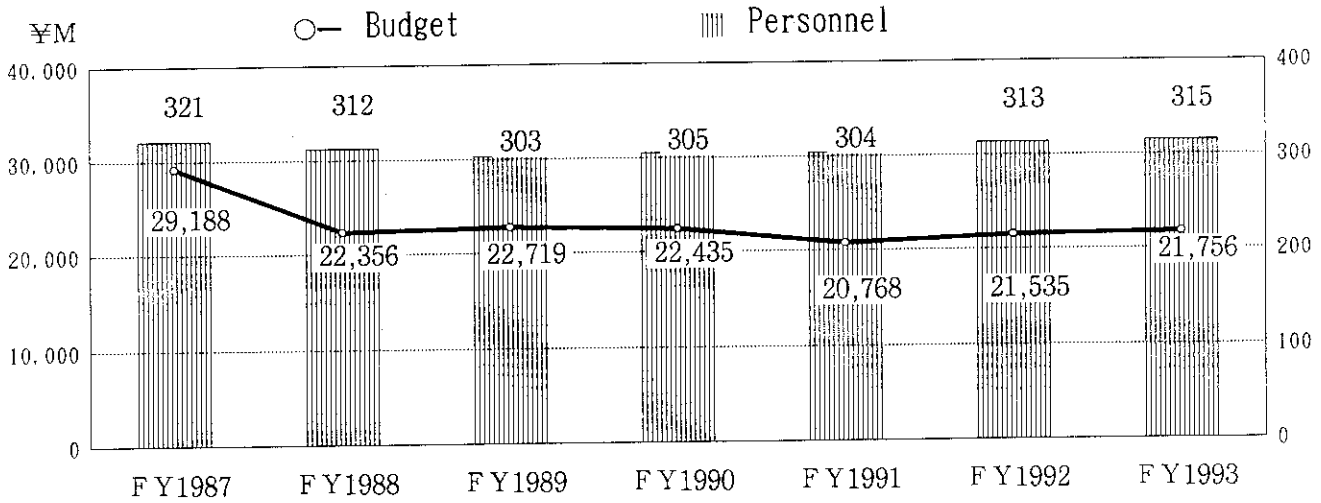

A.2.2 Organization chart (March 31, 1994)

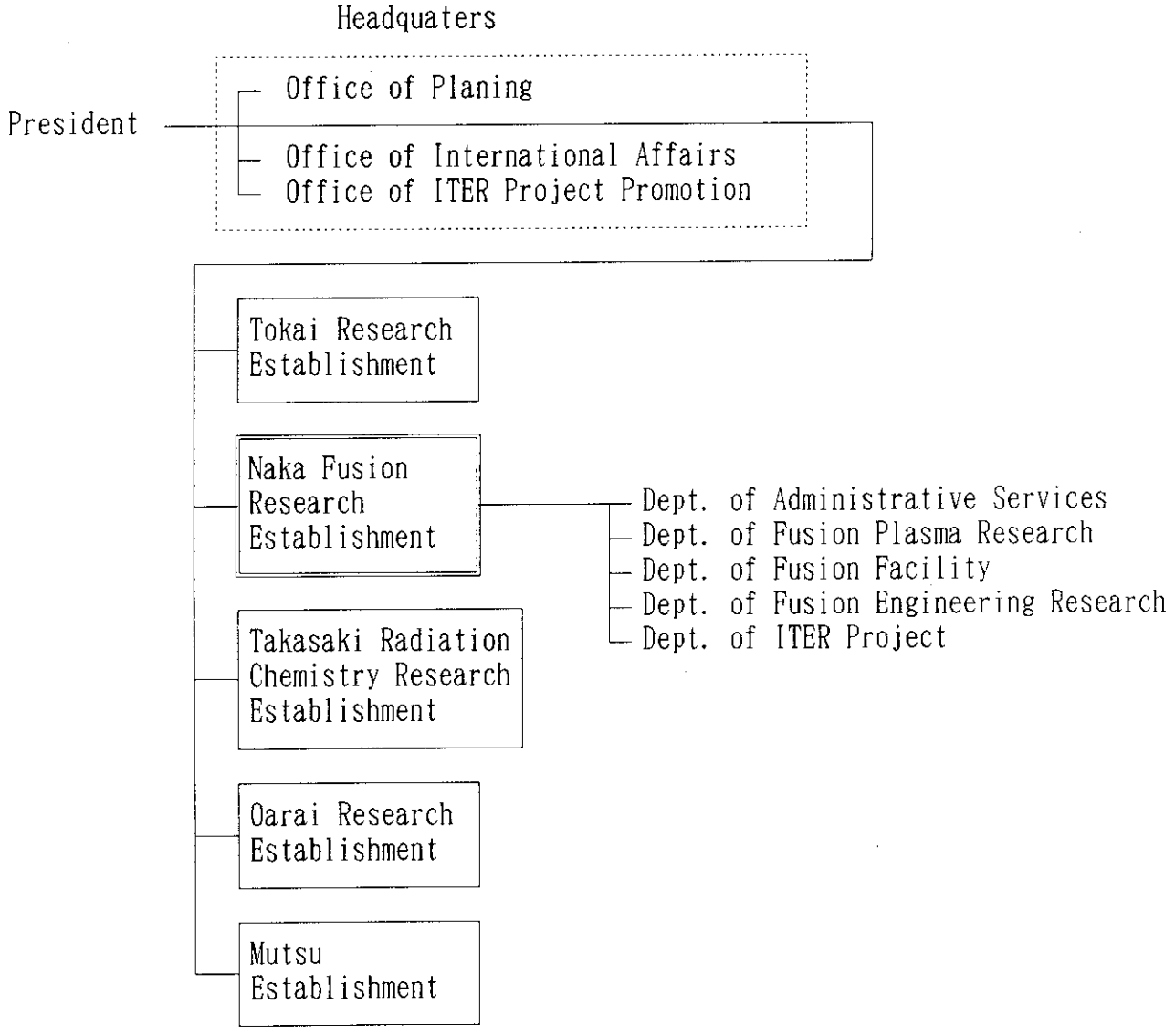

A.2.3 Scientific Staffs in the Naka Fusion Research Establishment (March 31, 1994)

Naka Fusion Research Establishment
TAMURA Sanae (Director General)
MIYAMOTO Goro (Scientific Advisor)
SEKIGUCHI Tadashi (Scientific Advisor)
TANAKA Masatoshi (Scientific Advisor)

Depertment of Adminisatrative Services
TEZUKA Kihachiro (Director)

Department of Fusion Plasma Research
KISHIMOTO Hiroshi (Director) KANAZAWA Tetsuo (Administrative Manager)

Tokamak Program Division
FUNAHASHI Akimasa (Head)

KAMADA Yutaka	KONOSHIMA Sigeru	MIYA Naoyuki
NAKAGAWA Shouji	NAKAJIMA Shinji	NINOMIYA Hiromasa
OGURI Shigeru	SAKASAI Akira	TOYOSHIMA Noboru

Plasma Analysis Division
AZUMI Masafumi (Head)

AOYAGI Tetsuo	HAGINOYA Hirofumi (*91)	HAMAMATSU Kiyotaka
NISHIMURA Yasutaro (*50)	OHSHIMA Takayuki	OZEKI Takahisa
SAITO Naoyuki	SAKATA Shinya	SATO Minoru
SHIRAI Hiroshi	TANI Kenji	TSUCHIYA Satoru (*85)
TSUJI Shunji	TSUGITA Tomonori	TSURUOKA Takuya (*49)
YAGI Masahiro		

Large Tokamak Experiment Division I
NAGAMI Masayuki (Head)

CHIBA Shinichi	FUKUDA Takeshi	GUNJI Souichi
HATAE Takaki	HIGASHIJIMA Satoru	HOSOGANE Nobuyuki
ISEI Nobuyuki	ISHIDA Shinichi	IWAHASHI Takaaki
KAZAMA Daisuke	KIKUCHI Mitsuru	KITAMURA Shigeru
KOIDE Yoshihiko	KONDOH Takashi	MORI Masahiro
NAGAYA Susumu	NAITO Osamu	NEYATANI Yuzuru
OHZEKI Masahiro	ONOSE Yoshiaki	OYEVAAR Ing. Therdorus (*89)
SATO Masayasu	SHITOMI Morimasa	SUNAOSHI Hidenori
TSUKAHARA Yoshimitsu	URAMOTO Yasuyuki	YAMASHITA Osamu
YOSHIDA Hidetoshi	YOSHINO Ryuji	

Large Tokamak Experiment Division II
NAGAMI Masayuki (Head)

ASAKURA Nobuyuki	FUJITA Takaaki	HOEK Magnus (*89)
IDE Shunsuke	ITAMI Kiyoshi	KAWANO Yasunori
KIMURA Haruyuki	KUBO Hirotaka	KUSAMA Yoshiki
MORIOKA Atsuhiko	NAGASHIMA Akira	NAKAMURA Hiroo
NEMOTO Masahiro	NISHITANI Takeo	SHIMADA Michiya
SHIMIZU Katsuhiro	SUGIE Tatsuo	TOBITA Kenji
USHIGUSA Kenkichi	VAN BLOCLAND Arjen (*89)	

Plasma Theory Laboratory
TAKEDA Tatsuoki (Head)
KAWANOBE Mitsuru (*49), KISHIMOTO Yasuaki, KURITA Gen-ichi
NAKAMURA Yukiharu, TAKIZUKA Tomonori, TOKUDA Shinji
TUDA Takashi, YAMAGIWA Mitsuru

Experimental Plasma Physics Laboratory
MAEDA Hikosuke (Head)
AIKAWA Hiroshi, HOSHINO Katsumichi, KAWAKAMI Tomohide
KAWASHIMA Hisato, MAENO Katsuki, MATSUDA Toshiaki
MORI Masahiro, MIURA Yukitoshi, NAGASHIMA Keisuke
OGAWA Hiroaki, OGAWA Toshihide, OHASA Kazumi
SHIINA Tomio, SHOJI Teruaki, TAMAI Hiroshi
UEHARA Kazuya, YAMAUCHI Toshihiko

Department of Fusion Facility
TANAKA Yuji (Director), OHTA Mitsuru (Deputy Director)

Fusion Facility Administration
KANAZAWA Tetsuo (General Manager)

JT-60 Facility Division I
KONDO Ikuo (Head), KIMURA Toyoaki (Deputy Head)
AKASAKA Hiromi, AKIBA Ken-ichi (*79), ARAKAWA Kiyotsugu
HISADA Kenji (*28), ISAKA Masayoshi, KAWAMATA Youichi
KIUCHI Shigemi (*30), KUSAKA Makoto (*28), MATSUZAKI Yoshimi
MIYACHI Kengo, NAKAKUKI Riichi (*49), OKANO Jun
OMORI Ken-ichiro, OMORI Shunzo, OMORI Yoshikazu
SEIMIYA Munetaka, SHIMONO Mitugu, TAKAHASHI Minoru
TERAKADO Tsunehisa, TOTSUKA Michiharu, YONEKAWA Izuru
YOSHIDA Michiharu

JT-60 Facility Division II
SHIMIZU Masatsugu (Head)
ANDO Toshiro, ARAI Takashi, HIRATSUKA Hajime
HONDA Masao, ICHIGE Hisashi, JIMBOU Ryutaro (*2)
KAMINAGA Atsushi, KODAMA Kozo, KOIKE Tsuneyuki
MASAKI Kei, MIYAKE Kazuyuki (*39), MIYO Yasuhiko
OGIWARA Norio, OHUCHI Yutaka, SAIDOH Masahiro
SASAJIMA Tadashi, SASAKI Noboru (*2), TAKASAKI Mamabu (*2)
TANAKA Takejiro, TSURUMI SATOSHI (*2), YAGYU Jun-ichi

RF Facility Division
YAMAMOTO Takumi (Head)
ANNOU Katsuo, FUJII Tsuneyuki, FUKUDA Hiromi (*29)
IKEDA Yoshitaka, IKEDA Yukiharu, IGARASHI Kouichi (*79)
KITAI Tatsuya (*28), KIYONO Kimihiro, MORIYAMA Shin-ichi
SATO Tomio (*30), SAWAHATA Masayuki, SEKI Masami
SHINOZAKI Shin-ichi, SUGANUMA Kazuaki, SUZUKI Norio
TERAKADO Masayuki, YOKOKURA Kenji

NBI Facility Division
KUNIEDA Toshisuke (Head) KURIYAMA Masaaki (deputy Head)
AKINO Noboru EBISAWA Noboru HOONOKI Toshio (*31)
KAWAI Mikito KASHIMURA Takanori (*30) KAZAWA Minoru
MATSUOKA Mamoru MIZUNO Makoto MOGAKI Kazuhiko
OHGA Tokumichi OOHARA Hiroshi SHIMIZU Kazuhiko (*30)
TAKAHASHI Shunji SUZUKI Yasuo (*28) TAKAYASU Toshio (*79)
USAMI Hiroji (*2) USUI Katsutomi YAMAMOTO Masahiro

JFT-2M Facility Division
SUZUKI Norio (Head)
HASEGAWA Koichi KASHIWA Yoshitoshi KIKUCHI Kazuo
KOMATA Masao OKANO Fuminori SAITO Masaya (*30)
SAWAHATA Masayuki SHIBATA Takatoshi SUZUKI Sadaaki
TANAKA Takejiro TANI Takashi TOKUTAKE Toshikuni

Department of Fusion Engineering Research
SHIMAMOTO Susumu (Director) SHOJI Kuniaki (Administrative Manager)

Plasma Engineering Laboratory
MURAKAMI Yoshio (Head)
ABE Tetsuya HIROKI Seiji KANEKO Kazuhiko (*94)
KASAI Satoshi UEHARA Toshiaki (*30)

Superconducting Magnet Laboratory
TSUJI Hiroshi (Head)
ANDO Toshinari HAMADA Kazuya HIYAMA Tadao
HOSONO Fumikazu (*87) KATO Takashi KAWANO Katsum
KOIZUMI Norikiyo MIYAKE Akihiro (*14) NAKAJIMA Hideo
NISHI Masataka NISHIDA Kazuhiko (*18) NOZAWA Masanobu (*4)
NUNOYA Yoshihiko OGATA Hirosige (*58) OSHIKIRI Masayuki (*30)
SASAKI Tomoyuki (*4) SEKI Shuichi (*30) SUGIMOTO Makoto
TAKAHASHI Yoshikazu TAKANO Katsutoshi (*30) TSUKAMOTO Hideo (*2)
WAKABAYASHI Hiroshi (*30) YASUKAWA Yukio (*58) YOSHIDA Kiyoshi

NBI Heating Laboratory
OHARA Yoshihiro (Head)
AKIBA Masato ARAKI Masanori DAIRAKU Masayuki
HANADA Masaya INOUE Takashi MAENO Shuichi (*59)
MIYAMOTO Kenji NAGASE Akihiko (*2) NAKAMURA Kazuyuki
NISHINO Yoshihiko OKUMURA Yoshikazu SATOH Kazuyoshi
SMID Ivica (*88) SUZUKI Satoshi TANAKA Shigeru
WATANABE Kazuhiro YOKOYAMA Kenji

RF Heating Laboratory
IMAI Tsuyoshi (Head)
FUJITA Hideo (*30) KASUGAI Atsushi KIKUCHI Masaya (*30)
MAEBARA Sunao SAIGUSA Mikio SAKAMOTO Keishi
SHIHO Makoto STEPHEN Musyoki (*90) TSUNEOKA Masaki
WATANABE Akihiko (*40)

Tritium Engineering Laboratory
OKUNO Kenji (Head)
ARITA Makoto (*35), ENOEDA Mikio, HARA Masahide (*23)
HAYASHI Takumi, HONMA Takashi, KAWAMURA Yoshimori
KONISHI Satoshi, MATSUDA Yuji, NAKAMURA Hirofumi
OBATA Hirofumi (*16), O`HIRA Shigeru, SUZUKI Takumi
TANJI Nobuo (*29), YAITA Yumi (*4), YAMADA Masayuki
YAMAI Hideki, YAMANISHI Toshihiko

Reactor Structure Laboratory
SEKI Masahiro (Head)
FURUYA Kazuyuki, KAKUDATE Satoshi, KANAMORI Naokazu (*2)
KURASAWA Toshimasa, MURAKAMI Shin (*4), NAKAHIRA Masataka
NISHIO Satoshi, OBARA Kenjiro, OKA Kiyoshi
SATO Satoshi, TADA Eisuke, TAGUCHI Kou (*30)
TERAKADO Takuya (*31), TOGAMI Ikuhide (*95)

Fusion Reactor System Laboratory
SEKI Yasushi (Head)
AOKI Isao, UEDA Shuzo

Department of ITER Project
MATSUDA Shinzaburo (Director)
TOMABECHI Ken (Invited Researcher)
FUJISAWA Noboru, NAGASHIMA Takashi, TAKATSU Hideyuki

Administration Group
YAMANE Yoshifumi (Leader)
IDE Toshiyuki, OHKUBO Keiko, YAMASHITA Tetsuyuki

Project Management Group
SEKI Syogo (Leader)
MATOBA Tohru

Joint Central Team Group
SEKI Syogo (Leader)
HORIKIRI Hitoshi (*97), IIDA Humio (*2), IIZUKA Takayuki
ISHIMOTO Kazuyuki (*96), IOKI Kimihiro (*7), ITOH Kazuyoshi (*29)
KONDOH Mitsunori (*4), MATSUKAWA Makoto, MATSUMOTO Hiroshi
MIZOGUCHI Tadanori (*2), MORI Seiji (*16), MOHRI Kensuke (*16)
NAKAMURA Hiroo, ODAJIMA Kazuo, OIKAWA Akira
OKUNO Kiyoshi, SAJI Gen (*7), SATO Kouichi (*83)
SHIBANUMA Kiyoshi, SHIMADA Mamoru (*4), SHIMIZU Katsusuke (*23)
SUGIHARA Masayoshi, TANAKA Eiichi (*98), TANAKA Shigeru
YAMAMOTO Shin, YONEKAWA Izuru, YOSHIDA Hiroshi

Home Team Design Group
TSUNEMATSU Toshihide (Leader)
HASHIMOTO Toshiyuki (*16), HOTTA Masataka (*58), KOIZUMI Kouichi
MURAKAMI Yoshiki (*4), NOMURA Yukio (*17), OOKAWA Yoshinao
SASAKI Takashi (*15), SAWA Masafumi (*14), SHIBUI Masanao (*4)
ZIMIN Sergei (*90)

Safety Evaluation Group
INABE Teruo (Leader)
UDA Tatsuhiko (*2)

*1 General Atomics, USA
*2 Hitachi Ltd.
*3 Lawrence Livermore National Laboratory, USA
*4 Toshiba Corp.
*5 Max-Planck Institute fur Plasmaphysik, Germany
*6 Massachusetts Institute of Technology, USA
*7 Mitsubishi Atomic Power Industory Inc.
*8 The University of Tokyo
*9 Nagoya University
*10 Osaka University
*11 Kyoto University
*12 Hiroshima University
*13 Institute fur Reaktorbauelements, KfK, Germany
*14 Ishikawajima-Harima Heavy Industries, Ltd.
*15 Mitsubishi Electric Co., Ltd.
*16 Kawasaki Heavy Industries, Ltd.
*17 Hazama-gumi Ltd.
*18 Kobe Steel Ltd.
*19 Oak Ridge National Laboratory, USA
*20 Century Research Center Corp.
*21 Northwestern Laboratory
*22 Institute of Plasma Physics, Nagoya University
*23 Mitsubishi Heavy Industries, Ltd.
*24 NAIG Nuclear Research Laboratory
*25 Japan Atomic Industrial Forum
*26 Central Research Institute for Electric Power
*27 NEC Co.
*28 Kaihatsu Denki Co.
*29 Sumitomo Heavy Industries, Ltd.
*30 Nuclear Engineering Co., Ltd.
*31 Tomoe Shokai
*32 Ibaraki Kohsan
*33 Tokyo Nuclear Service Co., Ltd.
*34 ULVAC Corp.
*35 Kyushu University
*36 Contract Researcher
*37 Princeton Plasma Physics Laboratory, USA
*38 LITEC Co., Ltd.
*39 Japan Expert Clone Corp.
*40 Nissei Sangyo Co., Ltd.
*41 JET Joint Undertaking, UK
*42 Hodaka Seiki Ltd.
*43 Sumitomo Electric Industries, Ltd.
*44 Nikon Corp.
*45 National Laboratory for High Energy Physics
*46 University of Tsukuba
*47 Los Alamos National Laboratory, USA
*48 Japan Radiation Engineering Co.
*49 Nuclear Energy Data Center Co.
*50 Osaka University
*51 IMPRIAL COLLEGE, UK
*52 Institute of Research Hydro-Quebec, Varenns, Canada
*53 KFA-IPP, Germany
*54 Ewic Engineering Co., Ltd.
*55 ORC Manufacturing Co., Ltd.
*56 Koike Sanso Kogyo Co., Ltd.

*57 Hitachi Sanso Co., Ltd.
*58 Fuji Electric Co., Ltd.
*59 Nissin Electric Co., Ltd.
*60 Sandia National Laboratory, USA
*61 JGC Corp.
*62 Tokyo Institute of Technology
*63 Nuclear Research Center Karlsruhe, Germany
*64 Argonne National Laboratory, USA
*65 ITER Team
*66 Yokohama National University
*67 Nihon Software Kaihatsu, Inc.
*68 Kanazawa Computer Service Corp.
*69 University of California at Los Angeles, USA
*70 University of Texas, USA
*71 Varian Company Co., Ltd.
*72 Nagaoka University of Technology
*73 Denki Kogyo Co., Ltd.
*74 The NET Team
*75 National Institute for Fusion Science
*76 I.V. Kurchatov Institute of Atomic Energy
*77 Keio University
*78 Mitsubishi Cable Industries, Ltd.
*79 Nippon Advanced Technology Co., Ltd.
*80 Hamamatsu Photonics KK
*81 University of California at San Diego, USA
*82 University of Maryland
*83 Atomic Data Service Corp.
*84 Nihon Houshasen Engineering Co., Ltd.
*85 ACE
*86 Hitachi Works
*87 Hitachi Cable, Ltd.
*88 Austrian Research Center Seibersdorf
*89 STA Fellowship
*90 JAERI Fellowship
*91 Nuclear Information Service Co.
*92 Tokai University
*93 Ibaraki Software
*94 Ebara Research Co., Ltd.
*95 Kumagai-gumi Ltd.
*96 Shimizu Corporation
*97 Shinryo Corporation
*98 Kajima Corporation